Cell manipulating surface topographies for biomedical applications

In vitro and in vivo evaluation of cell and tissue response to micro- and nanometric organized patterns

Alexey Klymov

Colophon

Thesis Radboud University Medical Center, Nijmegen, The Netherlands, with summary in English and Dutch.

Surface-topographies for cell manipulation in tissue engineering: In vitro and in vivo evaluation of cell and tissue response to micro- and nanometric organized patterns

Lay-out and cover design: **Alexey Klymov**

Printed by: **Ipskamp Drukkers, Enschede**

Cell manipulating surface topographies for biomedical applications

In vitro and *in vivo* evaluation of cell and tissue response to micro- and nanometric organized patterns

Proefschrift

ter verkrijging van de graad van doctor
aan de Radboud Universiteit Nijmegen
op gezag van de rector magnificus,
volgens besluit van het college van decanen
in het openbaar te verdedigen op dinsdag 26 januari 2016
om 12:30 uur precies

door

Alexey Klymov
geboren op 13 december 1983
te Kiew (Oekraïne)

Cell manipulating surface topographies for biomedical applications

In vitro and *in vivo* evaluation of cell and tissue response to micro- and nanometric organized patterns

Doctoral Thesis

to obtain the degree of doctor
from Radboud University Nijmegen
on the authority of the Rector Magnificus,
according to the decision of the Council of Deans
to be defended in public on Tuesday, January 26, 2016
at 12:30 hours

by

Alexey Klymov
born on 13 december 1983
in Kiew (Ukraine)

Contents

1

General Introduction

Organization of multi-cellular life

The development of the human organism is fascinating in many aspects. It begins with a single fertilized egg and dramatically expands to a total number of approximately 37 trillion (37.000.000.000.000) individual cells.[1] Despite being genetically identical, our cells differentiate into hundreds of cell-types, and can be characterized based on their genotype as well as on phenotype, i.e. cell morphology, function and purpose.[2] Remarkably, single cells can orient inside our bodies, interact and communicate with other cells, migrate to places of destination, and execute various programs, eventually building up higher order structures that are nearly identical for almost 8 billion human beings. Such perfection of blueprint execution is only possible since cells possess inherited intrinsic mechanisms that allow cellular organization and coordination inside multi-cellular organisms. Understanding how we can use these mechanisms to manipulate cell-behavior might help us to exploit such phenomena also for clinical applications, such as for improvement of implantable materials.

Cell-implant surface interactions

One of the key intracellular mechanisms that have evolved during the past 1 billion years is the ability to interact with the cell-surrounding environment. Especially the recognition of the surface-features such as stiffness, bio-chemical cues, and topography are nowadays thought to be the influential factors the orchestration of cell-behavior.[3-5] Therefore, it is not surprising that the fate of a material brought into a living system is strongly defined by its surface properties; hydrophillicity and hydrophobicity, chemical groups, charge distribution, and topography.[6] Immediately upon implantation, these properties will define the ionic profile from the host serum at the surface of the implanted material.[7] As the next step, proteins and peptides will adhere to the implant either by weak charge-based non-covalent bonds, or by the stronger permanent covalent bonds.[8] Since proteins are the main interaction point between cells and the substrate, the protein-profile eventually defines the cellular binding. That means that substrate surfaces not only can be designed to allow or prohibit cell binding, they moreover can be designed in order to determine a specific cellular subset.

This bio-chemically based interaction is achieved through transmembrane integrins, which attach to the extracellular proteins, serve as anchoring points during migration, and transmit information into the intracellular space by activating intracellular signaling pathways. Different cell-types can express different subsets of integrins, which in term strictly define the ligand the cells can bind to. Some cell-types express a broad range of different integrin types allowing them recognition and binding to a big subset of extra-cellular proteins. Endothelial cells express $\alpha_1\beta_1$, $\alpha_2\beta_1$, $\alpha_3\beta_1$, $\alpha_5\beta_1$ and $\alpha_6\beta_1$ integrins, which allow them binding to extra-cellular collagen, laminin, fibronectin, and invasin. Contrary, certain cell-types express a very specific integrin combination that allows only for binding to a small subset of proteins. For example the specific $\alpha_L\beta_2$ integrin expressing leukocytes are the only subset of cells being able to bind to a glycoprotein motif on the surface of antigen presenting cells.[9] Except being the link between cells and extracellular matrix, the integrin interaction has been shown to steer cell-behavior and can influence processes like migration, attachment, proliferation, differentiation, and even cell death.[2]

Topographies were often shown to influence the integrin organization *in vitro*. In fact, also distinct tissues, organs and niches were found to feature very specific topographies.[10] Characterization of these topographies reveals a strongly repetitive setup of features on a scale spanning between millimeters down to nanometers. Such a hierarchically structure is collagen, which is the most abundant protein of the extra-cellular matrix. Collagen is build up from fibrils having dimensions of approximately 20 nm, which build up higher structure fibers of micrometer size and which are found normally in higher order bundles.[11] As a direct consequence of the collagen design, contact guidance of cells has been found to occur, which induce cell polarity and cell migration along collagen fibrils.[12]

It is to be elucidated how the natural topographies contribute to the cell-behavior in a healthy living system. Several experiments showed that cellular response can be indeed initiated by pattern-features with sizes of only few nanometers also in an *in vitro* system.[13] However, the manner in which topographies are influencing cell-behavior can be different. To date two main ideas were described that can explain the cellular reaction, namely direct and indirect topographical mechanotransduction.

1

Direct mechanotransduction explains the deformation of the intracellular organization including the nucleus, by means of mechanical forces.[14] These forces can occur either through direct deformation of the cells by prominent topographical features on the substrate surface, or by transfer of forces via integrin and focal adhesions through the cytoskeleton to the nucleus. The deformation of the nucleus is thought to change the gene expression and thereby the behavior of the cell. The indirect mechanotransduction is independent of the intracellular cytoskeleton organization.15 The relevant process occurs at the focal adhesions, which will change cell-behavior through signaling as a direct consequence of focal adhesion formation and distribution.

Surface topographies on implant surfaces

The advantage of applying specific patterns onto the surface of implantable materials can for example be seen in the field of dental and orthopedic implants, and bone tissue engineering. The trial-and-error based development of osseintegrative implants has eventually led to the design of metallic implants with a wide range of surface roughness.[16] Roughness, which is the direct result from the various processing steps of the implant-manufacturing, has been shown to positively influence bone-regeneration related cell-behavior *in vitro*. However, studying the effects of topographies on cell-behavior is complicated on rough surfaces, as "roughness" is a rather abstract term, including a wide variety of topographical features. Therefore, to understand the fundamental cell-topography interaction that can allow improvement of the implantable material design, predefined and organized patterns should be the pivotal choice. Production of such topographies is possible with a high precision due to strongly developed lithography based processes also utilized for the semi-conductor industry (Chapter 2 reviews in detail which methods for production, functionalization and characterization are available to date).

Objectives of this study

In literature a vast amount of evidence is provided on the intrinsic potential of eukaryotic cells to respond to the topographical features of the cellular environment. Being one of the naturally evolved mechanisms

to interact inside of a multicellular complex organism, the cell-topography interaction can be exploited to communicate with cells, allowing a direct intervention with the intra- and extracellular processes. Although such cell-manipulation can only occur on the interface between cells and a solid material, the results might be essential for various bone implant and tissue engineering approaches. This thesis describes the biological response towards organized surface topographies in *in vitro* and *in vivo* experiments. It was extensively analyzed how cells react to topographies, regarding organization and migration. Moreover, it was studied how combinations of topographies with bio-chemical stimuli can influence the potential of bone-forming cells to proliferate, differentiate and eventually to mineralize on the substrate-surface. Ultimately, topographies were tested on the surfaces of implants in an animal model for their ability to influence trabecular bone regeneration.

The general hypothesis of the given studies was that *in vitro* and *in vivo* biological response to surface-topographies could be triggered, changed and manipulated by direct cellular exposure to specifically designed surface cues.

The following research questions were assessed:

1. Which technologies can be used to manipulate solid matter to produce designed strictly organized topographies, and how can the cellular response to such substrates be assessed? (Chapter 2)

2. To which extent can neuronal cells and their neurite extensions react and interact with nanosized grooves? (Chapter 3)

3. To which extent can cells recognize and preferentially migrate on patterned surfaces? (Chapter 4)

4. Can a calcium-phosphate based coating change the response of mineralizing cells to nanosized grooves, regarding organization, proliferation, differentiation and mineralization? (Chapter 5)

5. Can nanosized grooves on the surface of spherical implants influence the regeneration of trabecular bone in an animal model? (Chapter 6)

6. Can microsized grooves on the surface of bioactive elastin-like recombinamer membrane influence the biological response, including differentiation and mineralization? (Chapter 7)

1

References

1. Bianconi, E., et al., An estimation of the number of cells in the human body. Annals of Human Biology, 2013. 40(6): p. 463-471.
2. Lamond, A.I., Molecular biology of the cell, 4th edition. Nature, 2002. 417(6887): p. 383-383.
3. Engler, A.J., et al., Matrix elasticity directs stem cell lineage specification. Cell, 2006. 126(4): p. 677-89.
4. Rowlands, A.S., P.A. George, and J.J. Cooper-White, Directing osteogenic and myogenic differentiation of MSCs: interplay of stiffness and adhesive ligand presentation. Am J Physiol Cell Physiol, 2008. 295(4): p. C1037-44.
5. McBeath, R., et al., Cell shape, cytoskeletal tension, and RhoA regulate stem cell lineage commitment. Dev Cell, 2004. 6(4): p. 483-95.
6. Anderson, J.M., A. Rodriguez, and D.T. Chang, Foreign body reaction to biomaterials. Semin Immunol, 2008. 20(2): p. 86-100.
7. Kasemo, B. and J. Gold, Implant surfaces and interface processes. Adv Dent Res, 1999. 13: p. 8-20.
8. Kasemo, B. and J. Lausmaa, Material-tissue interfaces: the role of surface properties and processes. Environ Health Perspect, 1994. 102 Suppl 5: p. 41-5.
9. Elangbam, C.S., C.W. Qualls, and R.R. Dahlgren, Cell adhesion molecules - Update. Veterinary Pathology, 1997. 34(1): p. 61-73.
10. Turner, L.-A. and M. J. Dalby, Nanotopography - potential relevance in the stem cell niche. Biomaterials Science, 2014. 2(11): p. 1574-1594.
11. Birk, D.E., et al., Collagen Fibrillogenesis Insitu - Fibril Segments Are Intermediates in Matrix Assembly. Proc Natl Acad Sci U S A, 1989. 86(12): p. 4549-4553.
12. Petrie, R.J., A.D. Doyle, and K.M. Yamada, Random versus directionally persistent cell migration. Nature Reviews Molecular Cell Biology, 2009. 10(8): p. 538-549.
13. Loesberg, W.A., et al., The threshold at which substrate nanogroove dimensions may influence fibroblast alignment and adhesion. Biomaterials, 2007. 28(27): p. 3944-3951.
14. Dalby, M.J., Topographically induced direct cell mechanotransduction. Medical Engineering & Physics, 2005. 27(9): p. 730-742.
15. Kasper, C., F. Witte, and R. Portner, Tissue Engineering III: Cell-Surface Interactions for Tissue Culture Preface. Tissue Engineering Iii: Cell-Surface Interactions for Tissue Culture, 2012. 126: p. Xi-Xii.
16. Svanborg, L.M., M. Andersson, and A. Wennerberg, Surface characterization of commercial oral implants on the nanometer level. J Biomed Mater Res B Appl Biomater, 2010. 92(2): p. 462-9.

2

Understanding the role of nano-topography on the surface of a bone-implant

Alexey Klymov, Ljupcho Prodanov, Edwin Lamers, John A Jansen, X Frank Walboomers

Introduction

During the lifetime of an organism tissue-damage can occur due to reasons like accidents, disease or aging. When lost tissues cannot be restored by natural regeneration processes, biomaterials can be used to (at least partially) replace the natural function. The term "biomaterial" is often used as the synonym for synthetic or non-living materials that, due to their physical and/or chemical properties, resemble natural tissues and can be introduced into a biological system.

Nowadays implant treatment has become routine, but still more advanced related regenerative medicine approaches remain challenging in clinics. The steadily increasing average age of patient-populations, and risk factors like diabetes, high blood pressure, osteoporosis and smoking habits can result in poor device performance.[1-6] Interestingly, also younger patients from healthy and risk groups show significantly higher failure rates than older patients,[7-9] which could be explained by the higher mechanical loads during the daily life activities. Moreover, revision surgery of a failed medical device usually is ever more challenging. These facts show that there is still the need for improvement of the implants and implant materials used today. Therefore the number of implantable biomaterials used for tissue regeneration of bone is growing at a high pace. Materials frequently used in clinics are metals, ceramics and polymers, which are systematically tested and improved to optimize their properties. Features like strength, hardness and wear resistance are desirable, whereas adverse reactions like abundant inflammatory responses or toxicity should not occur.

However, in the ambition to produce biomaterials, principles and rules of natural tissue formation are often overlooked or simply ignored. Bringing a biomaterial into a living system, does not only disturb the biologically equilibrated state of the organism, but also confronts this system with a material of foreign structure and (bio-) chemical properties. Studying the natural mechanisms of tissue formation and regeneration on the one hand, and cellular interaction with that tissues on the other hand, will not only increase fundamental understanding of organogenesis, but will also allow utilization of this knowledge for efficient and intelligent tissue-reconstruction applications.

The rather complex process of tissue formation and organization in humans is mainly driven by the interaction of single cells with their environment. During the one billion years after the transition from single-cell organisms to multicellular living systems, efficient features have developed that allow cell-control on an almost single-cell level. These control mechanisms make it possible for a single fertilized oocyte to develop into a systematically organized multibillion-cell organism, which is able to maintain, reshape and regenerate many of its tissues. The three important coordination systems within an organism are: (1) cell signaling using cytokines and hormones, (2) direct interactions between cells, and (3) interactions between cells with non-cellular tissues.

The ability of single cell organisms to sense a gradient of chemical compounds and to follow or to avoid the highest concentration evolved very early. The process, that is called chemotaxis, allowed the organisms to find sources of nutrients, or to stay away from toxic compounds. The main mechanism behind it is the recognition of compounds (ligands) by a specific receptor expressed on the cellular membrane. Ligand-binding to the receptor activates an intracellular signal transition process, which allows regulation of transporters, gene expression and cell-migration. Information about the concentrations of nutrients, growth factors, cytokines and hormones is sensed and integrated by cells, resulting in adaptation of cellular behavior. The process can be controlled on different levels but mainly depends on ligand concentrations and receptor expression levels. However, cells are able to sense, but also produce and release ligands, thereby allowing signaling processes that for instance are crucial during regeneration and inflammation processes. Following that, principle mesenchymal stem cells (MSCs) have been shown to follow the concentration gradient of 9 out of 26 chosen growth factors, of which the platelet-derived growth factor (PDGF) showed the strongest effect.[10] Combinations of different growth factors have been shown to synergistically increase the cellular response, or to block each other and thereby to decrease the migration. Interestingly, thrombin could attract MSCs but not fibroblasts, explained by different sub-sets of expressed receptors. These findings show that cells possess a fine-tuning system, which allows them to react to different situations very specifically. It is possible that the PDGF that is strongly released after

bone-injury will stimulate chemo-attraction of MSCs,[11] which will migrate to the place of injury and differentiate into bone-forming cells under the stimulation by additional factors.[12]

Second, cell–cell recognition and interaction is crucial for a proper development and function of a multicellular organism. We can distinguish between stable and transient cell–cell interactions. Stable interactions are provided by tight- and gap-junctions, which allow the formation and organization of organ tissues. Transient cell–cell interactions are based on the interaction of cell-surface adhesion proteins and recognition of transmembrane and glycoprotein motifs on the extracellular site of one cell by receptors on the membrane of another cell. Transient bindings are crucial for processes like recognition of cells during immunological processes and migration. During bone remodeling cell–cell interactions strictly control the phases of periodic bone resorption and bone formation. The interaction between osteoclast-precusor cells and osteoblasts induces the formation of bone-resorbing osteoclast cells, while bidirectional signaling between osteoclasts and osteoblast precursors initiates osteoblast differentiation.[13] Finally, cellular receptors play also an important role in cellular interaction with the non-cellular environment such as the matrix of connective tissue, bone and cartilage. Protein patterns from the connective tissue, like the three amino acid arginine–glycine–aspartic acid (RGD) motif, are directly recognized by receptors. Recent research has shown that cells are also capable of sensing mechanical features like elasticity,[14] size[15] and topography[16] on the culturing surfaces, leading to changes in their behavior. By utilizing this knowledge cells can be directed to execute the required performance, such as the differentiation of MSCs to bone-producing osteoblast(-like) cells. For instance, when culturing the progenitor MSCs on a rigid matrix-material,[14] surfaces that allow cell spreading instead of restricting the cell size[15] or surfaces featuring disordered nano-scale pillars instead of ordered[16] the cells will differentiate into the osteogenic lineage. These properties could allow a rapid repopulation on the implant surface with osteogenic cells, thereby inducing osteogenesis.

Although some implantable biomaterials that feature protein motifs or release chemo-attractants and growth factors to stimulate cellular behavior have been studied, in this review we will mainly focus on the interaction

of cells with nano-topographical features of implants, how these can be manufactured and characterized.

Characterization of surfaces

A plausible starting point for biomaterial-implant design is the observation of local conditions and environment in the living organism. Most tissues will feature a hierarchical organization ranging from macroscopic scales to sizes in the nanometer-range. Such strongly standardized and systematic arrangement of certain tissues can provide unique and pivotal clues about tissue–cell interactions. For example, collagen in the extracellular matrix (ECM) that is packed in dense parallel nano-sized fibers, which not only provide strong mechanical properties,[17] but seem also crucial for cell-migration.[18] This knowledge can be applied in biomaterials-design, for instance as production of surfaces having nano-grooved structures can partly mimic collagen-like topography.[19] Moreover, the topography can be varied thereby providing a fine-tuning mechanism to manipulate cellular behavior. However, one crucial part when reproducing such advanced surface features is the characterization of living tissues as well as biomaterials allowing a goal-oriented design and optimization of implants. In this part, the most frequently used methods for analysis will be presented, which can be subdivided in microscopic, physical and chemical analysis.

Of course, routine microscopic techniques can be used for determination of tissue-properties like surface macro- and micro-topographical structure size and feature distribution. Morphology of single cells and cellular organelles can be obtained using the same techniques giving more insight in the dimensions of cellular-movement mechanisms, membrane structures and how these can be influenced by biomaterial topography. Conventional optical microscope techniques could be a useful and easy to use method for surface analysis. However, due to the nature of visible light-waves, the maximal resolution of the microscopes is limited to about 200 nm[20] and thus unsuitable for more detailed characterization of nano-metric features, which by definition are below 100 nm.[21] Lately, the development of new generation lenses[22] and several fluorescence based techniques[23–26] could reduce the theoretical diffraction limit to dimensions

of only few nanometers. Although so far not being used for surface analysis, these so called super-resolution microscopes might become a helpful tool in that area of research.

Nowadays one of the most extensively used techniques for surface-imaging is electron microscopy (EM) that utilizes a dense electron beam to scan the probe of interest. Electrons interact with substrate-surface atoms and can penetrate, be absorbed or reflected by the material. Scanning electron microscopes (SEM) produce contrast images with a resolution of less than 2 nm by detection of reflected electrons.[27] One disadvantage of SEM is the need for sputtering of conductive material and placement of the specimen into a vacuum chamber, making a trustful analysis of nanostructure biological samples challenging. This problem can be resolved by the use of the environmental SEM technique, which works following the same principles but without the need for electrical conductivity and vacuum environment[27] reaching image resolutions that are comparable with that of SEM.[28] Also, the transmission electron microscope utilizes electrons for image acquisition, but contrary to SEM detects the electrons that are penetrating the sample, and allows resolutions down to single angstroms.[29]

Although SEM and TEM provide excellent resolution dimensions, the obtained quantitative information is limited to the longitudinal axis. This disadvantage can be circumvented by the use of the atomic force microscope (AFM), which combines mechanical interaction and imaging.[30] Although a disadvantage of AFM is a slow scanning process, it is outweighed by the fact that measurements can be done with living tissues, almost without preparation and at a resolution of atomic sizes.[31]

A structure perfectly rebuilt from a biomaterial does not necessary mean that it will behave in the same manner as the real tissue it is mimicking during *in vitro* or *in vivo* experiments or at a later time-point during clinical applications. Adverse physical properties can interfere and bias the interaction of the substrate with living cells and tissues. For this reason factors like roughness, stiffness, energy and charge should also be determined, compared and eventually optimized.

Roughness analysis of surface topographies has become a routine method in material design.[32–34] One of the reasons is the observation that cellular

function strongly depends on the grade of roughness,[35,36] which has also been confirmed by *in vivo* experiments.[37,38] Roughness can be analyzed by profilometric techniques, which can be subdivided into mechanical contact and optical measurements. Contact methods are based on physical interaction of a stylus or a cantilever with the surface topography. Stylus profilometers and AFM are examples that due to small dimensions of the interacting tip can sense roughness features in the nanometer range. The non-contact optical profilometers make use of a beam of light that is reflected by the surface and picked up by a detector. On a completely plane surface, the angle of entry would result in a predicted same dimensional angle of reflection. However, when hitting a rough surface, the light detection would occur with a non-predicted angle of reflection, which will be relative to the grade of roughness. No need for physical interaction with the surface is a big advantage of the optical techniques, since it is faster and more cost-effective. However, because of the diffraction limit of light the lateral resolution is less accurate. Therefore similar methods like X-ray reflectometry, which is based on reflection of X-rays from the surface, can be used for roughness measurements at the nanometer scale.

Another important physical characterization method is the determination of surface-wettability, usually assessed by contact-angle measurements. High surface tension will result in a low contact angle, and low surface tension in a high contact angle between the edge of a liquid-drop and the surface it is placed on (Figure 1). However, measuring of wettability on nano-topographic or even porous materials remains challenging, since the measured angle will reflect not only the surface energy, but also the topographic features. Advancing and receding contact angle tests can be performed to increase the sensitivity of this approach for patterned surfaces. Another disadvantage of the test is that it can only give an average value of the surface-area underneath the droplet and thereby is not suitable to study single isolated nano-sized features. Nevertheless, differences in wettability seem not only to have an influence on liquid interaction with the surface, but have also been shown to result in changes in cellular behavior. When increasing the wettability of titanium discs by argon plasma treatment, Duske et al. showed fibroblast spreading was significantly higher on treated compared to non-treated samples.[39]

For some purposes, like the above mentioned mimicking of collagen fibers *in vitro* by using nano-grooved structures, capillary forces should also be taken into account. These for instance can be observed when dipping a thin tube into water, which instantly will begin to rise (Figure 1B). Anisotropic wetting measurements, consisting of a combined wettability test and liquid dispersion measurements,[40] can be performed to allow relative estimations of the capillary forces.

Cells are also able to sense and react to surface stiffness or elasticity[41] as has been shown by the interesting finding made by Engler et al. when culturing MSCs on surfaces having different elasticity.[14] While MSCs cultured on soft surfaces differentiated into neuron-like cells, culturing on intermediate and rigid materials drove the cells into entering the myogenic and osteogenic differentiation-pathways respectively. AFM interaction with the surface and the micro-indentation (MI) technique can be used for surface stiffness characterization. Since the force of the AFM cantilever that is affecting the surface is adjustable, the counterforce of the surface can be interpreted as the surface stiffness. For MI, a diamond stylus of predefined geometry is pressed against the surface with a predefined force, the data of which are integrated and used for stiffness value calculations. The same methods can also be used to define elastic properties of cellular membranes and how these are affected by surface topographies.

AFM can also be used to evaluate the adhesion forces of a nano-topographic
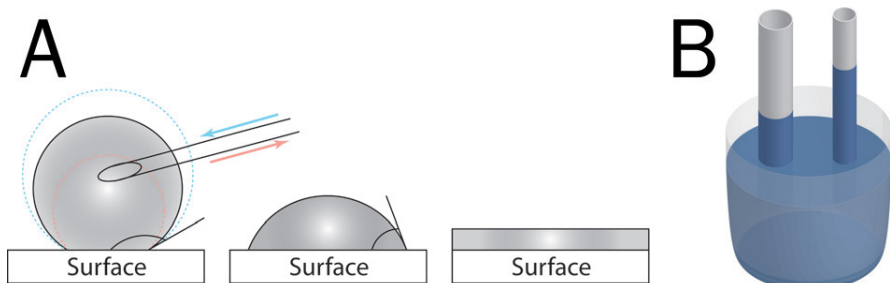
Figure 1: Wettability and capillary action. A) Wettability, the property of a surface to interact with liquids, can be defined by placement of a liquid drop on the surface and measuring their contact angle. Low wettability will result in a high contact angle (left), high wettability in a low contact angle (right) between the edge of a liquid-drop and the surface. Advancing and receding contact angle tests can be performed to increase the sensitivity of this approach. B) Capillary action can be visualized by dipping a thin glass tube into water, which instantly will begin to rise. The height of the water column is relative to the diameter of the tube.

surface at a high resolution and precision.[42] The measured adhesion force is often the sum of various separate forces like the Van der Waals forces, electrostatic forces, capillary forces and chemical-bond forces. For the measurement the cantilever is brought into contact with and removed from the surface, while the forces that act on the cantilever during both motions are recorded. Depending on the experimental setup the material of the cantilever as well as the functionalization of the cantilever-surface can be performed. Chemical groups, proteins, or even cells can be attached to the cantilever tip, thereby allowing the measurement of cell-surface adhesion interactions.[43] However, when measuring surfaces with nano-topographies the relative roughness has to be taken into account for which the calculations should be corrected.[44]

As implant-materials are confronted with a wet local environment full of charged ions, proteins and cells when brought into a patient, it is of high importance to take the zeta potential (Figure 2) into account when designing and testing a biomaterial.[45] Charged particles in a suspension medium are surrounded by two layers of ions. The inner "fixed" or Stern

IMPLANT SURFACE
WITH CHARGED
GROUPS

Stern layer
Slipping plane
Diffuse layer
Bulk solution
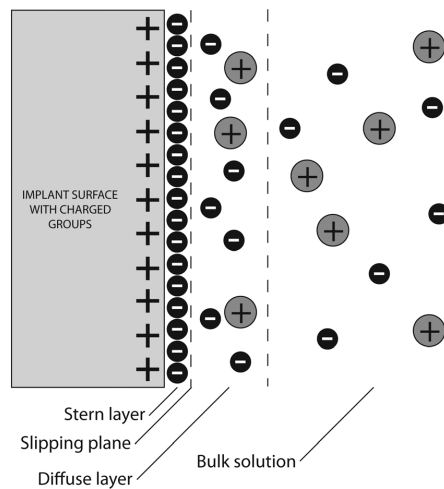
Figure 2: Schematic overview of ion-distribution at the surface of positively charged implanted biomaterial originating in zeta potential. Polarized particles in the suspension medium are surrounded by two layers of ions. The inner "fixed" or Stern layer consists of strongly bound, and the outer "diffuse" layer of loosely bound ions. During motion and interactions of the particle, the outer ions begin to move, thereby leading to a shear effect between the two layers inducing the development of an electrokinetic potential.

2

layer consists of strongly bound ions, the outer "diffuse" layer of loosely bound ions. During motion and interactions of the particle, the outer ions begin to move, thereby leading to a shear effect between the two layers. The arising electrokinetic potential—the zeta potential—can influence the behavior of these particles and has been shown to be utilized by evolution for natural behavior of living systems.[46] The surface zeta potential can be calculated from streaming potential experiments and allows estimations of available functional groups and thereby also of the overall charge of the surface.[47] Similar to the wetting experiments, zeta potential measurements can only give information about the average potential of the measured surface.

Chemical characterization can be used to obtain spatial and quantitative information about the composition of surface elements. The underlying theoretical background of many characterization techniques is the fact that every element has its own specific and unique atomic structure, which allows element-differentiation based on radiation produced by atoms as a result of electron ejection. Energy-dispersive X-ray spectroscopy (EDS) makes use of electron-beams that, when hitting and ejecting an electron from an atom, will produce X-rays. Since the same process occurs as a byproduct during electron microscopy, EDS is often combined with (S)EM, allowing parallel analysis and mapping of visual and chemical properties of a material in the range of only few nanometers. X-Ray photoelectron spectroscopy (XPS) uses X-ray-beams instead of electrons. However, it is following the same basic principles of element-characteristic measurements of energy spectra that are produced by electrons ejected by X-rays. The rather poor XPS resolution of several micrometers can be improved with X-ray photoelectron emission microscopy allowing resolutions down to 30 nm.[48,49] Exploitation of ion beams can also be used for characterization of the chemical surface composition in secondary ion mass spectrometry. Also here goes a similar principle. When an ion hits an electron, it can generate secondary electrons that are detected by a mass spectrometer. The lateral resolution of this technique goes down to about 50 nm.[50]

The advantage of the Raman spectroscopy technique compared to the previously described characterization methods is the possibility to obtain not only the atom composition, but also molecular structures of

the surface-compounds. This approach is based on the interaction of monochromatic photons with molecular electrons. Similar to fluorescence, the photon will interact with one of the molecules' electrons thereby exciting it to a higher energy state. Upon relaxation of the molecule, the electron will return to a lower energy state, while releasing the remaining energy in form of a photon. Contrary to fluorescence where the emitted photon always has less energy than the exciting photon, Raman scattered electrons can either remain at the same energy state, loose, or gain energy thereby shifting in wavelength. The resultingspectrum of the emitted light, however, molecule-specific and can therefore be used to make conclusions about the surface chemistry. Additional to molecule structures, Raman spectroscopy can be used for determination of crystal structures.

X-Ray diffraction (XRD) techniques utilize X-rays that are scattered by surfaces under certain conditions. Therefore the sample needs to be scanned by, or rotated in front of the X-ray-beam. Information about scattered angle, wavelength or the polarization of the scattered X-rays can be used to determine the crystal structure, texture and orientation, crystal phases, lattice parameters, but also chemical compositions of the surface material at the nanometer level.

Manufacturing of nano-patterned surfaces

Characteristic features of the tissue structure ideally can be replicated for *in vitro* or *in vivo* experiments. Most of the basic principles used for production of surface topographies are the same as (or at least have evolved from) techniques that were used for already more than 50 years for the semiconductor industry. In 1965, Gordon Moore stated that the number of transistors on integrated circuits is doubling almost every two years.[51] This statement has proven to be true and is nowadays known under the term of Moore's Law. However, to keep such pace it was necessary to miniaturize all produced materials, leading to an immense investment and drive of streamlining development-pathways allowing fast and parallel production of microchips at a cheap price. In particular, the focus on cost-effectiveness has allowed these techniques to step into life-science research.

A huge number of new techniques for nano-topography production have

2

been invented so far and can be used, separately or in combination, allowing control over the generation of specific surface features. Description of all of these methods and combinations would go far beyond the scope of this review and only the common used methods will be described. Approaches can be subdivided into production of rough or non-organised surface structures, like chemical etching, machining, polymer demixing, self-organization, laser ablation/deposition and electrospinning, production of semi-ordered structures by anodic oxidation and production of organized textures produced by writing and replicating techniques.

Depending on the scientific question to be answered, not every experimental setup is based on ordered nano-topography. The production of non-ordered surface-features is usually less elaborate and less expensive than ordered-surface production techniques, nevertheless allowing research on nano-patterned surfaces. The most straightforward method is chemical etching as it is applicable for practically all solid materials using acids, bases or other aggressive chemicals like peroxides. Such agents will remove parts of the used material thereby introducing random topographic features. By variation of chemicals, their concentration and the time of exposure the amount of etched away material can be regulated, thereby allowing certain control over the dimensions of the produced features that can reach dimensions down to the size of few nanometers[52] and probably beyond that. Another easy to perform technique is machining, which is a mechanical introduction of scratches resembling grooves into the surface of a solid material. The size of the grooves is dependent on the force and size of the scratch inducing aperture. A third inexpensive straight forward method is polymer demixing. This phenomenon is based on phase separation of different immiscible polymer blends, like the combination of polystyrene and poly(4-bromostyrene), when mixing and using them for spin casting on silicon-wafers. The dimensions of the thus created topographies like pits, island and ribbons can be controlled by varying the polymer ratio, concentrations, solving agent, humidity and the speed of spinning, being at sizes of about 10 nm.[53] Self-organization is a "bottom-up" process, meaning that single (nano-) particles aggregate to form higher order structures under the influence of thermodynamic forces. Despite the fact that self-organization again cannot be used for the production

of ordered textures, fine-tuning of the process can induce the formation of semi-ordered rough structures in the nano-scale range.[54] Although the above described methods can be used to obtain surface features in the nano-scale range, usually also formation of structures of higher-order sizes will occur.

Laser ablation and deposition are easy-to-implement and cost effective techniques that can be exploited to change surface properties and to produce nano-size topographic features. Therefore, laser ablation makes use of irradiation of various solid material-surfaces by a high-energy pulsed laser system. The photon energy is absorbed by electrons on the material-surface, thereby inducing material heating and evaporation or formation of plasma. By adjustment of the laser-wavelength, pulse repetition and dwell time it is possible to fine-tune the dimensions of the ablated material. The ablated material can be further transferred to other materials and surfaces during the process of pulsed laser deposition, where it can form roughness- or pillar-like structures. Both techniques have been shown to be able to produce features of sub-micron and nano-sized (down to 16 nm–20 nm) dimensions.[55,56]

Another method to produce nano-fibers is the electrospinning method using various polymer materials. A polymer is mixed with a solvent to form a viscous solution (also melting can be performed to avoid solvent incorporation into the end-product), which is extruded from a needle thereby forming a droplet at an electrode. The droplet can be electrically charged leading to the formation of a cone structure arising due to an electrical field. Increase of the electrical field will result in the ejection of a polymer-jet from the cone into the direction of a grounded collector, where the fiber will randomly form a mesh-like membrane structure. By optimizing factors like polymer properties, viscosity of the solution, conductivity, electrical properties, distance between needle and collector, humidity and temperature it is possible to fine-tune the resulting product and to obtain fibers with average diameters below 100 nm.[57] Adjusting the method of collecting through a water bath allows for scaffolds of near infinite thickness.[58]

Anodic oxidation can be used to self-organize nano-tubes on titanium- or various titanium alloy- surfaces.[59,60] The substrate is brought into a fluoride-

based electrolyte-filled two-electrode electrochemical cell and connected to an anode, while platinum is used as the cathode. An increase of anodizing voltages induces a topography change of the titanium surface from porous, over particulate to nano-tube featuring at voltages higher than 10 V (reviewed by [61]). Nano-tube properties like pore diameter, wall thickness and tube height can be fine-tuned by changing the anodizing voltage, electrolyte composition and time of anodizing and feature dimensions in the range of few nanometers (diameter 22 nm–110 nm; wall thickness 7 nm–34 nm; height 200 nm–6000 nm).[61]

Writing techniques form "top-down" processes, in which direct removal of bulk material can be used for production of (semi-)ordered nano-topography surfaces. Photolithography is the progenitor of many used nano-manufacturing techniques all following the same principles (Figure 3 left). The fundamental principle for the lithography approach is the fact that some materials can be influenced to change their properties by interaction with energy from light sources. Upon exposition to light, positive resist materials change their physical state and become soluble when in contact with a developer solution. Negative resist-materials behave in the opposite way and cross-link, becoming insoluble after illumination. Dependent on the experimental setup, a wafer with a silicon-dioxide surface is coated with either a positive or negative photoresist. On top of the resist a chrome-layer photomask is placed, into which a desired pattern is reproduced. When illuminated, light hitting the metal will be reflected, whereas passing light will interact with the resist. Subsequently the mask is removed and the wafer is exposed to developer solution. The removed photoresist will expose the silicon oxide layer on the wafer that subsequently is etched away. In the last step, the remaining resist is stripped away leaving the wafer with the positive or negative silicon oxide replicate of the photomask. The wafer can be used afterwards as a template for the reproduction of nano-topographic structures into polymers (Figure 3 right), allowing a theoretically unlimited production of replicates with only one single master-wafer.

Photolithography can also be used to generate patterns without using a mask. However, comparable to microscopy, the resolution of patterns thus created is strongly dependent on the wavelength of the used light source.

Mercury lamps have been used for a long time because of their strong near-ultraviolet (UV) peaks that could be isolated and used for the production of patterns in the sub-micrometer range.[62] With the development of deep UV-light excimer lasers the use of lower wavelength light sources has pushed the resolution limit down to dimensions below 100 nm. Other examples of radiation sources that can be exploited for lithographical patterning are ions, X-rays and electrons.

One of the commonly used lithography-based techniques in life-science research is electron beam lithography (EBL) (Figure 4 left), which has been used for the generation of pits, pillars and grooves in several
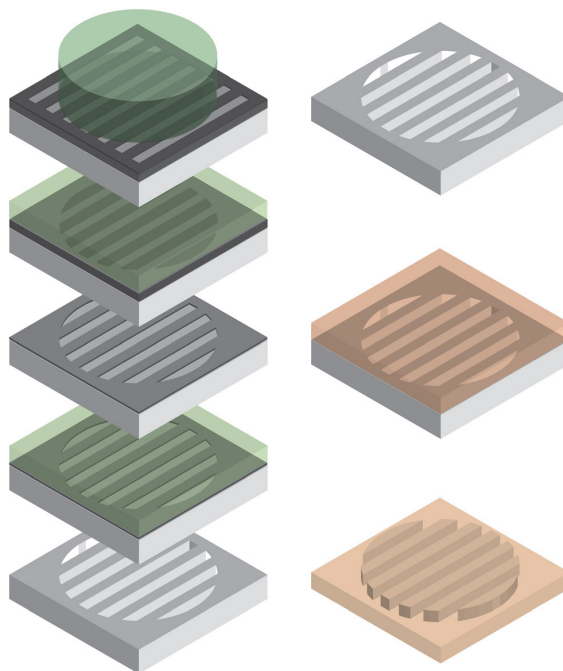
Figure 3: Photolithography production of grooved patterns and replication. Left: photolithography is based on the fact that resist material that has been exposed to light becomes soluble in development solutions. A physical mask can be used to reproduce a pattern into the resist by shielding it from light. The non-protected regions will dissolve after contact with the developer solution, thereby uncovering the underneath material, which is usually silicon. Etching and the final removing of the photoresist will remain the replicated (nano-)pattern within the substrate. Right: the patterned silicon replicate can be used as a master for reproduction of the pattern into different polymeric materials. Replication allows a cost-effective production of practically unlimited (nano-)patterned copies of one single master.

studies.[16,63-69] An electron-sensitive polymer resist, coated on a substrate, is exposed to a high-energy electron beam thereby allowing precise and maskless patterning. Although rather elaborate, timely and thus expensive, EBL allows software-controlled generation of isolated features down to a resolution of 5 nm on flat surfaces.[70] However, due to electron scattering, patterning of larger surface areas reduces the accuracy to resolutions between 30 and 40 nm.[70]

Another maskless lithographic technique to create periodic nano-structures is laser interference lithography. Additional advantages of LIL are no need for finalizing processes like etching or photoresist development, production
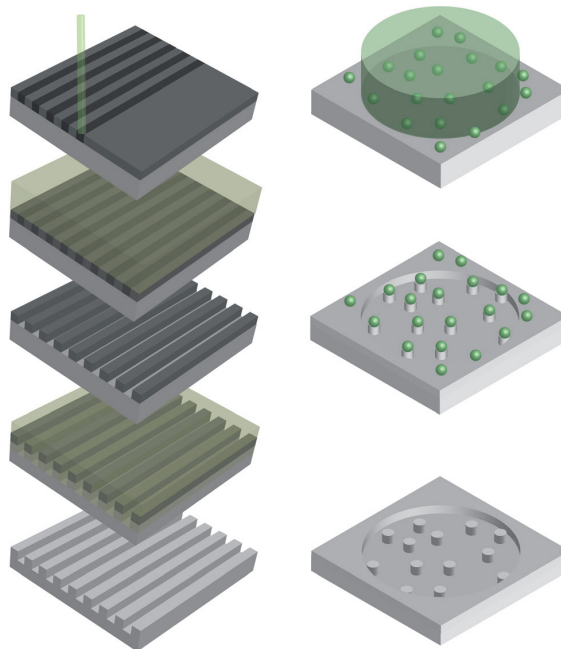
Figure 4: Lithography based nano-topography manufacturing methods. Left: electron beam lithography makes use of a high-energy electron beam to expose an electron-sensitive resist layer, thereby allowing a maskless introduction of nano-dimensional features into a substrate. The exposed area can be removed during development and the underlying area is etched away. After removing the non-exposed resist, the substrate surface will contain nano-sized features. Right: colloidal lithography makes use of randomly dispersed nano-sized colloid particles that serve as a physical barrier against ion bombardment of the substrate- surface, which will etch away the particles and the particle-surrounding area. After removing the remnants of the particles by a lift-off process the nanosized features will remain in the substrate-surface.

of nano-topographies with sizes less than 30 nm[71] on surface-materials like ceramics, metals and polymers and areas up to square meters. The patterns are produced directly onto the surface by an interference of two or more coherent light beams from one laser source. Often one laser-beam is divided into two that are recombined at the surface plane resulting in grooved structures.[72] However, use of additional laser-beams can be exploited to produce other types of topographies. While three-beam interference can be used for hexagonal dot or hole formations,[73] applying four beams will result in rectangular patterns.[71,74]

When not interested in strongly ordered textures, colloidal lithography (Figure 4 right) can produce features of about 20 nm[75–77] cost effectively and over large areas. Instead of a pre-produced rigid mask, colloidal lithography is making use of randomly dispersed colloid nano-particles. Using particles of the same dimensions allows production of surfaces having features of identical shape and height. One additional dimension of order can be controlled by the adjustment of the electrostatic particle–particle interaction during the adsorbing process, resulting in a specific distance of separation.[77] After the particles have been immobilized on the surface they and the surface material surrounding them can be etched away by using ion-beams to produce nanocolumns[78] or by film evaporation for nano-pit production.[62]

In vitro studies

Experiments showing that cells can respond to, and change their behavior dependent on the underlying surface have been performed since more than a century ago. When culturing frog embryonic cells in 1911 Ross Harrison noticed that cells showed differences in attachment, migration and morphology on different topographies.[79] That process was confirmed by Paul Weiss, who coined the term "contact guidance"[80] and by Curtis and Varde, who could prove that the cellular response indeed directly resulted from the experience of surface topography.[81]Later it was proposed that the alignment to micro-grooved patterns that was observed by Rovensky et al.[82] could be varied by manipulation of substrate-characteristics[83] and included the interaction between cellular focal adhesions and the

surface.[84] The development of micro- and nano-fabrication techniques led to an increase in experimental setups using micro- (reviewed by[85–88]) and nano-patterns for *in vitro* experiments.

The next chapter will focus on the nano-topography induced changes and control of cellular behavior, which can be measured on different levels. Since direct interaction between cells and surface are crucial for cellular function[89] factors like kinetics and force of cellular adhesion to a surface, migration, deposition of ECM-proteins and minerals, changes in gene expression, proliferation and differentiation can all be obtained and related to the experienced topography. The most commonly used topographic features are different grades of stochastic roughness, (semi-)ordered tubes, pits and pillars, and highly organized grooves.

Various experiments have shown that surface-roughness can influence cell behavior like adhesion, migration, proliferation and differentiation. Surface nano-roughness introduced by acid-etching usually is reported to have positive influence on cell activity as for example has been shown by Takeuchi et al., who found that when cultured on dual acid-etched titanium surface with a roughness average (Ra) of 110 nm rat bone-marrow derived osteoblast differentiation increased compared to machined titanium samples (Ra = 49 nm).[90] Similar observations have been made by de Oliveira et al. on acid-etched titanium surfaces when using calvaria derived osteogenic cells.[91,92] Contrary to this, rat periosteal cell-differentiation into osteoblasts, which could be seen on machined titanium surfaces (Ra = 49 nm), was inhibited on acid etched surfaces (Ra = 183 nm), while chondrocyte specific genes were activated.[93] The proliferation of periosteal cells was measured to be increased on machined surfaces compared to the acid etched substrates. However, the aspect of nano-roughness being the determining factor for specific effects on cellular behavior remains controversial, since the roughness-generating methods generate features not exclusively having dimensions in the nano-range. Moreover, when culturing human osteoblast-like cells on ordered and non-ordered surfaces with similar surface roughness Ball et al. observed that ordered patterns induced higher metabolic activity and alignment than non-ordered features.[94] This observation shows that cells do recognize patterns and necessitates studies on (semi-)organized topographies to

elucidate the underlying phenomena of cellular response.

It has been shown that acid etching can be used to generate a surface that in combination with TiO_2-sputtering can self-assemble to form nodule-like structures of similar sizes down to dimensions of about 100 nm.[95,96] Using these methods Kobo et al. have studied rat osteoblast behavior on surfaces with micro-pits, which either featured nano-nodules (diameter = 100 nm, 300 nm, 500 nm) or had no nodular features.[96] The group found osteoblast function was stimulated by the nano-nodules, which on the other hand had no effect on fibroblast function. The 300 nm nodule pattern showed the most prominent effect concerning cell attachment, differentiation and proliferation. Also, the biomechanical testing using a rat femoral model showed the advantage of the nano-nodules on the implant surface. Forces needed to push-in the implant after 2 weeks of healing were 3 times higher with the 300 nm structures than the force that was needed for the micro-pit only implants. Regarding the easy to use method and the possible benefit that could be achieved in clinics by adapting the surface production method, it would be interesting to evaluate the topography in more detail in an *in vivo* model.

Straightforward production of nanotubes by anodic oxidation improves hydrophilic properties of titanium-surfaces[97] and shows a semi-ordered nano-sized pattern,[60] which has been applied for *in vitro* studies. When culturing rat MSCs on titanium oxide nanotubes (pore size 80 nm; depth 400 nm) Popat et al. observed higher adhesion, proliferation and viability during the first 7 days of culture compared to non-oxidized titanium surfaces.[98] Moreover, cells cultured on the patterned surface demonstrated higher alkaline phosphatase (ALP) activity and 50% more matrix mineralization. Similar results have been found by Yao et al. when observing osteoblast behavior after 3 weeks of culturing[99] and Yu et al. after 2 and 3 weeks of pre-osteoblast culturing.[100] Likewise, chondrocyte functions like adhesion, synthesis of collagen, ALP activity and mineralization could be increased by nanotubes (pore 70–80 nm: depth 100–200 nm).[101] In combination with electrical stimulation, Ercan and Webster were even able to increase osteoblast long-term functions like ALP synthesis, collagen type I synthesis and mineral deposition onnanotube surfaces (pore 40–60 nm; depth 80–120 nm).[102] The last result shows that providing combinations

2

of cues to cells can result in a synergistic improvement of desired cellular functions. Nevertheless, it should be taken into account that the same combinations could also increase unwanted effects. However, the positive effect of nano-tubes on the behavior of bone forming cells and the rather easy to perform production method also on non-planar surfaces could be utilized for implant production.

When not specifically interested in the material itself, but more in the physical interaction between topographic features and cells, polymer-based techniques can be used for large array studies. When comparing osteoblast adhesion properties on poly-L-lactic acid (PLLA)/polystyrene demixed thin film blends that resulted in different nano-topographic features, Lim et al. demonstrated nano-islands (height 9–21 nm; area 0.01–0.06 µm^2) having a stronger adhesion-stimulation than nano-pits having comparable dimensions (depth 3–29 nm; area 0.01–0.18 µm^2) and smooth surfaces.[103] The same group found osteoblast-proliferation and differentiation increased on shorter islands (height 11 nm) compared to higher islands (height 38–85 nm) produced by demixing of polybromostyrene and polystyrene.[104] Cell adhesion was stronger on smaller islands, which could be seen by a prominent focal adhesion formation and cytoskeleton formation. Similar results have been obtained by Dalby et al. who performed several polystyrene–polybromostyrene demixed nano-island based studies, showing that fibroblasts and endothelial cells adhered stronger to and formed greater focal adhesions on shorter islands (13 nm) than on higher islands (33–45 nm).[53,65,105–108] On the other hand higher islands (height 160 nm; diameter 100 nm; centre-to-centre spacing 230 nm) that have been produced bycolloidal lithography have been shown to decrease adhesion and proliferation of fibroblasts[54,87,88] and osteoblasts[65] when compared to flat controls. Although cells react differently to the height of nano-islands, the density of the features seems to have less influence. When evaluating the adhesion, proliferation and growth of osteoblasts and macrophages cultured on 110 nm high islands Rice et al. have found no significant differences that have been induced by different nano-island densities (3–43%).[109] Interestingly, not only migration, proliferation and differentiation can be affected by nano-islands. When studying mouse osteoblast cells on nano-islands with dimensions between 11 and 38 nm, Hansen et

al. demonstrated increased cell stiffness when nano-topography was introduced.[110] Also, mechanosensitivity can be influenced by nano-patterns as has been shown by Salvi et al., who have studied mechanosensitivity of hMSCs on nano-islands (height 10–80 nm).[111] They observed a stronger intracellular calcium increase as a response to fluid flow on smaller islands compared to cells cultured on higher islands and proposed that topography, synergistically with mechanical cues, could increase downstream signaling and thereby proliferation and differentiation.

The height/depth of nano-features seems to be a crucial factor during the initial phase of cell–surface interaction. Cells cultured on nano-pits, which are more uniform in size than nano-islands, also show a diminished response. Several experiments have been performed by the group around Curtis et al.,[64] Dalby et al.[16,65,68,69] and Biggs et al.[63,66,67] on nano-pit structures (often in combination with nano-pillars), which have been produced by electron beam lithography in combination with dry etch techniques on silicon surfaces. By optimization of the EBL technique an area of 1 cm^2 could be produced within 1 hour and replicated into polymers such as poly(methyl methacrylate) (PMMA), polycaprolactone or polycarbonate. When cultured on nano-pits (diameter 37–120 nm; centre-to-centre spacing 100–300 nm; high 160 nm) cell spreading of fibroblasts was significantly decreased on patterned substrates compared to flat control substrates.[112] Moreover, proliferation occurred at a higher pace on the control flat surface. Similarly, when culturing human fibroblasts on PMMA nano-pillars produced by colloidal lithography(diameter 100 nm; center-to-center spacing 230 nm; height 160 nm) reduced adhesion, a less organized cytoskeleton and decreased growth was observed.[113] A strong formation of filopodia could be seen on the pitted surfaces and direct interaction with the substrates occurred on 75 and 120 nm pits.[112] Nano-pit recognition by cells seems to be a size-specific event with a lower limit of about 35 nm as has been shown for fibroblasts.[65,112] Also, osteoblasts cultured on ordered nano-pit patterns displayed decreased adhesion ability compared to smooth control surfaces.[63,66,67] Interestingly, osteoblast spreading increased when the pit-pattern became more random, although still being less when compared to plane controls[66] and differentiation-specific gene and protein expression was generally induced on nano-patterned surfaces

in MSCs and osteoblasts.[16,66]

Nano-grooved structures can be produced by various techniques and in different forms. Several factors of these topographic features can have nano-sized dimensions, such as the pitch, the height of the ridge and the depth of the groove. The grooves themselves can be rectangular, V-shaped, truncated V-shaped or U-shaped, which is often defined by the limitations of the production mechanisms. When mammalian cells are cultured on nano-grooves, it has been shown that cells do not penetrate grooves narrower than 2 μm or deeper than 500 nm, but in contrast primarily bind to the ridges.[114,115] However, a study of contact-guidance induced morphological behavior on nano-grooved (width 20–1000 nm and depth 5–350 nm) surfaces showed that fibroblasts could react and aligned to groove sizes down to 100 nm in width and 35 nm in depth.[116] Alignment to nano-grooves (Figure 5) has also been found for stem cells,[117] smooth muscle cells,[118] epithelial cells,[119] endothelial cells,[120] kidney cells[121] and fibroblasts.[116,122] Limitations of topography-induced orientation-change on nano-grooves having dimensions beneath 100 nm have also been reported
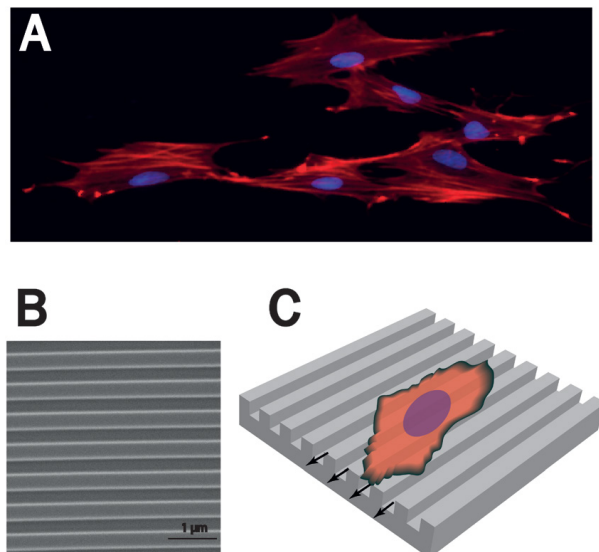

Figure 5: Cellular response to (nano-)grooved surfaces. A) When cultured on nano-grooved surfaces cells feature elongated spindle-like morphologies. B) SEM obtained image of a 500 nm pitch grooved polystyrene surface. C) The cellular elongation occurs parallel to the groove direction.

by other groups and seem to be rather cell-type specific.[19,119]

Lamers et al. have systematically studied the nano-scale topography influence on osteoblast behavior.[19] Therefore different nano-grooved patterns (pitch sizes between 40 and 2000 nm; depth 10–360 nm) have been created by EBL and LIL on silicon wafers and reproduced in cell culture plastic polystyrene (PS). Cell alignment to the grooves was evaluated and showed a significant response on grooves with dimensions down to 75 nm in width and 33 nm in depth. Interestingly, the cell-driven generated calcium phosphate deposition was found to be aligned to even smaller nano-patterns. Vinculin staining analysis showed that focal adhesions mainly resided on top of the ridges. Moreover, gene expression analysis demonstrated that osteoblast-specific genes were activated on the patterned samples, when compared to smooth controls. In a different experimental setup the group has found that also the ratio between the ridge and the groove of nano-grooved patterns can influence morphology and migration of osteoblasts.[123] It was discovered that grooves having a groove:ridge ratio of 1:3 (especially 400 nm pitch) have induced the highest migration speed and were correlating with short focal adhesions.

Yang et al. have investigated the influence of nano-grooved silicon surfaces, which were produced by EBL and dry etching, on morphology of osteoblast-like cells.[124] All of them used different nano-grooved patterns (ridge:groove 90–500 nm in width and 300 nm in depth) featured increased cell-spreading after 4 hours and cell-alignment after 24 hours of culturing compared to flat surfaces. Furthermore, the measured cell-spreading area was decreased on all nano-patterned surfaces. Interestingly, the nuclei also showed an elongated, groove-aligned morphology, which was also confirmed by other studies on nano-grooved textures.[125] The rearrangement of intracellular structures has been found also for other organelles using different substrate topographies and could be an important factor leading to observation of changes in gene expression, as reviewed by Dalby.[126,127]

An example for the ability of nano-grooves to synergistically increase cell function has been described by You et al.[128] Human mesenchymal stem (hMSCs) cells have been cultured in osteogenic medium for 8 days on nano-grooved (pitch sizes between 200 and 1200 nm; groove width between 150 and 600 nm) patterns that were produced by UV-assisted capillary

force lithography. A significantly higher osteogenic marker expression was measured on the 150 nm grooved pattern compared to cells cultured on a planar surface and grooves wider than 150 nm. In a similar experiment, hMSCs were cultured on nano-grooves (pitch 700 nm–20 µm; width 350 nm–10 µm; depth 250 nm) produced by nano-imprinting and soft lithography techniques on polydimethylsiloxane (PDMS).[125] Interestingly, the experiment also showed that the process of trans-differentiation into neuron-like cells in neuronal induction media could be significantly increased by the nano-grooved pattern. Moreover, Lee et al. were able to show that nano-grooved patterns can induce differentiation even in absence of differentiation medium.[117] When cultured on grooves (ridge:groove width 350 nm; depth 500 nm) human embryonic stem cells (hESCs) increased the expression of neuronal differentiation markers and decreased expression of markers of other lineages.

Interestingly, when combining topographic cues from nano-grooved (width 300 nm; depth 60 nm) silicon surfaces and mechanical loading cues, which were simulated by periodic stretching of the material parallel to the grooves, the alignment of osteoblast-like cells to the grooves could be overruled and resulted in anti-parallel alignment.[129] Moreover, in combination the two cues resulted in synergistic up-regulation of the genes involved in ECM generation and osteoblast differentiation. The development of such multi-factorial models can further aid in understanding the effectiveness of surface patterning and developing biomaterial surfaces with enhanced efficacy towards translation.

Considerable effort over the last decade was focused on the evaluation of behavior of primary-interest cells responding to differently patterned surfaces. Nevertheless, some groups have also studied also the interactions of materials with "fouling" components, such as various plasma proteins. Materials with different chemical properties have been investigated several times and have often been shown to have little influence on cell behavior, which could possibly be explained by adherence of ECM proteins that mask surface groups.[89,130] For this reason, surface chemical cues could be of high importance only during the first moments after implantation and in so far usually seem important to cell behavior as they could specifically attract different subsets of proteins. Once adsorbed to the implant surface, the

adhered proteins are the main interaction links between the biomaterials and cells.[131] The amount of fibronectin for example has been found to be an determining factor for cell-attachment.[132] However, nano-topographic features have been shown to interact with the cells during cell adhesion only limited in serum-free medium, but resulted in increased adhesion in combination with serum proteins.[104,130] This is an interesting finding, which allows speculations about surface design not for cells, but more prominently for proteins as primary targets as has been studied by MacDonald et al.[133] Wettability and charge of the surface will primarily determine the hydrophilic or hydrophobic properties and thus the overall charge of the proteins that will bind in first instance to the implant. For example it has been shown that albumin can block cell–implant interaction by binding strongly to hydrophobic surfaces so that it cannot be replaced by other ECM proteins.[134] On the other hand, when binding to hydrophilic groups, adsorbed albumin can indeed be replaced by ECM proteins.[134] These consequently will dictate cellular adhesion and migration processes. In particular, roughening has been shown to influence surface properties,[135] usually resulting in a higher wettability,[104,136] but its effect on protein adsorption remains controversial. Cai et al., were not able to show significant differences in amounts of adsorbed albumin and fibrinogen between titanium films displaying different degrees of nano-roughness.[137] However, experiments by other groups with nano-features have shown a roughness-dependent protein adhesion. Sela et al. have studied the adsorption of plasma proteins on titanium surfaces modified using machining, acid-etching and acid-etching followed by grit blasting.[138] It was found that most of the tested proteins preferably bound to surfaces having higher roughness. Similar results showing that roughness has a positive effect on protein adhesion have been obtained on surfaces of various other materials like tantalum,[139,140] alumina,[141] platinum[142] and polymers.[143,144] Nevertheless, the fact that some proteins are undergoing conformational change under certain of the above mentioned conditions should also be taken into account, since exposition of the organism unknown epitopes could result in adverse effects not only having an influence on cell–implant interactions, but could also provoke immune responses.

As stated above, after implantation of a biomaterial into a living system, the

2

local environment will act on and interact with the material surface. The first wave of compounds to arrive at the surface is the body fluid mainly consisting of water, proteins and ions. Since an inflammatory response is provoked by the operation, secondary to arrive in high concentrations are white blood cells of the inflammatory system. Especially neutrophils and later macrophages will accumulate at the damaged area in order to protect the tissue from pathogens and by production of cytokines to attract additional immune system cells and to stimulate tissue repair. Cells that arrive last are the ones that the surface topography is often aimed at. These cells are actively producing the tissues and have the power to integrate the implant into the host organism. It would be ideal to consider all of the factors and cell types that get in contact with the surface when designing an implantable bio-material, since the interaction with soluble factors and cells can change the long term behavior of the implant *in vivo*. The properties of the surface will mainly dictate how and which proteins and ions will bind to it, thereby determining the later interaction with cells. Depending on the topographic features and sizes it is even thinkable that due to protein accumulation cells, which should be influenced by the surface, will encounter a completely different topography when getting in contact with the implant for the first time, which can ultimately lead to a different response than observed from *in vitro* experiments.

In vivo studies

The first period after implantation of a biomaterial into a living system is crucial for further implant–host development and will determine whether the implant will be integrated successfully into the organism or whether complications will occur. Close proximity to the epithelium can lead to extrusion of the implant, meaning that epithelial cells will form a continuous layer on the border between implant and tissue, ultimately leading to a physical displacement of the implant from the organism. Sometimes it is of advantage to have a "space holder" biomaterial that is destined to be degraded temporally while being replaced by host-material. On the other hand non-degradable biomaterial can evoke the so called "foreign body response",[145] which is often the result of the immune-

system failure to remove a harmful compound by macrophages from the organism. After a period of time macrophages fuse in order to form giant cells that will produce chemo-attractants to recruit fibroblasts.[146] In turn, fibroblasts will secrete a collagen-layer and fibrous tissue capsule around the material, thereby isolating and also "camouflaging" it from the local environment[146] and allowing a physical separation of system-own from system-foreign.

Although frequently observed after biomaterial implantation, encapsulation does not necessary mean a drawback, and in fact could even serve as a scaffold for bone regeneration processes like protein adhesion and hydroxyapatite nucleation.[147] Nevertheless, generally fibrous encapsulation of bone implants is seen as a negative result, whereas direct contact of newly formed bone on the implant-surface is considered to be a positive outcome.[148]

So far the ability of implant-surface topography to influence the rate and quality of bone healing has been recognized.[149] However, before application of *in vitro* favorable nano-topographies on implant surfaces can occur for clinical purposes, the biocompatibility, which by definition is the ability of a material to perform with an appropriate host response in a specific application,[150] has to be evaluated. The difficulty to make the step from *in vitro* to *in vivo* is evident by the fact that fewer animal-studies have been published so far. One underlying reason for this could be the problematic reproduction of the nano-topographies on (concave) surfaces of implantable materials.

Only one single study can be found that uses polymer implants having an ordered nano-pattern surface topography. For this study Giavaresi et al. made use of colloidal lithography and hot embossing for polymer-reproduction of nano-scale pillars (depth 100 nm; width 120 nm) and pits (height 160 nm; width 100 nm).[151] Polymers featuring the topographic cues and a control non-structured polymer were subcutaneously introduced into rats and a histological and histomorphometric analysis was performed after 1, 4 and 12 weeks. Generally, nano-pit structures increased the fibrous capsule development and decreased vascular density, while nano-pillars increased fibroblast cellularity of the fibrous capsule and the vascular density.

Several groups have studied the *in vivo* behavior of polymer bio-composites with roughness nano-topography allowing comparison between the materials.[152,153] One interesting finding was made by Wu et al., who found poly(ether ether ketone) (PEEK), which is known to have good biomechanical properties, to perform better when used in combination with nano-TiO_2 (n-TiO_2).[152] Four different substrates were prepared, which were smooth (Ra > 0.1 μm) PEEK and n-TiO_2–PEEK, and rough (Ra = 1 μm–2.2 μm) PEEK and n-TiO_2/PEEK. Osteoblasts cultured on the n-TiO_2–PEEK nanocomposite and PEEK control substrates preferably attached to surface areas where TiO_2 was present and showed a stronger attachment capability to the rough surface of the n-TiO_2–PEEK nanocomposite. Moreover, *in vivo* results using a Beagle dog tibia model showed a twice larger bone volume around the rough n-TiO_2–PEEK nanocomposite implants compared to the rough PEEK implants. The results show a clear advantage of titanium *in vivo* and it would be very interesting to compare these implants with pure titanium implants in order to validate the benefit of such composite-products.

In titanium bone implant material, it remains more challenging to produce ordered nano-size features on large surfaces at an affordable price. For this reason all of the studies made use of non-ordered or semi-ordered topographies.

One example for semi-ordered topographies are nano-tubes, which can be produced by chemical anodization. Popat et al. produced nano-tubular titanium oxide surfaces having a pore size of 80 nm and length of 400 nm.[98] The substrates were implanted subcutaneously into rats and showed no induction of fibrous scar tissue formation, suggesting that neither the material, nor the topography are inducing adverse immune responses. The authors were concluding that nano-tube architectures on implant-surfaces could promote long-term osseointegration. A later study by Bjursten et al. confirmed this theory when they compared bone bonding capacities between grit-blasted (roughness 6 μm) and by anodization produced nanotube (pore size 80 nm and length 250 nm) titanium dioxide implant surfaces.[154] For this purpose, the implants had been implanted into the tibia of rabbits for 4 weeks, after which pull-out testing and histological analysis were performed. Histology clearly showed greater bone–implant contact area and increased bone formation resulting

2

in a nine-fold higher strength that was necessary to pull out the nano-tube implant compared with the grid-blasted implant.

A more systematic study using titanium dioxide nanotubes *in vivo* has been performed by Wang et al.[155] in order to investigate implant with bone interaction. Therefore nanotubes with different diameters (30 nm, 70 nm and 100 nm) produced by anodization and a machined control have been implanted into cranial defects in minipigs. Like in the above described study histology analysis at 4, 5 and 8 weeks after implantation showed an increased bone-to-implant contact for all nano-patterned surfaces compared to the machined control. Also osteogenesis-related gene expression of alkaline phosphatase, osterix, collagen-I and tartrate-resistant acid phosphatase was upregulated in the bone attached to the implant. In particular, the 70 nm implants showed the significantly strongest effect.

Also, interactions between soft tissues and titanium dioxide nanotube implants have been studied. Smith et al. have compared by anodization produced nanotubes (pore size 70 nm and length 250 nm) with titanium dioxide control surfaces (surface roughness less than 1 µm) after implantation into the abdominal wall of rats.[156] The group has shown that nanotube implants induced less encapsulation and lower nitric oxide production at the implant surface. The authors propose that these results may occur due to increased catalytic properties of titanium dioxide on the nanotube structure.

Another commonly used technique for the generation of nano-topography on titanium surfaces for *in vivo* studies is the deposition of discrete calcium phosphate (CaP) or hydroxyapatite (HA) particles thereby increasing the nano-scale roughness. The work of Meirelles et al.compares the effect of nano-hydroxyapatite coated titanium surfaces and nano-titanium particle coated titanium surfaces on early bone response in a rabbit tibia bone model.[157] The average surface roughness of the HA-coated implant was with about 22 nm with a feature diameter of about 30 nm slightly higher than the topography of the titanium particle-coated surface (surface roughness 10 nm and feature diameter 24 nm). Although HA is a main component of bone and could be thought to be an excellent biomimetic material,[158] the texture did not increase the bone formation compared to the nano-titanium sample.

In two studies Mendes et al. have observed osteoconduction in a rat femur bone model, where they compared nano-CaP crystal coated titanium and titanium alloy surfaces with uncoated implants.[159,160] They report that nano-CaP (size 20–100 nm) coating induced a significantly stronger osteoconduction than non-patterned implants and conclude that this effect mainly is induced by the nano-CaP increased surface topography complexity.

Similarly, it has been shown that rod-shaped nano-CaP particle (width 10–20 nm and length 100–200 nm) coated titanium had favorable effects in a rabbit tibia bone model compared to the non-coated control.[161] Summed up, the nano-CaP patterned implants enhanced the early osseointegration, since more force was needed to remove the implants from the bone tissue after 2 weeks. Moreover, the surface suppressed inflammatory responses and significantly up-regulated the expression genes involved in bone production.

Some groups have used commercially available implants, which they have modified in order to obtain the desired nano-topographic features. Palmquist et al. have compared the behavior of machined laser-modified with machined non-modified titanium alloy implants.[162] While machined surfaces showed semi-ordered valleys and ridges, laser treatment resulted in micro- and nano-sized non-ordered globular features, giving the surface higher roughness and a thicker oxide surface layer. The implants had been shaped in screw-form and implanted into rabbit cortical bone. Analysis 8 weeks after implantation showed that laser-modified implants were strongly anchored to bone on the nano-level resulting in a 270% increase in shear strength during torsion compared to the machined sample. Similar results could be obtained using the same experimental setup after a long term experiment of 6 months.[163] In an additional study the same group studied the acute inflammatory response to machined titanium surfaces with and without additional laser treatment modification.[164] Implantation occurred subcutaneously in a rat model and resulted in the observation that significantly less inflammatory cells were attracted to the laser-modified surfaces and less pro-inflammatory cytokines have been measured around the surface compared to machined controls. In a recent study, commercial laser-modified implants were evaluated after retrieval at 10 weeks of

2

healing from a human patient.[165] Similar to the above described topographic features, the implants showed globular micro- and nano-topography. The analysis of the surface–bone interaction showed strong osseointegration properties on the nano-scale level between the laser-modified titanium surface and human bone.

Conclusion

The great variety of materials used nowadays, feature forms, sizes and cell lines makes it very difficult to integrate the experimental observations for development of a general model. Nevertheless, it is possible to state that topography (in combination with other surface properties and cues) is able to affect cellular behavior on different levels and should be the topic of more systematic research *in vitro* and *in vivo*. Interestingly, many of the clinically used implant materials, which have been proven to deliver good performance in patients, feature nano-scale roughness.[166] This shows that nano-topographic features have been probably automatically selected during the trial and error process of implant development. Nevertheless, the here described studies showed that the use of ordered and semi-ordered nano-topographies provide additional possibilities for manipulation of bone-growth and could probably be used to further increase the success rate of bone implants. The ability to design surfaces on a nano-metric scale could allow us to actively communicate with single cells by using a common language in the form of topographic features that are already used by our own organisms since the beginning of multi-cellularity.

References

1. D. Hwang and H. L. Wang, Medical contraindications to implant therapy: part II: relative contraindications, Implant Dent., 2007, 16(1), 13–23
2. D. Hwang and H. L. Wang, Medical contraindications to implant therapy: part I: absolute contraindications, Implant Dent., 2006, 15(4), 353–360
3. F. P. Strietzel, et al., Smoking interferes with the prognosis of dental implant treatment: a systematic review and meta-analysis, J. Clin. Periodontol., 2007, 34(6), 523–544
4. G. Hulleberg, et al., A clinical and radiographic 13-year follow-up study of 138 Charnley hip arthroplasties in patients 50–70 years old: comparison of university hospital data and registry data, Acta Orthop., 2008, 79(5), 609–617
5. K. T. Makela, et al., Total hip arthroplasty for primary osteoarthritis in patients fifty-five years of age or older. An analysis of the Finnish arthroplasty registry, J. Bone Jt. Surg., 2008, 90(10), 2160–2170
6. G. Alsaadi, et al., Impact of local and systemic factors on the incidence of oral implant failures, up to abutment connection, J. Clin. Periodontol., 2007, 34(7), 610–617
7. O. L. Harrysson, O. Robertsson and J. F. Nayfeh, Higher cumulative revision rate of knee arthroplasties in younger patients with osteoarthritis, Clin. Orthop. Relat. Res., 2004,(421), 162–168
8. S. P. Johnsen, et al., Patient-related predictors of implant failure after primary total hip replacement in the initial, short- and long-terms. A nationwide Danish follow-up study including 36 984 patients, J. Bone Jt. Surg., Br. Vol., 2006, 88(10), 1303–1308
9. S. D. Ulrich, et al., Total hip arthroplasties: what are the reasons for revision?, Int. Orthop., 2008, 32(5), 597–604
10. Y. Ozaki, et al., Comprehensive analysis of chemotactic factors for bone marrow mesenchymal stem cells, Stem Cells Dev., 2007, 16(1), 119–129
11. A. Tokunaga, et al., PDGF receptor beta is a potent regulator of mesenchymal stromal cell function, J. Bone Miner. Res., 2008, 23(9), 1519–1528
12. R. Bielby, E. Jones and D. McGonagle, The role of mesenchymal stem cells in maintenance and repair of bone, Injury, 2007, 38(Suppl 1), S26–S32
13. K. Matsuo and N. Irie, Osteoclast–osteoblast communication, Arch. Biochem. Biophys., 2008, 473(2), 201–209
14. A. J. Engler, et al., Matrix elasticity directs stem cell lineage specification, Cell, 2006, 126(4), 677–689
15. R. McBeath, et al., Cell shape, cytoskeletal tension, and RhoA regulate stem cell lineage commitment, Dev. Cell, 2004, 6(4), 483–495
16. M. J. Dalby, et al., The control of human mesenchymal cell differentiation using nanoscale symmetry and disorder, Nat. Mater., 2007, 6(12), 997–1003
17. M. J. Buehler, Nature designs tough collagen: explaining the nanostructure of collagen fibrils, Proc. Natl. Acad. Sci. U. S. A., 2006, 103(33), 12285–12290
18. F. Grinnell and W. M. Petroll, Cell motility and mechanics in three-dimensional

collagen matrices, Annu. Rev. Cell Dev. Biol., 2010, 26, 335–361

19. E. Lamers, et al., The influence of nanoscale grooved substrates on osteoblast behavior and extracellular matrix deposition, Biomaterials, 2010, 31(12), 3307–3316

20. M. Born and E. Wolf, Principles of Optics: Electromagnetic Theory of Propagation, Interference and Diffraction of Light, 7th expanded edn, Cambridge University Press, Cambridge, New York, 1999, xxxiii, 952 p

21. D. Williams, The relationship between biomaterials and nanotechnology, Biomaterials, 2008, 29(12), 1737–1738

22. E. G. van Putten, et al., Scattering lens resolves sub-100 nm structures with visible light, Phys. Rev. Lett., 2011, 106(19), 193905

23. M. Bates, et al., Multicolor super-resolution imaging with photo-switchable fluorescent probes, Science, 2007, 317(5845), 1749–1753

24. T. A. Klar and S. W. Hell, Subdiffraction resolution in far-field fluorescence microscopy, Opt. Lett., 1999, 24(14), 954–956

25. M. J. Rust, M. Bates and X. Zhuang, Sub-diffraction-limit imaging by stochastic optical reconstruction microscopy (STORM), Nat. Methods, 2006, 3(10), 793–795

26. E. Betzig, et al., Imaging intracellular fluorescent proteins at nanometer resolution, Science, 2006, 313(5793), 1642–1645

27. G. Michler, Electron Microscopy of Polymers, Springer, 2008

28. M. Toth, et al., Nanostructure fabrication by ultra-high-resolution environmental scanning electron microscopy, Nano Lett., 2007, 7(2), 525–530

29. R. Erni, et al., Atomic-resolution imaging with a sub-50 pm electron probe, Phys. Rev. Lett., 2009, 102(9), 096101

30. C. A. Siedlecki and R. E. Marchant, Atomic force microscopy for characterization of the biomaterial interface, Biomaterials, 1998, 19(4–5), 441–454

31. J. V. Lauritsen and M. Reichling, Atomic resolution non-contact atomic force microscopy of clean metal oxide surfaces, J. Phys.: Condens. Matter, 2010, 22(26), 263001

32. H. K. Webb, et al., Roughness Parameters for Standard Description of Surface Nanoarchitecture, Scanning, 2012, 34(4), 257–63

33. V. D'Anto, et al., Evaluation of Surface Roughness of Orthodontic Wires by Means of Atomic Force Microscopy., Angle Orthod, 2012

34. A. Dugal and G. Thakur, Surface analysis of indigenous stainless steel miniplates used in facial fractures, Journal of Maxillofacial and Oral Surgery, 2010, 9(4), 403–406

35. U. Hempel, et al., Response of human bone marrow stromal cells, MG-63, and SaOS-2 to titanium-based dental implant surfaces with different topography and surface energy, Clin. Oral Implants Res., 2011

36. D. Geblinger, et al., Effects of surface microtopography on the assembly of the osteoclast resorption apparatus, J. R. Soc. Interface, 2012, 9(72), 1599–608

37. A. Ungersböck, O. Pohler and S. M. Perren, Evaluation of the soft tissue interface

at titanium implants with different surface treatments: experimental study on rabbits, Biomed. Mater. Eng., 1994, 4(4), 317–325

38. A. Chakraborty, et al., In vivo bone response and interfacial properties of titanium-alloy implant with different designs in rabbit model with time, Indian Journal of Dental Research, 2011, 22(2), 277–284

39. K. Duske, et al., Atmospheric plasma enhances wettability and cell spreading on dental implant metals, Journal of Clinical Periodontology, 2012, 39(4), 400–407

40. S. Lenhert, et al., Capillary-induced contact guidance, Langmuir, 2007, 23(20), 10216–10223

41. S. Kress, et al., Stem cell differentiation depending on different surfaces, Adv. Biochem. Eng. Biotechnol., 2012, 126, 263–283

42. H. J. Butt, B. Cappella and M. Kappl, Force measurements with the atomic force microscope: Technique, interpretation and applications, Surf. Sci. Rep., 2005, 59(1–6), 1–152

43. E. Lamers, et al., Dynamic cell adhesion and migration on nanoscale grooved substrates, Eur. Cell Mater., 2012, 23, 182–193; discussion 193–4.

44. E. J. Thoreson, J. Martin and N. A. Burnham, The role of few-asperity contacts in adhesion, J. Colloid Interface Sci., 2006, 298(1), 94–101

45. G. Altankov, K. Richau and T. Groth, The role of surface zeta potential and substratum chemistry for regulation of dermal fibroblasts interaction, Materialwiss. Werkstofftech., 2003, 34(12), 1120–1128

46. K. M. Jan and S. Chien, Role of surface electric charge in red blood cell interactions, J. Gen. Physiol., 1973, 61(5), 638–654

47. A. B. García, et al., Zeta potential as a tool to characterize plasma oxidation of carbon fibers, Journal of Colloid and Interface Science, 1997, 192(2), 363–367

48. J. P. Szaflarski, et al., Constraint-induced aphasia therapy stimulates language recovery in patients with chronic aphasia after ischemic stroke, Med. Sci. Monit., 2008, 14(5), CR243–CR250

49. M. Stamm, Polymer Surfaces and Interfaces, Springer, 2008

50. M. L. Kraft, et al., Phase separation of lipid membranes analyzed with high-resolution secondary ion mass spectrometry, Science, 2006, 313(5795), 1948–1951

51. G. E. Moore, Cramming more components onto integrated circuits (Reprinted from Electronics, pg 114–117, April 19, 1965), Proc. IEEE, 1998, 86(1), 82–85

52. Y. W. Fan, et al., Culture of neural cells on silicon wafers with nano-scale surface topograph, J. Neurosci. Methods, 2002, 120(1), 17–23

53. M. J. Dalby, et al., In vitro reaction of endothelial cells to polymer demixed nanotopography, Biomaterials, 2002, 23(14), 2945–2954

54. G. M. Whitesides and B. Grzybowski, Self-assembly at all scales, Science, 2002, 295(5564), 2418–2421

55. A. Tavangar, B. Tan and K. Venkatakrishnan, Synthesis of bio-functionalized three-dimensional titania nanofibrous structures using femtosecond laser ablation, Acta Biomater., 2011, 7(6), 2726–2732

2

56. M. Fusi, et al., Titanium oxide nanostructured films by reactive pulsed laser deposition, Appl. Surf. Sci., 2009, 255(10), 5334–5337

57. L. Li and Y. L. Hsieh, Chitosan bicomponent nanofibers and nanoporous fibers, Carbohydr. Res., 2006, 341(3), 374–381

58. S. H. Shang, et al., The Effect of Electrospun Fibre Alignment on the Behaviour of Rat Periodontal Ligament Cells, Eur. Cells Mater., 2010, 19, 180–192

59. V. Zwilling, et al., Structure and physicochemistry of anodic oxide films on titanium and TA6V alloy, Surf. Interface Anal., 1999, 27(7), 629–637

60. D. Gong, et al., Titanium oxide nanotube arrays prepared by anodic oxidation, J. Mater. Res., 2001, 16(12), 3331–3334

61. G. K. Mor, et al., A review on highly ordered, vertically oriented TiO2 nanotube arrays: Fabrication, material properties, and solar energy applications, Sol. Energy Mater. Sol. Cells, 2006, 90(14), 2011–2075

62. J. J. Norman and T. A. Desai, Methods for fabrication of nanoscale topography for tissue engineering scaffolds, Ann. Biomed. Eng., 2006, 34(1), 89–101

63. M. J. Biggs, et al., Regulation of implant surface cell adhesion: characterization and quantification of S-phase primary osteoblast adhesions on biomimetic nanoscale substrates, J. Orthop. Res., 2007, 25(2), 273–282

64. A. S. Curtis, et al., Substratum nanotopography and the adhesion of biological cells. Are symmetry or regularity of nanotopography important?, Biophys. Chem., 2001, 94(3), 275–283

65. M. J. Dalby, et al., Investigating the limits of filopodial sensing: a brief report using SEM to image the interaction between 10 nm high nano-topography and fibroblast filopodia, Cell Biol. Int., 2004, 28(3), 229–236

66. M. J. Biggs, et al., Interactions with nanoscale topography: adhesion quantification and signal transduction in cells of osteogenic and multipotent lineage, J. Biomed. Mater. Res. A., 2009, 91(1), 195–208

67. M. J. Biggs, et al., The effects of nanoscale pits on primary human osteoblast adhesion formation and cellular spreading, J. Mater. Sci.: Mater. Med., 2007, 18(2), 399–404

68. M. J. Dalby, N. Gadegaard and C. D. Wilkinson, The response of fibroblasts to hexagonal nanotopography fabricated by electron beam lithography, J. Biomed. Mater. Res. A., 2008, 84(4), 973–979

69. M. J. Dalby, et al., Osteoprogenitor response to defined topographies with nanoscale depths, Biomaterials, 2006, 27(8), 1306–1315

70. C. Vieu, et al., Electron beam lithography: Resolution limits and applications, Appl. Surf. Sci., 2000, 164(1–4), 111–117

71. C. Tan, et al., Ordered nanostructures written directly by laser interference, Nanotechnology, 2009, 20(12), 125303

72. D. W. Hamilton, et al., Migration of periodontal ligament fibroblasts on nanometric topographical patterns: influence of filopodia and focal adhesions on contact guidance, PLoS One, 2010, 5(12), e15129

73. J. de Boor, et al., Three-beam interference lithography: upgrading a Lloyd's interferometer for single-exposure hexagonal patterning, Opt. Lett., 2009, 34(12), 1783–1785

74. K. V. Sreekanth, J. K. Chua and V. M. Murukeshan, Interferometric lithography for nanoscale feature patterning: a comparative analysis between laser interference, evanescent wave interference, and surface plasmon interference, Appl. Opt., 2010, 49(35), 6710–6717

75. M. A. Wood, Colloidal lithography and current fabrication techniques producing in-plane nanotopography for biological applications, J. R. Soc. Interface, 2007, 4(12), 1–17

76. M. A. Wood, M. Riehle and C. D. W. Wilkinson, Patterning colloidal nanotopographies, Nanotechnology, 2002, 13(5), 605–609

77. P. Hanarp, et al., Control of nanoparticle film structure for colloidal lithography, Colloids Surf., A, 2003, 214(1–3), 23–36

78. M. J. Dalby, et al., Changes in fibroblast morphology in response to nano-columns produced by colloidal lithography, Biomaterials, 2004, 25(23), 5415–5422

79. R. G. Harrison, On the stereotropism of embryonic cells, Science, 1911, 34(870), 279–281

80. P. Weiss, Experiments on cell and axon orientation in vitro; the role of colloidal exudates in tissue organization, J. Exp. Zool., 1945, 100, 353–386

81. A. S. Curtis and M. Varde, Control of cell behavior: topological factors, J. Natl. Cancer Inst., 1964, 33, 15–26

82. Y. A. Rovensky, I. L. Slavnaja and J. M. Vasiliev, Behaviour of fibroblast-like cells on grooved surfaces, Exp. Cell Res., 1971, 65(1), 193–201

83. G. A. Dunn and J. P. Heath, A new hypothesis of contact guidance in tissue cells, Exp. Cell Res., 1976, 101(1), 1–14

84. P. T. Ohara and R. C. Buck, Contact guidance in vitro. A light, transmission, and scanning electron microscopic study, Exp. Cell Res., 1979, 121(2), 235–249

85. A. F. von Recum and T. G. van Kooten, The influence of micro-topography on cellular response and the implications for silicone implants, J. Biomater. Sci., Polym. Ed., 1995, 7(2), 181–198

86. A. Curtis and C. Wilkinson, Topographical control of cells, Biomaterials, 1997, 18(24), 1573–1583

87. X. F. Walboomers and J. A. Jansen, Cell and tissue behavior on micro-grooved surfaces, Odontology, 2001, 89(1), 2–11

88. R. G. Flemming, et al., Effects of synthetic micro- and nano-structured surfaces on cell behavior, Biomaterials, 1999, 20(6), 573–588

89. C. C. Berry, et al., Human fibroblast and human bone marrow cell response to lithographically nanopatterned adhesive domains on protein rejecting substrates, IEEE Trans. NanoBiosci., 2007, 6(3), 201–209

90. K. Takeuchi, et al., Enhanced intrinsic biomechanical properties of osteoblastic mineralized tissue on roughened titanium surface, J. Biomed. Mater. Res. A., 2005, 72(3), 296–305

2

91. P. T. de Oliveira and A. Nanci, Nanotexturing of titanium-based surfaces upregulates expression of bone sialoprotein and osteopontin by cultured osteogenic cells, Biomaterials, 2004, 25(3), 403–413

92. P. T. de Oliveira, et al., Enhancement of in vitro osteogenesis on titanium by chemically produced nanotopography, J. Biomed. Mater. Res. A., 2007, 80(3), 554–564

93. K. Kubo, et al., Microtopography of titanium suppresses osteoblastic differentiation but enhances chondroblastic differentiation of rat femoral periosteum-derived cells, J. Biomed. Mater. Res. A, 2008, 87(2), 380–391

94. M. Ball, et al., The effect of different surface morphology and roughness on osteoblast-like cells, J. Biomed. Mater. Res. A, 2008, 86(3), 637–647

95. T. Ogawa, et al., Ti nano-nodular structuring for bone integration and regeneration, J. Dent. Res., 2008, 87(8), 751–756

96. K. Kubo, et al., Cellular behavior on TiO2 nanonodular structures in a micro-to-nanoscale hierarchy model, Biomaterials, 2009, 30(29), 5319–5329

97. I. H. Bae, et al., Anodic oxidized nanotubular titanium implants enhance bone morphogenetic protein-2 delivery, J. Biomed. Mater. Res. B: Appl. Biomater., 2010, 93(2), 484–491

98. K. C. Popat, et al., Influence of engineered titania nanotubular surfaces on bone cells, Biomaterials, 2007, 28(21), 3188–3197

99. C. Yao, E. B. Slamovich and T. J. Webster, Enhanced osteoblast functions on anodized titanium with nanotube-like structures, J. Biomed. Mater. Res. A., 2008, 85(1), 157–166

100. W. Q. Yu, et al., In vitro behavior of MC3T3-E1 preosteoblast with different annealing temperature titania nanotubes, Oral Dis., 2010, 16(7), 624–630

101. K. Burns, C. Yao and T. J. Webster, Increased chondrocyte adhesion on nanotubular anodized titanium, J. Biomed. Mater. Res. A., 2009, 88(3), 561–568

102. B. Ercan and T. J. Webster, The effect of biphasic electrical stimulation on osteoblast function at anodized nanotubular titanium surfaces, Biomaterials, 2010, 31(13), 3684–3693

103. J. Y. Lim, et al., Osteoblast adhesion on poly(L-lactic acid)/polystyrene demixed thin film blends: effect of nanotopography, surface chemistry, and wettability, Biomacromolecules, 2005, 6(6), 3319–3327

104. J. Y. Lim, et al., Human foetal osteoblastic cell response to polymer-demixed nanotopographic interfaces, J. R. Soc. Interface, 2005, 2(2), 97–108

105. M. J. Dalby, et al., Fibroblast reaction to island topography: changes in cytoskeleton and morphology with time, Biomaterials, 2003, 24(6), 927–935

106. M. J. Dalby, et al., Interactions of human blood and tissue cell types with 95-nm-high nanotopography, IEEE Trans. NanoBiosci., 2002, 1(1), 18–23

107. M. J. Dalby, et al., Polymer-demixed nanotopography: control of fibroblast spreading and proliferation, Tissue Eng., 2002, 8(6), 1099–1108

108. M. J. Dalby, et al., Rapid fibroblast adhesion to 27 nm high polymer demixed nano-topography, Biomaterials, 2004, 25(1), 77–83

109. J. M. Rice, et al., Quantitative assessment of the response of primary derived human osteoblasts and macrophages to a range of nanotopography surfaces in a single culture model in vitro, Biomaterials, 2003, 24(26), 4799–4818

110. J. C. Hansen, et al., Effect of surface nanoscale topography on elastic modulus of individual osteoblastic cells as determined by atomic force microscopy, J. Biomech., 2007, 40(13), 2865–2871

111. J. D. Salvi, J. Y. Lim and H. J. Donahue, Increased mechanosensitivity of cells cultured on nanotopographies, J. Biomech., 2010, 43(15), 3058–3062

112. M. J. Dalby, et al., Investigating filopodia sensing using arrays of defined nano-pits down to 35 nm diameter in size, Int. J. Biochem. Cell Biol., 2004, 36(10), 2005–2015

113. M. J. Dalby, et al., Fibroblast response to a controlled nanoenvironment produced by colloidal lithography, J. Biomed. Mater. Res., 2004, 69(2), 314–322

114. E. T. den Braber, et al., Quantitative analysis of fibroblast morphology on microgrooved surfaces with various groove and ridge dimensions, Biomaterials, 1996, 17(21), 2037–2044

115. X. F. Walboomers, et al., Attachment of fibroblasts on smooth and microgrooved polystyrene, J. Biomed. Mater. Res., 1999, 46(2), 212–220

116. W. A. Loesberg, et al., The threshold at which substrate nanogroove dimensions may influence fibroblast alignment and adhesion, Biomaterials, 2007, 28(27), 3944–3951

117. M. R. Lee, et al., Direct differentiation of human embryonic stem cells into selective neurons on nanoscale ridge/groove pattern arrays, Biomaterials, 2010, 31(15), 4360–4366

118. W. Hu, et al., Effects of nanoimprinted patterns in tissue-culture polystyrene on cell behavior, J. Vac. Sci. Technol., B, 2005, 23(6), 2984–2989

119. A. I. Teixeira, et al., Epithelial contact guidance on well-defined micro- and nanostructured substrates, J. Cell Sci., 2003, 116(Pt 10), 1881–1892

120. C. J. Bettinger, et al., Enhancement of in vitro capillary tube formation by substrate nanotopography, Adv. Mater., 2008, 20(1), 99–103

121. E. Rebollar, et al., Proliferation of aligned mammalian cells on laser-nanostructured polystyrene, Biomaterials, 2008, 29(12), 1796–1806

122. C. H. Choi, et al., Cell interaction with three-dimensional sharp-tip nanotopography, Biomaterials, 2007, 28(9), 1672–1679

123. E. Lamers, et al., The influence of nanoscale topographical cues on initial osteoblast morphology and migration, Eur. Cell Mater., 2010, 20, 329–343

124. J. Y. Yang, et al., Quantitative analysis of osteoblast-like cells (MG63) morphology on nanogrooved substrata with various groove and ridge dimensions, J. Biomed. Mater. Res., Part A, 2009, 90A(3), 629–640

125. E. K. F. Yim, S. W. Pang and K. W. Leong, Synthetic nanostructures inducing differentiation of human mesenchymal stem cells into neuronal lineage, Exp. Cell Res., 2007, 313(9), 1820–1829

126. M. J. Dalby, Topographically induced direct cell mechanotransduction, Med. Eng. Phys., 2005, 27(9), 730–742

2

127. M. J. Dalby, Cellular response to low adhesion nanotopographies, Int. J. Nanomedicine, 2007, 2(3), 373–381

128. M. H. You, et al., Synergistically enhanced osteogenic differentiation of human mesenchymal stem cells by culture on nanostructured surfaces with induction media, Biomacromolecules, 2010, 11(7), 1856–1862

129. L. Prodanov, et al., The interaction between nanoscale surface features and mechanical loading and its effect on osteoblast-like cells behavior, Biomaterials, 2010, 31(30), 7758–7765

130. T. J. Webster, et al., Specific proteins mediate enhanced osteoblast adhesion on nanophase ceramics, J. Biomed. Mater. Res., 2000, 51(3), 475–483

131. T. Brevig, et al., The recognition of adsorbed and denatured proteins of different topographies by beta2 integrins and effects on leukocyte adhesion and activation, Biomaterials, 2005, 26(16), 3039–3053

132. Y. Z. Yang, R. Cavin and J. L. Ong, Protein adsorption on titanium surfaces and their effect on osteoblast attachment, J. Biomed. Mater. Res., 2003, 67A(1), 344–349

133. D. E. MacDonald, et al., Thermal and chemical modification of titanium-aluminum-vanadium implant materials: effects on surface properties, glycoprotein adsorption, and MG63 cell attachment, Biomaterials, 2004, 25(16), 3135–3146

134. Y. Arima and H. Iwata, Effect of wettability and surface functional groups on protein adsorption and cell adhesion using well-defined mixed self-assembled monolayers, Biomaterials, 2007, 28(20), 3074–3082

135. L. Ponsonnet, et al., Relationship between surface properties (roughness, wettability) of titanium and titanium alloys and cell behaviour, Mater. Sci. Eng., C, 2003, 23(4), 551–560

136. F. Rupp, et al., Roughness induced dynamic changes of wettability of acid etched titanium implant modifications, Biomaterials, 2004, 25(7–8), 1429–1438

137. K. Cai, J. Bossert and K. D. Jandt, Does the nanometre scale topography of titanium influence protein adsorption and cell proliferation?, Colloids Surf., B, 2006, 49(2), 136–144

138. M. N. Sela, et al., Adsorption of human plasma proteins to modified titanium surfaces, Clin. Oral Implants Res., 2007, 18(5), 630–638

139. K. Rechendorff, et al., Enhancement of protein adsorption induced by surface roughness, Langmuir, 2006, 22(26), 10885–8

140. M. B. Hovgaard, et al., Fibronectin adsorption on tantalum: the influence of nanoroughness, J. Phys. Chem. B, 2008, 112(28), 8241–8249

141. T. J. Webster, et al., Mechanisms of enhanced osteoblast adhesion on nanophase alumina involve vitronectin, Tissue Eng., 2001, 7(3), 291–301

142. A. Dolatshahi-Pirouz, et al., Bovine serum albumin adsorption on nano-rough platinum surfaces studied by QCM-D, Colloids Surf., B, 2008, 66(1), 53–59

143. X. Wang, et al., Influence of physicochemical properties of laser-modified polystyrene on bovine serum albumin adsorption and rat C6 glioma cell behavior, J. Biomed. Mater. Res. A, 2006, 78(4), 746–754

144. D. V. Nicolau, et al., Protein immobilisation on micro/nanostructures fabricated by laser microablation, Biosens. Bioelectron., 2010, 26(4), 1337–1345

145. J. M. Anderson, A. Rodriguez and D. T. Chang, Foreign body reaction to biomaterials, Semin. Immunol., 2008, 20(2), 86–100

146. J. M. Anderson, Biological responses to materials, Annu. Rev. Mater. Res., 2001, 31, 81–110

147. B. D. Ratner, Replacing and renewing: synthetic materials, biomimetics, and tissue engineering in implant dentistry, J. Dent. Educ., 2001, 65(12), 1340–1347

148. T. Albrektsson and L. Sennerby, Direct bone anchorage of oral implants: clinical and experimental considerations of the concept of osseointegration, Int. J. Prosthodont., 1990, 3(1), 30–41

149. L. Le Guehennec, et al., Surface treatments of titanium dental implants for rapid osseointegration, Dent. Mater., 2007, 23(7), 844–854

150. D. F. Williams, The Williams Dictionary of Biomaterials, Liverpool University Press, Liverpool, 1999, xvii, 343 p

151. G. Giavaresi, et al., In vitro and in vivo response to nanotopographically-modified surfaces of poly(3-hydroxybutyrate-co-3-hydroxyvalerate) and polycaprolactone, J. Biomater. Sci., Polym. Ed., 2006, 17(12), 1405–1423

152. X. Wu, et al., Nano-TiO2/PEEK bioactive composite as a bone substitute material: in vitro and in vivo studies, Int. J. Nanomedicine, 2012, 7, 1215–1225

153. H. Liu and T. J. Webster, Ceramic/polymer nanocomposites with tunable drug delivery capability at specific disease sites, J. Biomed. Mater. Res. A, 2010, 93(3), 1180–1192

154. L. M. Bjursten, et al., Titanium dioxide nanotubes enhance bone bonding in vivo, J. Biomed. Mater. Res. A, 2010, 92(3), 1218–1224

155. N. Wang, et al., Effects of TiO2 nanotubes with different diameters on gene expression and osseointegration of implants in minipigs, Biomaterials, 2011, 32(29), 6900–6911

156. G. C. Smith, et al., Soft tissue response to titanium dioxide nanotube modified implants, Acta Biomater., 2011, 7(8), 3209–3215

157. L. Meirelles, et al., Effect of hydroxyapatite and titania nanostructures on early in vivo bone response, Clin. Implant Dent. Relat. Res., 2008, 10(4), 245–254

158. S. S. Liao, et al., Hierarchically biomimetic bone scaffold materials: nano-HA/collagen/PLA composite, J. Biomed. Mater. Res., 2004, 69(2), 158–165

159. V. C. Mendes, R. Moineddin and J. E. Davies, Discrete calcium phosphate nanocrystalline deposition enhances osteoconduction on titanium-based implant surfaces, J. Biomed. Mater. Res. A, 2009, 90(2), 577–585

160. V. C. Mendes, R. Moineddin and J. E. Davies, The effect of discrete calcium phosphate nanocrystals on bone-bonding to titanium surfaces, Biomaterials, 2007, 28(32), 4748–4755

161. R. Jimbo, et al., Genetic responses to nanostructured calcium-phosphate-coated implants, J. Dent. Res., 2011, 90(12), 1422–1427

2

162. A. Palmquist, et al., Biomechanical, histological, and ultrastructural analyses of laser micro- and nano-structured titanium alloy implants: a study in rabbit, J. Biomed. Mater. Res. A, 2010, 92(4), 1476–1486

163. A. Palmquist, et al., Biomechanical, histological and ultrastructural analyses of laser micro- and nano-structured titanium implant after 6 months in rabbit, J. Biomed. Mater. Res. B: Appl. Biomater., 2011, 97(2), 289–298

164. A. Palmquist, et al., Acute inflammatory response to laser-induced micro- and nano-sized titanium surface features, Clin. Implant Dent. Relat. Res., 2011

165. A. Palmquist, et al., Bone-titanium oxide interface in humans revealed by transmission electron microscopy and electron tomography, J. R. Soc. Interface, 2012, 9(67), 396–400

166. L. M. Svanborg, M. Andersson and A. Wennerberg, Surface characterization of commercial oral implants on the nanometer level, J. Biomed. Mater. Res. B: Appl. Biomater., 2010, 92(2), 462–469

3

Nanogrooved Surface-Patterns induce cellular organization and axonal outgrowth in neuron-like PC12-Cells

Alexey Klymov, Charlotte T Rodrigues Neves, Joost te Riet, Martijn J H Agterberg, Emmanuel A M Mylanus, Ad F M Snik, John A Jansen, X Frank Walboomers

Introduction

Congenital or acquired severe to profound sensorineural deafness, which results from defective loss or damage of sensory hair cells, is preferentially treated by placement of a cochlear implant (CI). More than 324000 patients worldwide have received such a CI to date.[1] The implants are bypassing the damaged hair cells, allowing direct stimulation of the spiral ganglion cells (SGCs). Although the quality of the implants and thereby the patient perception- and understanding-ability improved during the last decade, CI-based hearing still has substantial shortcomings. High fidelity hearing might be limited due to the poor spatial resolution on the interface between the electrode and SGCs. Sounds are perceived by separated stimulation of approximately 30000 neurones of the auditory nerve in a healthy situation, while only 4 – 8 broad range areas of SGCs can be triggered by up to 22 electrodes in the most recent devices.[2] Transfer of temporal information is difficult in this situation leading to limited possibilities for speech recognition-in-noise and music appreciation. A possible explanation for the rather crude stimulation of the SGCs in limited filter bands is the relatively large distance of about 150 µm between the electrode contacts, situated in the scala tympani of the cochlea, and the SGCs in Rosenthal's canal. This results in an interaction of electrical stimuli and thereby in reduction of resolution. Approximation of the electrodes closer to the target cells has shown an improvement in implant performance,[3] allowing speculation about a possible CI-optimization based on direct electrode-SGC contact. Furthermore, *in vivo* experiments and post mortem explantation studies, have shown the formation of fibrous tissue and occasionally even bone on the electrode surface, which can also affect the interaction between the electrode and SGCs.[4-7] A direct electrode-SGC contact might also reduce this irritating factor.

Manipulation of the electrode surface topography in combination with delivery of neurotrophins,[8-10] may be a possible solution for the reduction of fibrotic tissue formation and consequently a more direct electrode-auditory nerve contact.[11] Moreover this combination can also be a method for a spatially designed interaction between the implant and the SGCs. The last would allow (1) the achievement of a higher resolution in stimulation

3

and therefore higher fidelity of patient-experienced perception, and (2) an optimization of the electrode surface that could provide increased affinity for the outgrowing neurons towards the electrode. Studies in other biomedical device applications have shown that especially grooves with micro- and nanodimensions are able to control cell-body organization and alignment of different cell types,[12] making such patterns interesting for the utilization on CI electrode-surfaces. It should be taken into account that the introduced electrode length is highly limited (20 – 30 mm) and relative to damage that is induced in the patient ears.[13] As in an ideal situation up to 30000 cells have to be stimulated by the electrode surface, only nanosized patterns may deliver the necessary separation of signal transduction. Moreover, microgrooves may not be sufficient for control of orientation of outgrowing axons, which have width dimensions in the submicron range[14] and would need contact guidance by templates of comparable size. The efforts of the semi-conductor industry have led to development of powerful techniques that allow design and structural manipulation of various material-surfaces effectively down to sizes of only few nanometers. Interestingly, several *in vitro* studies have shown already small-scale nanotopographical features to have enormous influence on cellular behaviour, such as proliferation, differentiation, gene expression and migration.[12] However, the effect that a topography can have on the cell is strongly cell-type dependent. Furthermore, the topography might interact with neurotrophins that stimulate neurite outgrow.

A mechanism by which microgrooves direct neurite organization strongly depends on the axonal localization inside the groove. Due to cellular dimensions these mechanisms may not be effective on nanogrooved surfaces, as cells including the neurites would always be located on top of the grooves. It is not known to which extent neuronal cells can sense and more importantly can be influenced in their behaviour by nanotopographies and what would be the smallest topography on which a recognizable effect could be observed. We hypothesize that a threshold exists for pattern recognition of neuronal cells and that the textures will have an effect on the outgrowth length of the axons. For the current study we made use of a polystyrene culturing surface that featured 5 different nanosized grooved surface topographies and a smooth control. The surfaces were used for

cell-culture of PC12 neuron-like cells during a period of 7 days, in which the cells were treated with nerve growth factor allowing differentiation and axon formation. After culture the cells were evaluated in terms of overall pattern-size recognition and subsequent organization (measured as pattern-induced cell and axon alignment) and the affinity for the surface pattern (measured as axon outgrowth).

Material and Methods
Substrate production

A lithography-based process was utilized to produce five 4″ silicon wafers featuring different grooved topographies as described before.[15] In short, silicon wafers were spin-coated with a tri-layer resist (bottom antireflective coating, photosensitive resist and a top anti-reflective coating). A laser interference setup based on the Lloyd's interferometer method was used with a laser of 266 nm wavelength. By adjustment of the incidence angles (between 7.6° and 62.4°) linear patterns were introduced into the resist having different dimensions, with pitches between two grooves varying between 150 nm and 1000nm. In a two-step process the lines were reproduced into the silicon wafer. First, the bottom antireflective coating was removed by oxygen plasma etching, revealing the silicon surface. Second, the grooves were etched into the silicon surface by $SF_6:O_2$ gas and silicon reactive ion etching.

 The produced grooved wafers, as well as one smooth wafer, were separated into sextant pieces and glued together resulting in a multi-patterned master that was further used to replicate the topographies into tissue culture plastic polystyrene (Acros, Geel, Belgium, Figure 1). Polystyrene was dissolved in chloroform in a proportion of 1:6 and 5 ml of the solution were used for solvent casting of a Ø6 cm replicate. For sterilization and wettability increase the replicates were treated by radiofrequency glow-discharge (Harrick, Ossining, USA) for a period of 5 minutes in Argon gas at an atmospheric pressure of about 10^{-2} mbar. Thereafter, the polystyrene substrates were directly used for cell culture experiments.

Atomic force microscopy (AFM)

For quality control of the surface topographies atomic force microscopy (AFM) was utilized. The atomic force microscope (Bioscope Catalyst, Bruker, Santa Barbara, CA, USA) was used in tapping mode with a 118 μm long silicon cantilever (NW-AR5T-NCHR, NanoWorldAG, Wetzlar, Germany) having average nominal resonant frequencies of 317 kHz and average nominal spring constants of 30 N/m. This type of AFM probe has a high aspect ratio (7:1) portion of the tip with a nominal length of >2 μm and a half-cone angle of <5°. Nominal radius of curvature of the AFM probe tip was less than 10 nm. Height images of each field/sample were captured in ambient air at 50% humidity at a tapping frequency of 266.4 kHz. The analyzed field was scanned at a rate of 0.5 Hz and 512 scanning lines.
 The AFM images were analysed and processed with NanoScope Analysis Software 1.40 (Bruker). For illustration purposes noise has been removed by use of the median filter (Median order 11x11).

Cell culture

Rat pheochromocytoma derived cell line (PC12) was maintained in proliferation medium (Dulbecco's Modified Eagle Glutamax Medium (Gibco/Life technologies, Breda, the Netherlands) supplemented with 7% horse serum (Gibco), 7% fetal calf serum (FCS; Sigma; F7524, Taukirchen, Germany), penicillin (100 U/mL) and streptomycin (10 μg/mL) (Gibco)). The cells were allowed to proliferate at 37 °C and 5% CO_2 in a humidified incubator for 7 days. At a confluence of about 80% the cells were trypsinized (trypsin/EDTA; 0.25%w/v trypsin, 0.02% EDTA; Sigma) and seeded onto textured substrates (1000 cells / cm² for microscopy-based analysis and 10000 cells / cm² for cell density analysis). Cells were maintained for 24 hours in proliferation medium to allow adherence to the substrates. After 24 hours the medium was replaced with differentiation medium (proliferation medium supplemented with 100 ng/ml nerve growth factor (NGF, 50385, Gibco)). After three days of cell culture, the substrates covered with cells were used for cell-density quantification. After one week, neural cell interaction with the surfaces, i.e. alignment of cell-bodies and axons to the grooves, and axonal outgrowth were assessed using scanning electron microscopy (SEM) and bright field microscopy.

Cell Density

To study the influence of the different topographies on cell density, substrates with a diameter of Ø1.2 cm were placed into 24-wells plates and cells were seeded with a density of 10000 cells / cm². Upon confluence, substrates with homogeneous cell-monolayers were carefully washed with PBS and placed into empty plates, where the cells have been lysed in 1 mL distilled water during two freeze-thaw processes. A dsDNA specific dye was used to quantify the DNA in solution by Quantifluor (Promega Benelux, Leiden, The Netherlands) fluorometric assay, according to the manufacturers specifications. Statistical analysis was performed by using Origin 8.6. Differences among groups were determined by one-way Analysis of Variance (ANOVA), with a Bonferroni post test. A p-value smaller than 0.05 was considered a significant difference.

Scanning Electron Microscopy (SEM)

Cells were washed in PBS and fixed for 5 minutes in 2% glutaraldehyde in 0.1 M sodium-cacodylate and washed for 5 minutes in 0.1 M sodium-cacodylate. Subsequently, cells were dehydrated in a graded series of ethanol (5 minutes in 70%, 80%, 90%, 96%, 100% ethanol and finally 100% water free ethanol) and dried to air in tetramethylsilane. The specimens were sputter-coated with a gold layer (10nm) and cell-surface interaction was examined by scanning electron microscopy (JEOL 6310, Jeol, Japan).

Bright Field microscopy and Image analysis

Cell were examined without further fixation by taking micrographs of cells (n ≥ 100 cells per pattern) with a bright field Zeiss Z1 microscope (Jena, Germany). Orientation measurements were performed on the neuronal cell bodies (soma). Additionally, the orientation and the length of axons were measured. The images were analysed with Image Pro Plus 6.0 (Media Cybernetics). Inclusion criteria for cells were: the cell-bodies/axons were lying apart from other cells, which made the contours of the cells clear and excluded the effects of neighbouring cells. Statistical analysis was performed by using Origin 8.6. Differences among groups were determined by one-way Analysis of Variance (ANOVA), with a Bonferroni post-test. A p-value smaller than 0.05 was considered a significant difference.

Results

Surface analysis

SEM and AFM analysis showed a good reproduction quality of patterned silicon masters into PS (Figure 1). The depth of the grooves increased with the pitch size. The dimensions of the grooved patterns as measured by AFM are summarized in Table 1.

Cell Density

After 3 days the PC12 cells reached a confluent monolayer state on all tested patterns. The results of DNA quantification are shown in Figure 2. There were no significant differences between the groups.

Cell-surface interaction

After seven days of culture, PC12 cells displayed typical neuronal characteristics, namely a prominent cell soma with (in most cases) at least one outgrowing axon (as shown by light microscopy and SEM in Figure 3 and 4). On smooth surfaces and grooved patterns with pitches of 150 nm and 200 nm, no clear orientation of somata and axons, was seen. Most of the cells were organized in smaller groups. On the other hand, cells were distributed more homogeneously on surfaces with grooves having pitches wider than 300 nm, while somata and axons aligned parallel to the grooves (Figure 4). In many cases the axonal terminus filopodia (growth cone) were widely spread and not following a specific direction. Due to the dimensions of cells compared to the topographical features of the used surfaces, soma and axons were localized on top of the ridges. No prediction can be made by means of visual observation about the localization of cells inside the grooves. However, Figure 5 demonstrates that on the somal and axonal borders membrane and filopodial interaction with the substrate occurred predominantly with the ridge-areas.

Soma and axon orientation

The results from the alignment measurements are depicted in Figure 6. The data are plotted as a box-whisker plot displaying the median (line in the box), 25% and 75% (box edges), and 5% and 95% (whiskers). The
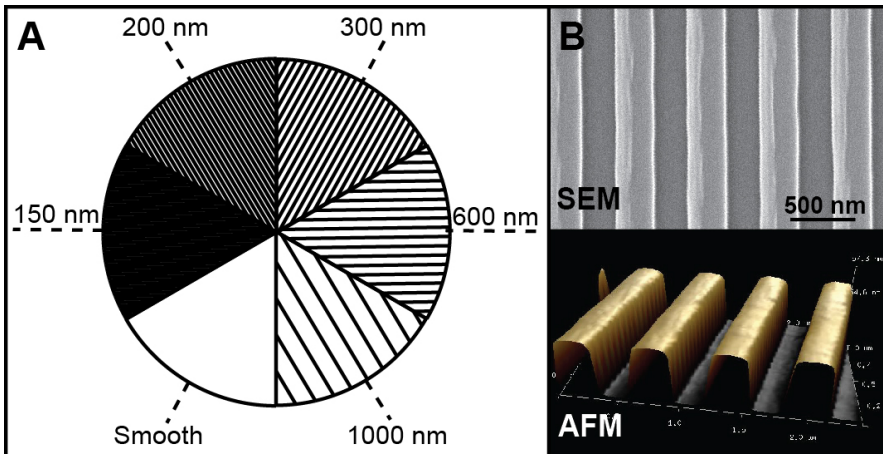
Figure 1: Overview of the multi-patterned culturing substrate. A) Sextant pieces of differently patterned silicon wafers (smooth and grooved with pitches between 150 nm and 1000 nm) have been utilized for the production of a master mold for solvent casting of culturing surfaces. B) For quality control the replicates have been analyzed by SEM and AFM (600 nm pitch pattern shown).

Table 1: Dimensions of the nanogrooved culturing substrates as measured by atomic force microscopy.

	Ridge	Groove	Depth
Pitch			
1000 nm	536.4 ± 10	453.1 ± 17.5	158 ± 10
600 nm	318.4 ± 16.3	304.8 ± 8.2	143 ± 10
300 nm	174.9 ± 5.4	130 ± 7.7	70.4 ± 7.7
200 nm	81.7 ± 3.1	135 ± 2.9	51.8 ± 2.7
150 nm	71.9 ± 5.7	77.3 ± 6.2	32.7 ±2
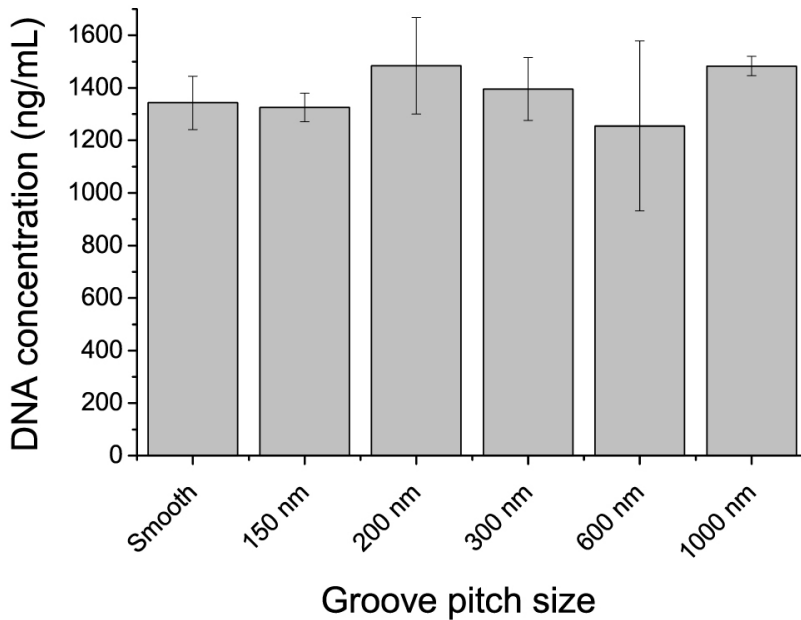
Figure 2: Assessment of cell number by DNA Assay on different substrates (n=3). Note that no significant differences (P<0,05) between the patterns was found.

Figure 3: Bright field light micrograph overview of PC12 cell behavior after 7 days of culture on differently patterned substrates. Compared to smooth surfaces, cells on grooved surfaces featuring pitches between 150 nm and 1000 nm significantly increased in axonal outgrowth length and alignment.

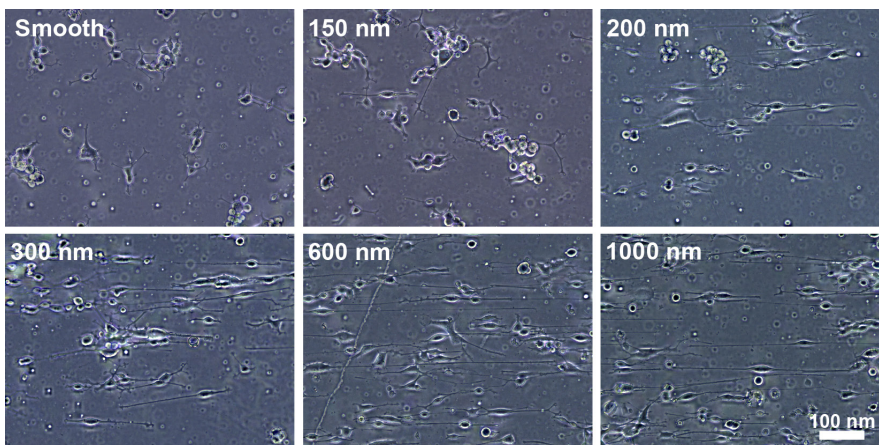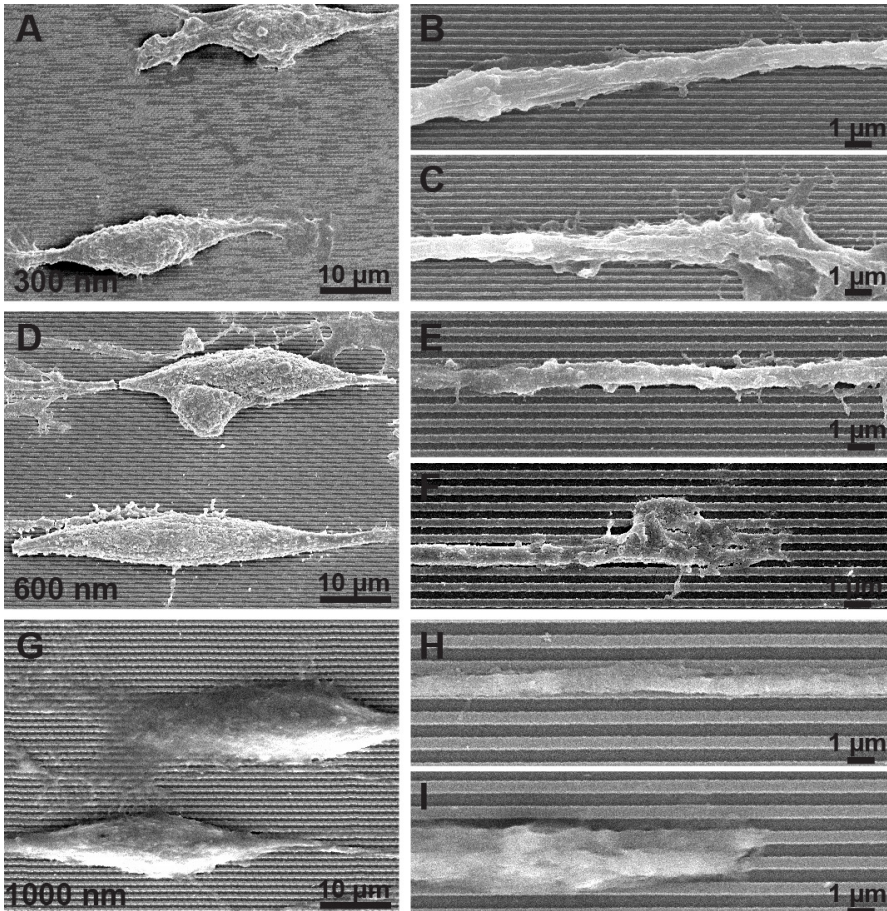**Figure 4: Scanning electron micrographs at 7 days of culture on nanogrooved substrates.** A) On 300 nm pitch surfaces cells aligned to the groove direction. B) Higher magnification of the 300 nm pitch pattern shown alignment of the axon. C) Note that the growth cone at the end of the axon is expanding over several grooves without apparent preferential orientation. D)E)F) Similar observations can be made on the 600 nm pitch pattern for cell bodies, the axon and the axonal growth cone and G)H)I) on the 1000 nm pitch pattern for cell bodies, axon and axonal growth cone.

Figure 5: Scanning electron micrograph of the axonal growth cone interacting with a 300 nm pitch grooved substrate. Cell extensions are often found to bridge from one ridge to another (white arrows), while very fe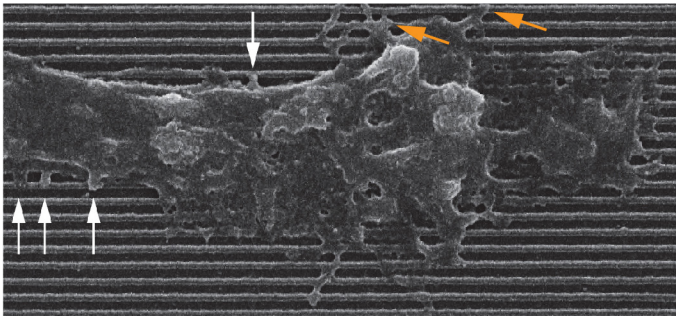w extensions are found to be located inside the groove. Moreover, thin filopodia-like formations can follow along single ridges (orange arrows), while no equivalent could be seen following the pattern inside the grooves.

shorter angle between cell/axon main axis and the groove direction was measured. In such measurement a random alignment would result in a value of approx. 45° with a very wide distribution of the boxes and whiskers, while near perfect alignment would result in a measurement close to 0°, with a very small distribution.

Cell soma alignment was found to occur significantly on grooved patterns with pitches down to 300 nm (median of ~10°), compared to the smooth surface. Axons aligned to smaller grooved patterns with pitches down to 200 nm (median of ~37°). Noticeably, a much stronger alignment of axons was induced by patterns with pitches of 300 nm (median of ~10°).

Axon length

A topography-dependent stimulation of axon-length of PC12 cells was found, as shown in Figure 7. All patterns including the smallest patterns with pitches of 150 nm induced significantly longer axonal outgrowth, compared to cells cultured on smooth surfaces ($P<0.05$). Moreover, cells on topographies with pitches wider than 200 nm showed significantly longer axons than cells on 150 nm pitch grooves, and the longest axons on 1000 nm pitch grooves were significantly longer than the axons on the 200 nm pitch grooves.
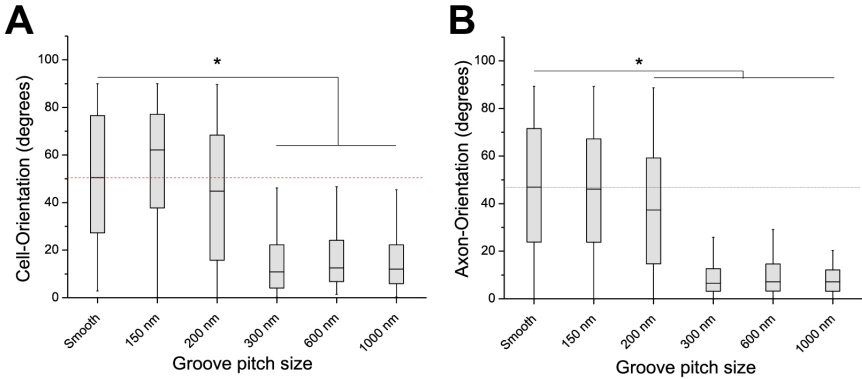
Figure 6: PC12 cell and axon orientation on smooth and grooved topographies. A) Cell-body alignment can be significantly ($p<0,05$) increased on grooved topographies with pitches between 300 nm and 1000 nm. B) While axons can already align significantly to grooves with a pitch of 200 nm, compared to cells on a smooth control. The red dashed line represents the median of the cell population cultured on a smooth surface.
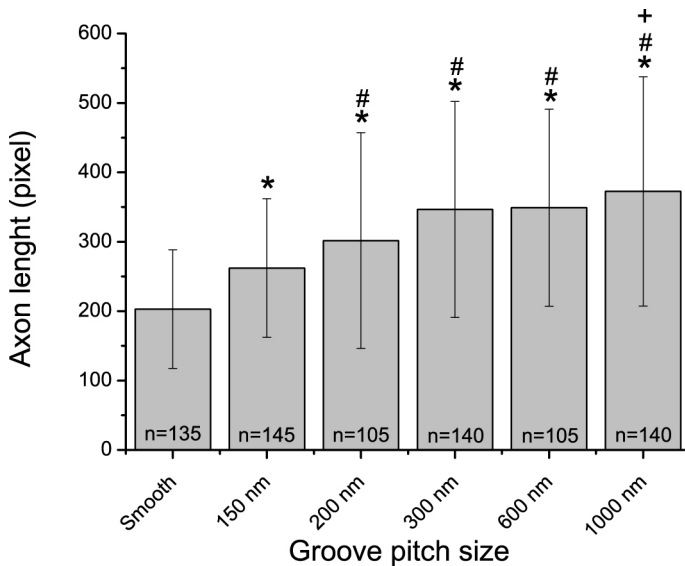
Figure 7: Differences in axon-outgrowth of PC12 cells as a response to differently patterned substrates. The smallest utilized grooves with a pitch of 150 nm have already induced a significant ($p<0,05$) increase in axon length. (* = significantly different with smooth, # = significantly different with 150 nm, + = significantly different with 200 nm)

3

Discussion

The aim of the present experiments was to evaluate a possible control-mechanism of neuron-like cell-behaviour by surface-nanotopography. Grooved micro-topography has already been tested and found to influence neuronal migration, alignment, and axon formation and outgrowth.[16-18] Based on literature it was suggested, that for an improved interaction between cochlear implant electrodes and the spiral ganglion cells, organized axon alignment would be required. Such organization would necessitate topographies of similar size as the axons, which can go down in width to nanometric dimensions.[14] Moreover, nanogrooves would allow parallelization of higher numbers of axons, thereby increasing the maximum possible perceptual resolution. Therefore, the current study investigated neuronal cell behaviour on a range of nanotopographies. The results showed evident cell attachment, normal neuronal-like cell morphology, and equal cell numbers on all topographies, indicating cytocompatibility of the applied nanotextured surfaces. When subsequently investigating cellular organisation by looking at alignment of soma and axons, the results clearly showed an evident threshold value; Grooves with pitches of 300 nm and depth of 70 nm could induce measurable changes in alignment of PC12-cell-bodies, whereas even smaller topographies could not. Also for axons a clear alignment becomes visible on grooved patterns having a pitch wider than 300 nm, although a statistical significance has been already been found on patterns with a 200 nm pitch and 52 nm depth. Therefore, grooved topographies with sizes in the found threshold range appear to be most interesting for the application on electrode surfaces.

Next to organisation, we also studied the effect of nanotopography on axon length. In contrast to the orientation behaviour, the effects on axon outgrowth did not show such a threshold value. Axon outgrowth, our measure for surface affinity, was stimulated significantly already on the smallest topographies tested (150 nm pitch; 33 nm depth), when compared to the smooth surface. This means that for the desired affinity between the electrode-surface and neurons any application of nanopatterns is of preference.

When looking at our study design, several comments can still be made.

The validity of any prediction about interaction between the cochlear implant electrode and the cells of the auditory nerve *in vivo* will also depend on the chosen cell-model. As for all cell-lineages there are three main sources available also for neuronal cells, namely *in vitro* differentiation, primary cells, and cell-lines. Differentiation of stem cells *in vitro* can be performed by using specific neuronal differentiation cues (e.g. growth factors, chemical compounds). This method has been rejected, as no golden standard has been established yet and some of the differentiation methods may even give rise to false positive cell phenotypes.[19] Primary differentiated spiral ganglion cells, being the main target of the research, would be ideal. Several protocols exist for the extraction and cultivation of SGCs from animal models, such as rats or mice.[20, 21] However, obtainment of human juvenile and therefore unaffected cells is rather complicated. The decision was made for the use of immortalized neuron-like cell lines, which give the advantage of a highly homogeneous cell population. Cell-lines are mostly chosen for strongly normalized experimental setups, marginalizing the bias induced by heterogeneous primary cell cultures. The chosen PC12 cells were discovered four decades ago and have been established to a well-studied neuronal cell model that is frequently used in fundamental research.[22, 23] Their responsiveness to NGF gives the PC12 cells the advantage that a controlled start of differentiation on the surface of interest is possible. This fact allows for observation of axonal formation behaviour as a direct response to the topography. This cannot be achieved for the already differentiated and neurites preformed primary cells. However, the immortalized phenotype of most cell-lines is often combined with metabolic variations in comparison to the parental cells. Also in the current experiment differences in expression of attachment and migration related proteins may interfere with the outcome that would be found for primary cells. A verification of the found effects should always occur with the application related cells. Such a comparison study between PC12 and spiral ganglion cells on grooved auditory implant surfaces was performed by Reich et al..[24] The presented data shows strong similarity in the response of the two cell types regarding the axonal alignment to microsized grooves. While both cell types aligned strongly to molded grooves on silicone elastomer and platinum sputtered grooves on glass, no

3

effect was found on grooves produced by ablation of silicone. Therefore, the authors suggest the PC12 cells as a convenient alternative model for inner ear derived cell-surface guidance studies.

The choice of the tested topographies was based on previous experiments in our laboratory. By far the most commonly used surface pattern has been grooves, because of the resemblance to the highly organized ECM in the living tissues (e.g. collagen fibers). The idea that physical stimuli can induce contact guidance of neuronal cells has been for the first time experimentally verified by Harrison in 1912, who used a spider web as a culturing substrate.[25] Since then, methods have been established that allow design and manufacturing of specific surfaces. Extensive research to date has been performed on topographies in the micrometer range. Such studies reported neuronal alignment and axonal outgrowth, although the microgrooves reached supra-cellular dimensions.[16, 26-32] Several groups demonstrated a maximum pitch threshold for alignment and a negative correlation between alignment and increasing pitch size.[16, 27, 33] This is a logical consequence, as axons of cells cultured on microgrooves have been found to reside inside the grooves and are being directed by the transition-wall between the groove and the ridge.[27] Therefore, an increase of periodicity will always result in a decrease of contact guidance. However, the need for a high channel separation on the electrode of a CI-device would require a decrease of periodicity. Research on the nanoscale could allow such characterization, but remained challenging, not least because the qualitative production of ordered nanosized (in x, y and z dimension) topographies was streamlined only during the past decade.[34] The here utilized nanopatterns induced significant changes in cellular behaviour. Contrary to the microgroove studies, a minimal pitch threshold for cell alignment, and a correlating increase in directionality with increasing pitch size were established.

Besides width, also the depth parameters have been found an important factor for cell alignment. Also on this aspect, the nanometric pattern proved superior to steer cell behaviour. While in microtexture studies increasing groove depth is correlated with the strength of axonal alignment, no response can be observed on grooves shallower than 200 nm.[26, 30-32] Our study shows that utilizing grooves with pitches on the nanoscale, cells can

respond even to the smallest tested depth of 32 nm by axonal outgrowth and to 70 nm deep grooves with organized soma and axonal orientation. Evidentially, the underlying mechanisms by which the nanogrooves influence cell behaviour partially differ from that of microgrooves. For the nanotextures our experimental setup found the ridge to be the dictating factor for orientation. Axons are located on top of the ridges. Likewise, the cell extension filopodiae seen around the growth cone seemed to interact with the top of the ridges only.

 Our study showed that nanosized parallel grooves can be used for CI-electrode optimization, while realizing a high number of separate channels that are needed for high fidelity hearing. The differences of cell and axon interaction with nano-/microgrooves can still be important in the manufacturing of cell manipulating surfaces. Several design principles are possible, namely grooves with dimensions to allow somata and axons to reside inside the grooves,[27] dimensions that only allow axons inside the grooves, while keeping the somata outside,[33] dimensions as utilized in our setup to retain both neuronal parts outside the grooves, and various combinations. Still, further validation is needed on the effect of texture on the axonal behaviour of spiral ganglion cells on auditory implant material *in vitro* and in an appropriate animal model. To date methods have been already developed to reproduce micro-sized grooves in platinum (electrodes) allowing such *in vivo* studies.[11, 35]

Conclusion

 This study showed the potential of nanogrooved topographies to direct neuronal cell behaviour. The used pattern with a size of 130 nm, depth of 70 nm, with a pitch of 300 nm resulted in a strong cell-body and axon orientation along the groove direction axis, whereas the smaller patterns did not. Therefore, especially nanogrooved topographies and a pitch of 300 nm should be considered as a possible fine tuning mechanism in cochlear implant electrode development, as they would allow desirable neuronal organization with the smallest possible resolution. Moreover, even the smallest nanotopographies with a width size of 75 nm, depth of 32 nm and a pitch of 150 nm resulted in significant outgrowth of axon-like structures.

In conclusion, surface nano-patterns have the potential to be utilized as an electrode modification for a stronger separation of cells on the one hand and the possibility of directing cells towards the electrode contacts of cochlear implants on the other.

References

1. U.S. Department of Health & Human Services. Cochlear Implants 2013 [cited 2013 Nov]; Available from: http://www.nidcd.nih.gov/health/hearing/pages/coch.aspx.
2. Wilson, B.S. and M.F. Dorman, Cochlear implants: a remarkable past and a brilliant future. Hear Res, 2008. 242(1-2): p. 3-21.
3. Cohen, L.T., et al., Psychophysical measures in patients fitted with Contour and straight Nucleus electrode arrays. Hear Res, 2006. 212(1-2): p. 160-75.
4. Xu, J., et al., Chronic electrical stimulation of the auditory nerve at high stimulus rates: A physiological and histopathological study. Hear Res, 1997. 105(1-2): p. 1-29.
5. Tykocinski, M., et al., Chronic electrical stimulation of the auditory nerve using high surface area (HiQ) platinum electrodes. Hear Res, 2001. 159(1-2): p. 53-68.
6. Li, P.M.M.C., et al., Analysis of intracochlear new bone and fibrous tissue formation in human subjects with cochlear implants. Annals of Otology Rhinology and Laryngology, 2007. 116(10): p. 731-738.
7. Somdas, M.A., et al., Quantitative evaluation of new bone and fibrous tissue in the cochlea following cochlear implantation in the human. Audiology and Neuro-Otology, 2007. 12(5): p. 277-284.
8. Gillespie, L.N., et al., Netrin-1 as a guidance molecule in the postnatal rat cochlea. Hear Res, 2005. 199(1-2): p. 117-23.
9. Miller, J.M., et al., Delayed neurotrophin treatment following deafness rescues spiral ganglion cells from death and promotes regrowth of auditory nerve peripheral processes: effects of brain-derived neurotrophic factor and fibroblast growth factor. J Neurosci Res, 2007. 85(9): p. 1959-69.
10. Agterberg, M.J., et al., Enhanced survival of spiral ganglion cells after cessation of treatment with brain-derived neurotrophic factor in deafened guinea pigs. J Assoc Res Otolaryngol, 2009. 10(3): p. 355-67.
11. Reich, U., et al., Differential fine-tuning of cochlear implant material-cell interactions by femtosecond laser microstructuring. Journal of Biomedical Materials Research Part B-Applied Biomaterials, 2008. 87B(1): p. 146-153.
12. Klymov, A., et al., Understanding the role of nano-topography on the surface of a bone-implant. Biomaterials Science, 2013. 1(2): p. 135-151.
13. Adunka, O. and J. Kiefer, Impact of electrode insertion depth on intracochlear trauma. Otolaryngol Head Neck Surg, 2006. 135(3): p. 374-82.
14. Berglund, A.M. and D.K. Ryugo, Hair cell innervation by spiral ganglion neurons in the mouse. J Comp Neurol, 1987. 255(4): p. 560-70.
15. Lamers, E., et al., The influence of nanoscale grooved substrates on osteoblast behavior and extracellular matrix deposition. Biomaterials, 2010. 31(12): p. 3307-16.
16. Tuft, B.W., et al., Photopolymerized microfeatures for directed spiral ganglion neurite and Schwann cell growth. Biomaterials, 2013. 34(1): p. 42-54.

3

17. Weigel, S., et al., Surface microstructures on planar substrates and textile fibers guide neurite outgrowth: a scaffold solution to push limits of critical nerve defect regeneration? PLoS One, 2012. 7(12): p. e50714.

18. Clarke, J.C., et al., Micropatterned methacrylate polymers direct spiral ganglion neurite and Schwann cell growth. Hear Res, 2011. 278(1-2): p. 96-105.

19. Osathanon, T., et al., Neurogenic differentiation of human dental pulp stem cells using different induction protocols. Oral Diseases, 2013: p. n/a-n/a.

20. Hansen, M.R., et al., Reciprocal signaling between spiral ganglion neurons and Schwann cells involves neuregulin and neurotrophins. Hear Res, 2001. 161(1-2): p. 87-98.

21. Vieira, M., et al., Survival and stimulation of neurite outgrowth in a serum-free culture of spiral ganglion neurons from adult mice. Hear Res, 2007. 230(1-2): p. 17-23.

22. Westerink, R.H. and A.G. Ewing, The PC12 cell as model for neurosecretion. Acta Physiol, 2008. 192(2): p. 273-85.

23. Greene, L.A. and A.S. Tischler, Establishment of a noradrenergic clonal line of rat adrenal pheochromocytoma cells which respond to nerve growth factor. Proc Natl Acad Sci U S A, 1976. 73(7): p. 2424-8.

24. Reich, U., et al., Directing neuronal cell growth on implant material surfaces by microstructuring. J Biomed Mater Res B Appl Biomater, 2012. 100(4): p. 940-7.

25. Harrison, R.G., The cultivation of tissues in extraneous media as a method of morpho-genetic study. The Anatomical Record, 1912. 6(4): p. 181-193.

26. Clark, P., et al., Topographical control of cell behaviour: II. Multiple grooved substrata. Development, 1990. 108(4): p. 635-44.

27. Beduer, A., et al., Engineering of adult human neural stem cells differentiation through surface micropatterning. Biomaterials, 2012. 33(2): p. 504-14.

28. Su, W.T., et al., Microgrooved patterns enhanced PC12 cell growth, orientation, neurite elongation, and neuritogenesis. J Biomed Mater Res A, 2013. 101(1): p. 185-94.

29. Morelli, S., et al., Influence of micro-patterned PLLA membranes on outgrowth and orientation of hippocampal neurites. Biomaterials, 2010. 31(27): p. 7000-11.

30. Miller, C., S. Jeftinija, and S. Mallapragada, Synergistic effects of physical and chemical guidance cues on neurite alignment and outgrowth on biodegradable polymer substrates. Tissue Eng, 2002. 8(3): p. 367-78.

31. Hirono, T., et al., Recognition of artificial microstructures by sensory nerve fibers in culture. Brain Res, 1988. 446(1): p. 189-94.

32. Walsh, J.F., M.E. Manwaring, and P.A. Tresco, Directional neurite outgrowth is enhanced by engineered meningeal cell-coated substrates. Tissue Eng, 2005. 11(7-8): p. 1085-94.

33. Yao, L., et al., Effect of functionalized micropatterned PLGA on guided neurite growth. Acta Biomater, 2009. 5(2): p. 580-8.

34. Loesberg, W.A., et al., The threshold at which substrate nanogroove dimensions may influence fibroblast alignment and adhesion. Biomaterials, 2007. 28(27): p. 3944-3951.

35. Fadeeva, E., et al., Surface patterning of cochlear implant electrode arrays. Biomedical Engineering-Biomedizinische Technik, 2013. 58.

3

4

Bone Marrow-derived mesenchymal Cells feature selective Migration Behavior on submicro- and nano-dimensional multi-patterned Substrates

Alexey Klymov, Ewald M Bronkhorst, Joost te Riet, John A Jansen and X Frank Walboomers

Introduction

Modern titanium bone-implants are commonly modified e.g. by grit blasting in combination with acid etching, laser machining, or oxidation.[1] These industrially utilized methods introduce modifications of all surface properties, most prominently substantial changes to the topography. The increasing surface-complexity in form of roughness consists of isolated features, with sizes down to the nanoscale 2 and was shown to positively influence bone integration in clinical applications (reviewed in [3,4]). Remarkably, isotropic and anisotropic macro-, micro- and nanometer-sized features seem not only to be effective on the organ level, but can stimulate various types of cell-behavior. Multiple in vitro studies have shown that attachment, migration, proliferation and differentiation can be manipulated by utilizing different topographies on culturing surfaces (reviewed in [5]). The fact that cells have evolved to interact with the likewise hierarchically organized extracellular matrix (ECM) allows speculations about the ability of a modern implant surface to interact with cellular functions in a more natural way, while stimulating desirable behavior. Such a phenomenon could be of instrumental importance for design of biomaterials in regenerative medicine approaches.

However, it is interesting that cell behavior, like differentiation, not only can be provoked, but also inhibited by use of topography. It was shown that specific nano-pit surfaces can keep stem cells in an undifferentiated state maintaining their self-renewing capacity.[6] This is an effect that can usually only be seen in nature for stem-cells being in direct contact with their "niches", which are known to have specific bio-chemical properties.[7] The question arises whether other cellular phenomena, like repopulation of stem-cell niches after chemotherapy – known as homing, could also be a result of cell-surface pattern recognition. For such a process to occur the cells would need to have the ability of recognition of, distinction between and preference for different patterns. This effect could be used in development of bone-implants by the production of an intelligent surface having the ability to attract and stimulate bone forming cells or their progenitors in a more efficient manner, thereby increasing the ultimate bone-to-implant contact. Contrary, also cell-repelling topographies could

be utilized in production of organs and prosthesis that are normally prone to unwanted cell attachment, or fouling by cellular debris. For example additional modifications of devices, like stents (e.g. by anti-fouling polymer coatings), would be redundant, as the repelling effect could be achieved just by surface-modification of already used materials.

 To evaluate the possibility of a cellular-migration selectivity based on the cell-topography interaction, we made use of a multi-patterned "biochip" culturing platform containing multiple topographies between 10 and 500 nanometers.[8, 9] The biochips were seeded with rat bone marrow derived cells, which were allowed to migrate on the substrates while "choosing" between patterns. It was postulated that cell-surface interactions during the first hours after cell seeding would be determined mainly by specific cell attachment to the substrate, while numbers of later time points would be defined by selective cell migration and proliferation. Therefore, it is
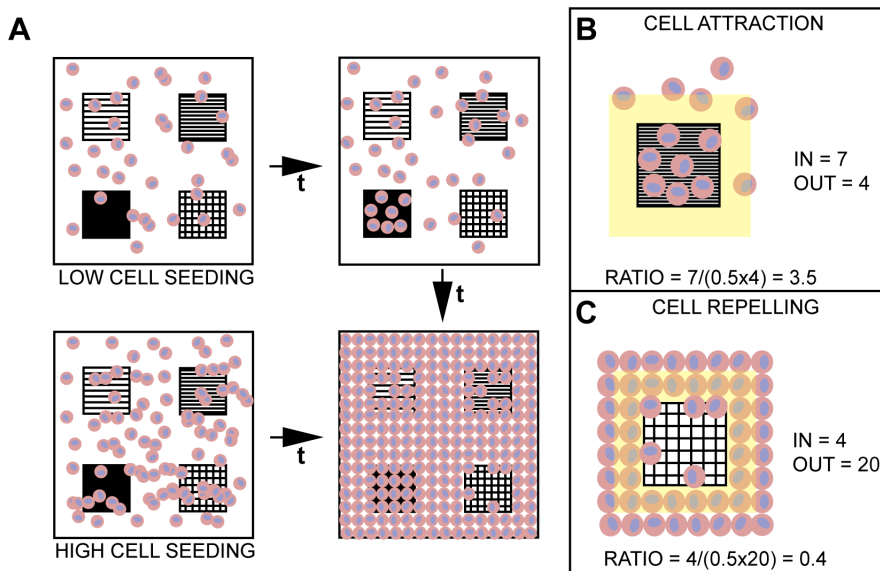
Figure 1: Theoretical model for a cell-migration preference study on a multi-patterned surface. A) In time, randomly seeded cells should accumulate on patterns of preference, while avoiding not favored patterns. Adaptation of initial seeding density and culturing time can increase or decrease the effects. B) cell-attracting patterns display more cells per area, compared to the surrounding smooth surface. C) cell-repelling patterns display less cells per area, compared to the surrounding smooth surface.

hypothesized that randomly seeded cells will accumulate in time on patterns of preference, while cell-repelling patterns should lead to a reduced cell retaining and smaller numbers compared to the surrounding area (Figure 1). Theoretically, an optimal timeframe for detection of attracting/repelling surfaces should exist. While low cell-density will result in a relatively high ratio between attracting patterns and the smooth surrounding, the effect will diminish in time when cell numbers increase. Contrary, the repelling effect will be most evident with high cell-densities, resulting in a relatively low ratio between pattern and smooth surrounding. In time, all of the effects will be not detectable, as cells will completely cover the culturing surface. The obtained data was interpreted by using a regression analysis model leading to a selection of the topographies with strongest differences in cell attraction or repelling, which were further analyzed for additional properties.

4

Materials and Methods

Substrate production

A silicon-wafer "biochip" was produced by electron beam lithography employing Hydrogen Silsesquioxane as described previously by van Delft et al..[8, 9] As shown in Figure 2A, the "biochip" consisted of 42 squared (500 x 500 µm²) fields that were separated by a smooth surface. Each of the fields contained either a submicron-/nanosized pattern, or was a smooth control that was processed identically to the topographical fields. The topographies inside the 36 patterned fields were designed as checkerboard organized squares with pitch sizes of 60 – 600 nm and grooves with pitch sizes of

Table 1: Nanotopography design dimensions on the polystyrene "biochip" replicate.

	Pitch (nm)									
	40	60	80	100	160	200	300	400	600	1000
Topography										
Grooves 3:1 (R:G nm)		45:15	60:20	75:25	120:40	150:50	225:75	300:100	450:150	
Grooves 1:1 (R:G nm)	20:20	30:30	40:40	50:50	80:80	100:100	150:150	200:200	300:300	500:500
Grooves 1:3 (R:G nm)	10:30	15:45	20:60	25:75	40:120	50:150	75:225	100:300	150:450	250:750
Squares (nm)		30	40	50	80	100	150	200	300	
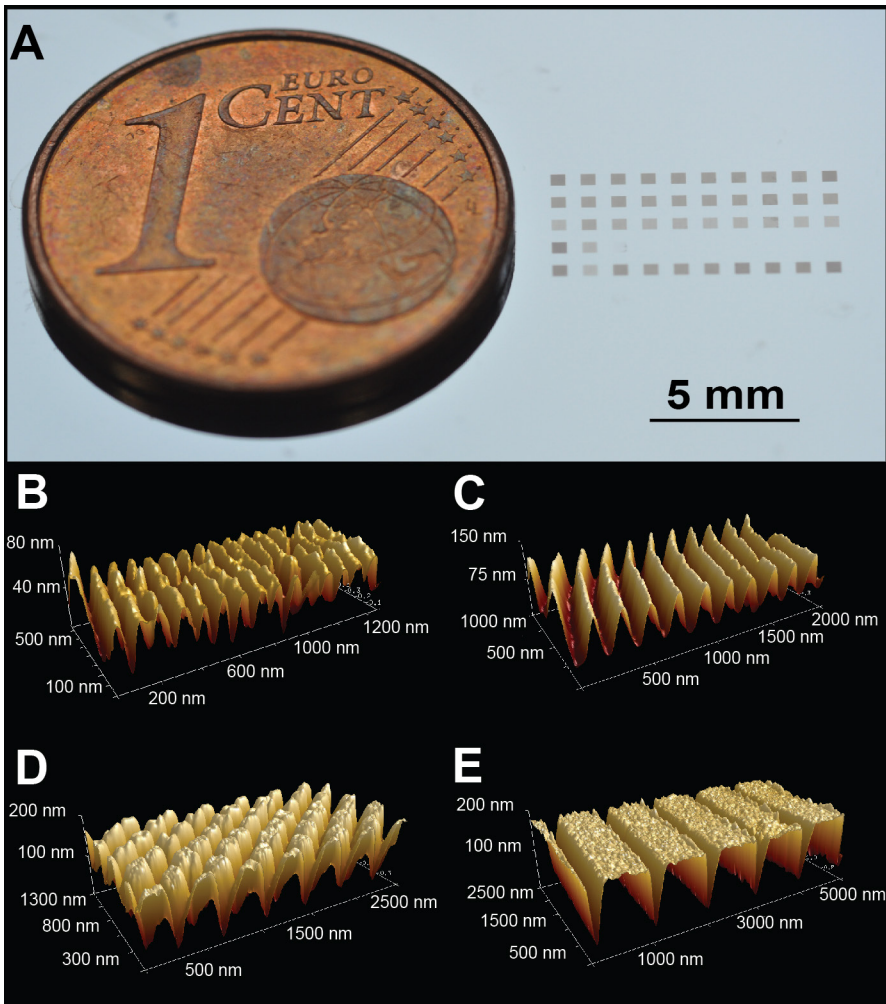
Figure 2: "Biochip" multi-patterned surface master and replicates. A) Silicon master featuring 36 differently patterned fields that was used for solvent casting of the cell-culturing substrates (The cent in the image is for size comparison purposes only). The grooves with ridge to groove ratios of 3:1 (upper row in the photograph), 1:1 (second row), 1:3 (third row), and squares (bottom row) were designed having features between 10 nm and 1000 nm. Quality was controlled by means of AFM. B) 100 nm pitch grooves with R:G 1:1, C) 200 nm pitch grooves with R:G 1:3, D) 400 nm squares and E) 1000 nm pitch grooves with R:G 3:1.

40 – 1000 nm having ridge to groove ratios of 1:1, 1:3 and 3:1 (Figure 2B - E, Table 1) and were used for the reproduction of the biochip into polystyrene (PS) cell culture plastic. Patterns with pitch sizes smaller than 100 nm reproduced poorly and were excluded from further analysis. Per chip 6 smooth fields were available, of which 4 were later used as a control. For reproduction, PS (Acros, Geel, Belgium) was dissolved in chloroform in a proportion of 1:6 and 5 ml of the solution were used for solvent casting of an Ø6 cm replicate. For sterilization and wettability increase the replicates were treated by radiofrequency glow-discharge (Harrick, Ossining, NY) in argon gas, for a period of 5 minutes at an atmospheric pressure of about 10^{-2} mbar. Thereafter, the PS biochips were used for cell culture experiments. The wafers were designed in a way in which the highest features of the different topographies on the PS replicates were on the same level with the smooth surrounding area, meaning that the first topographical feature a cell encounters entering a topographical field would be a groove or a square pit.

Atomic Force Microscopy

Atomic force microscope (AFM, Catalyst, Bruker, Santa Barbara, CA) analysis was done in tapping mode with a 118 µm long silicon cantilever (NW-AR5T-NCHR, NanoWorldAG, Wetzlar, Germany) having average nominal resonant frequencies of 317 kHz and average nominal spring constants of 30 N/m. This type of AFM probe has a high aspect ratio (7:1) portion of the tip with a nominal length of >2 µm and a half-cone angle of <5°. Nominal radius of curvature of the AFM probe tip was less than 10 nm. Height images of each field/sample were captured in ambient air at 50% humidity at a tapping frequency of 266.4 kHz. The analyzed field was scanned at a rate of 1.0 Hz and 512 scanning lines.

Cell retrieval and culture

Rat bone marrow cells (rBMCs) were obtained according to the local ethical approval protocol (RU DEC 2012-317) from femurs of 40 – 43 days old male Wistar WU rats. Femurs were washed three times in α Minimal Essential Medium (αMEM; Gibco, Invitrogen Corp., Paisley, Scotland) containing 0.5

mg/mL gentamycin (Gibco) and 3mg/mL fungizone (Gibco). The epiphyses were cut off to allow flushing out of the cells from the diaphyses using αMEM supplemented with 10 % fetal calf serum (FCS; Sigma F7524, Taukirchen, Germany) and 0.5 mg/mL gentamycin. The cells were brought into culturing flasks and non-adherent cells were removed after one day by medium refreshment (αMEM, 10% FCS, penicillin (100 U/mL) and streptomycin (10 μg/mL) (Gibco)). After additional 6 days of culture, the cells were collected by trypsinization (trypsin/EDTA; 0.25% w/v trypsin, 0.02 % EDTA; Sigma) and seeded onto the substrates in two densities, namely $5x10^3$ cells/cm² and 10^4 cell/cm². The lower density was chosen to detect patterns that favor cell retention, while higher cell seeding would show reduced cell numbers within cell repelling patterns and closing of the monolayer at the patterns during the progress of proliferation (Figure 1).

Three independent experiments were performed for the low and high seeding conditions. In each experiment one substrate was retrieved per time point and condition (low seeding condition after 4, 24, 48 and 72 hours; high seeding condition after 48 and 72 hours). While these substrates were used for the design of a regression analysis model, additional substrates were obtained after 216 hours for long term effect observations. The substrates were then processed for scanning electron- or fluorescence microscopy.

Scanning electron microscopy

For scanning electron microscopy the substrates were washed in phosphate buffered saline (PBS, Gibco), fixed for 5 minutes in 2% glutaraldehyde in 0.1 M sodium-cacodylate, and washed for 5 minutes in 0.1 M sodium-cacodylate. Subsequently, cells were dehydrated in a graded series of ethanol and dried to air in tetramethylsilane (Sigma). The specimens were sputter-coated with a gold layer (10 nm) and examined using scanning electron microscopy (JEOL 6310, Jeol, Tokyo, Japan).

Fluorescent microscopy, cell proliferation and analysis

To analyze cell morphology the cytoplasm was stained with CellTracker Green CMFDA Dye (Life Technologies, Paisley, Scotland, UK) according to

the manufacturer's description. For quantification of proliferating cells, a Click-iT™ 5-ethynyl-2´-deoxyuridine (EdU) imaging kit with AlexaFluor 555 azide (Invitrogen) was used. In short, cells were incubated for 4 hours before fixation in conditioned medium containing 50 µM EdU. Thereafter, the cells were washed three times with fresh medium and fixed using 3.3% paraformaldehyde in PBS for 15 minutes. After fixation, cells were permeabilized for 15 minutes with 0.5% Triton-X100 (Sigma) in PBS containing 10% FCS and incubated in reaction buffer containing AlexaFluor azide. The samples were washed and mounted on microscope slides using Mowiol 4.88 mounting medium (Polysciences, Eppeldorf, Germany) containing 4',6-Diamidin-2-phenylindol (DAPI, Roche Applied Science, Mannheim, Germany).

Image acquisition was performed using a Z1 microscope (Zeiss, Jena, Germany) with a 5X objective. Images of the whole biochip were obtained and stitched to one single image. A mask of the biochip was reproduced by brightfield microscopy, which allowed visualization of single fields. Subsequently, the mask was laid over the fluorescent images. A second region of interest was created around the mask, which was twice the size of the fields, to use as a smooth reference. Image analysis was performed using Photoshop X6 (Adobe, Hamburg, Germany) and Image Pro Plus 6 (Media Cybernetics Inc., Rockville, MD). For cell number analysis, a ratio was made between the cell-numbers within the topographic field, and half of the cell number inside the smooth region of interest, thus resulting in a value of 1 for equal cell distribution, <1 for a cell repelling surface, and >1 for a cell attracting surface.

Regression model design

Since this study utilizes a large number of different surfaces, direct statistical comparisons between experimental groups are ineffective, due to statistical disadvantages of massive multiple testing. For power-enhancement of such studies, regression models can be constructed.[10, 11] Two models were designed to estimate the relation between experimental parameters and the migration behavior, expressed in the ratio described in the previous paragraph. This was done separately for low and high density, although the approach in building the model was identical. The

independent variables in the model were the various "patterns" of the topographies (squared, grooved 3:1 etc.), "time", and finally the groove width "size". Next, it was questioned whether interactions between groove/pit width and time or pattern would improve the model, by varying the values for each parameter and then assessing the regression model for an increase in the determination-coefficient R^2. Finally, the model was extended with a quadratic term for the relation between groove/pit width and migration behavior, to allow non-linear relations between the two. As the shape of the relation between groove/pit width and migration behavior might differ for various patterns, an interaction of pattern and the squared groove/pit width was tested for model inclusion as well. Figure 1S shows a flowchart with a stepwise description of the modelling process.

As the resulting regression models contain both a linear term and a quadratic term for groove/pit width, and potentially interaction terms between groove/pit width and shape as well as between the square of groove/pit width and shape, the relation between the dimension of the shape and the migration behavior is difficult to assess from the model directly. Therefore, scatterplots were made, depicting the estimated ratio for all types of pattern relative to the groove/pit width ranging between 25 nm and 750 nm. The shape, slope and the extreme points of the resulting curves can be used to determine the extent to which a certain aspect of the topography influences the cell migration behavior. The 3 strongest attracting and 6 strongest repelling patterns have been defined based on the models, and used for statistical analysis of the proliferation data.

Statistics

Statistical analysis was performed using Origin 8.5 (OriginLab, Northampton, MA). For proliferation the ratios (EdU/DAPI per field) from 24, 48 and 72 hours were pooled. The data was compared using one-way analysis of variance (ANOVA) combined with a post-hoc Bonferroni Multiple Comparisons Test for detection of significant different groups at a significance level of $p < 0.05$. Only patterns have been chosen that have shown the strongest effects on attraction and repelling in the regression models.

Results

Substrates

The polystyrene replicates were checked routinely by SEM and AFM (Figure 2). The dimensions of the replicated topographies are summarized in Table 1. All the dimensions, such as ridge/pillar width, groove/pit width and depth were increasing with the increasing pitch size. No decrease in reproduction quality was observed between the early and later produced substrates.

Cell-surface interactions

Fluorescent microscopy showed no differences in the distribution of cells on the biochip after the time period of 4 hours. However, during the later periods a change in distribution was observed that most obviously resulted in fewer cells on certain topographical fields compared to the smooth surrounding (Figure 3). By visual inspection this effect increased in time as cells were allowed to migrate and proliferate.

SEM analysis of a "biochip" after 72 hours of cell culture corroborated such observation, as more cells were found to be distributed over the smooth surface than inside the topographical fields (Figure 4a). A repelling effect that could be maintained on some of the patterns even 9 days after seeding (Figure 4b and 4c). However, on all patterns cells could be found attached and spreading. Grooved surfaces induced cellular orientation along the grooves (Figure 5a), which was less strong with decreasing pitch size. Squared patterns did not induce a specific change in overall cellular morphology and orientation (Figure 5b). A further difference could be observed between the border region of squared/smooth and grooved/smooth surfaces. Figure 5c and 5d show cell interaction at the similar borders of the 600 nm pitch grooved 1:1 and 600 nm pitch squared surfaces. While cells on the border with the grooves were mostly entering the topographical field, the cells next to the squared field were found often aligned next to the topography without being in direct contact. Higher magnification of the cellular interactions showed thin cellular extensions following the squares in a rather organized manner by spanning the shortest distance between the square-edges, thereby aligning either parallel, or at a 45° angle (Figure 5e and f). In general, thin membrane regions were found

4

to be mainly located on top of the topographical features with cavities over the squared pits and grooved areas.
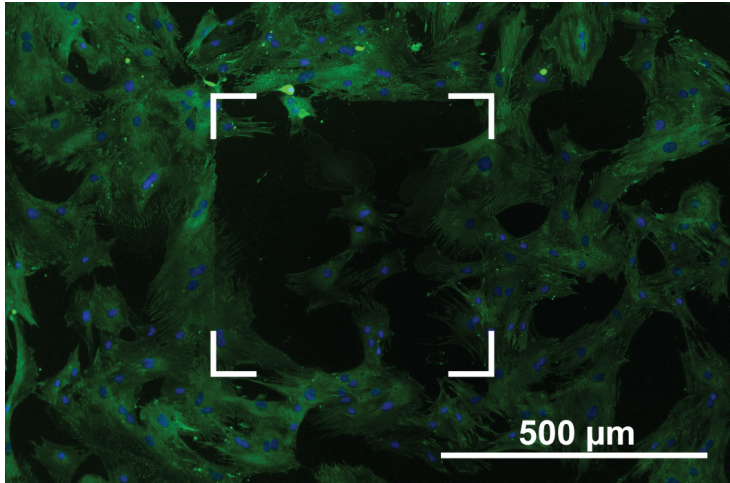
Figure 3: Fluorescent micrograph of the repelling effect of 600 nm pitch squares (highlighted) on cells after 72 hours on the "biochip" (nucleus is stained blue by DAPI, cell cytoplasm stained green with CellTracker).

Figure 4: Scanning electron micrograph of cells cultured on the "biochip". A) After 72 hours of culture less cells can be found on certain topographical fields than on the surrounding smooth surface. B) Also after 9 days of culture the repelling effect can be seen on squares with a pitch of 600 nm. C) A similar effect can be seen on grooves with a R:G 1:3 and a pitch of 1000nm.

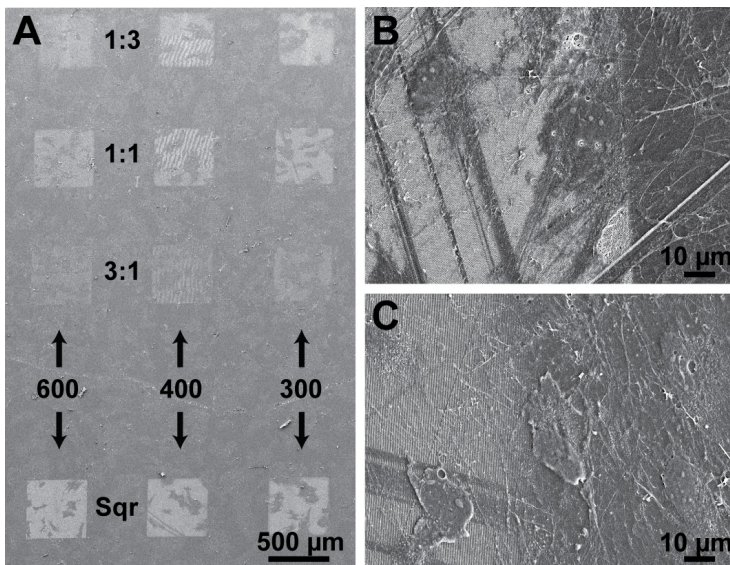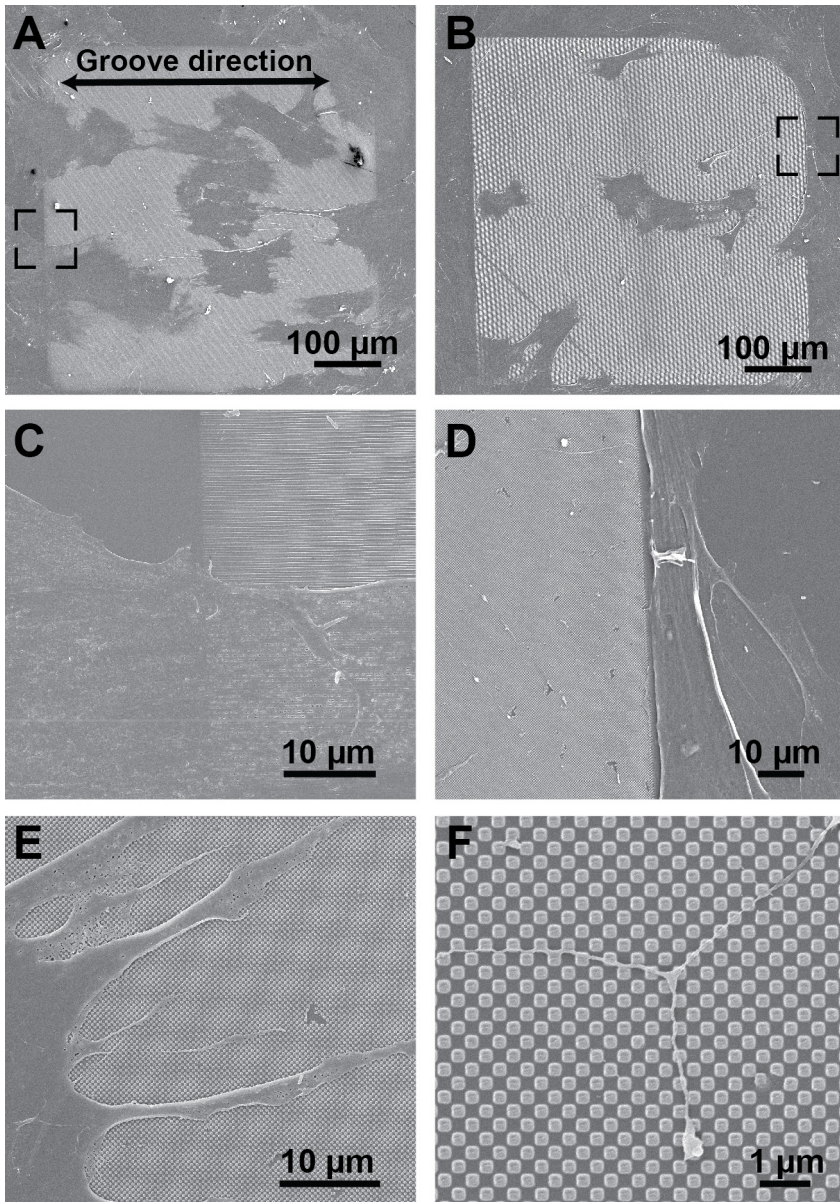**Figure 5: Scanning electron micrograph of cell surface topography interactions 72 hours after seeding.** A) Cells on grooves with 600 nm pitch, R:G 1:1 B) Cells on squares with 600 nm pitch C) and D) (magnification of A) and B). C) Cells were found entering grooves without evident changes in behavior. D) Contrary, numerous cells were found to align to the squared topographical field, without being in direct contact. E) And F) Higher magnification of cell-surface interaction on squared topographies

Model

 Figure S1 shows a flowchart of the model design process. In Table S1 the resulting regression models are represented. Both models have a similar structure. The main difference is that for the low density situation an interaction between time and groove/pit width did not improve the model, whereas in the high density situation an interaction between time and groove/pit width did improve model performance. To facilitate understanding of the models, an example is given for the low density experiment defining the local ratio at time = 24 of a 3:1 grooved surface with a groove/pit width of 200 nm. The corresponding effects from the Table have to be selected and added. In this case "Constant" (always present) + "24 Hours" + "Grooves 3:1" + 200 x "Size x Grooves 3:1"+ 2002 x "Size² x Grooves 3:1"= 0.961 + 0.019 - 0.011 + 200 x -1.675 x 10-3 + (200)² x 8.556 x 10-6 = 0.976.

 Figure 6 shows the resulting prediction for migration behavior depicted as ratio as a function of groove/pit width for the earliest obtained time-points. Each of the patterns possesses an individual parabolic function for the tested range of the groove/pit dimensions. In the low seeding model, the biggest part of all curves is underneath the ratio of 1. The only evidence for an attracting effect could be found for the bigger sized 3:1 grooves and medium sized 1:1 grooves as these were above the equated ratio. Contrary, both the low and high density models show a strong repelling effect, especially of the squared patterns. All tested square sizes were found to repel cells more strongly than the grooves with ratios around 0,6 - 0,7. The repelling effect became stronger with increasing feature size for all patterns. A comparison example between the measured data and the modelled data can be seen on the example shown in Figure S2 for high seeding density at Time=48 Hours.

Cell proliferation

 On basis of the models, the topographies with the strongest and lowest repelling capacity were chosen for cell proliferation analysis. The results showed no significant differences concerning EdU-positive cells compared to the smooth control (Figure 7a). However, the mean values of the chosen
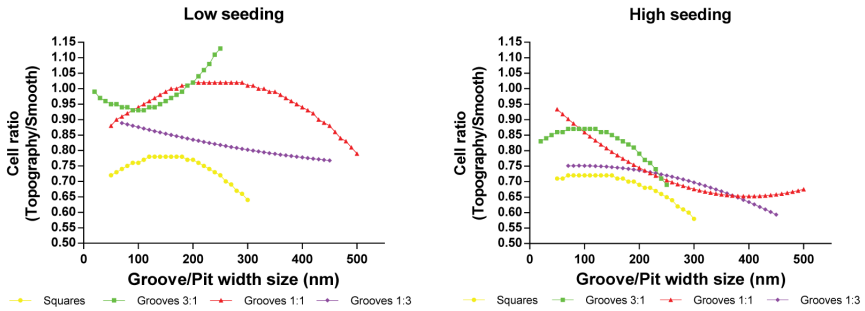
Figure 6: Visualization of the modulated migrational behavior as a function of the groove/ pit width size. The low and high density models show the squared patterns to repel the cells stronger than the grooved patterns with the different ridge to groove ratios. The grooves with the ridge to groove ratio of 1:3 repel cells most, while ridge to groove ratios of 3:1 repel the cells least.

4
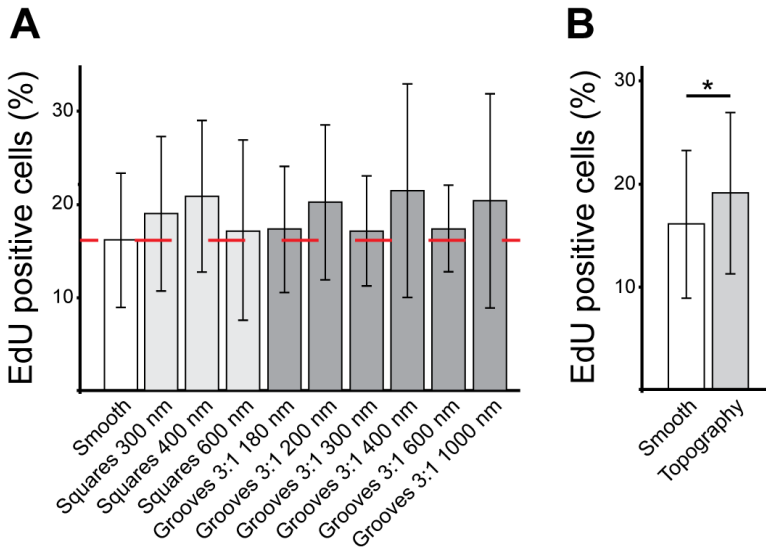
Figure 7: Cell proliferation on the "biochip" patterns. A) Percentage of EdU positive cells cultured for a period between 24 and 72 hours (strongest repelling topographies (light grey) and strongest attracting patterns (dark grey) retrieved from the regression models; n smooth=64, n per pattern=16, ± SD). B) Percentage of EdU positive cells as a comparison between the smooth and pooled patterned surfaces (n smooth=64, n patterns = 144, ± SD).

topographies are all higher that the means on the smooth patterns. Pooling of the data for comparison of the effects between topography in general and the smooth surface showed a minor but significant difference between topographies and the smooth control (Figure 7b).

Discussion

It is striking that most of the in vitro experiments regarding cell-surface interactions published to date, have studied the effects of specific uniform patterns. Contrary, the current experiment was utilizing a multi-patterned "biochip"-setup, in which cells were confronted with an array of different topographies without prominent borders. We discovered an intrinsic property in form of a preference-mechanism for surface features on the nano-scale.

Several remarks can be made regarding the experimental setup and the model design. To monitor heterogeneity in cell distribution, four smooth control fields were used that are positioned in the four corners of the "biochip", framing the patterned fields. Moreover, a ratio-based approach was chosen for cell attraction/repelling comparisons that would exclude cell-distribution and density related bias. Although only one replicate of the individual topographies was present on each "biochip", topographies of the same group (e.g. Squares, Grooves 1:3, Grooves 1:1, Grooves 3:1) are strongly related. The gradual change of feature sizes of a group was thought to induce also a gradual effect on cell behavior, allowing a reduction of experimental replicates. However, due to the amount of the individual variables in our experiment (time-points, topographical groups, feature sizes), conventional analysis would result in a large number of tests between small groups and therefore in low power. Hence, the decision was made to utilize a statistical model incorporating all effects in one single analysis, thereby gaining detail and power at the same time. As the number of tested topographies can strongly increase in future experiments and possible industrial screenings the performed etiological modelling seems to be a possibility for interpretation and visualization of the collected data. Since the model is build up by inclusion and exclusion of different independent parameters by adjusted R^2 value evaluation, it is possible to

define relevant and irrelevant factors involved in cell behavioral changes. For example our model shows that the ratio is dependent on the pattern, the feature size and the time that is experienced by the cells, as inclusion of these parameters increased the power of the models. The final R^2 value on the other hand can be used to evaluate the power of the underlying model. In our case the low density model is weaker (R^2=0.1) than the high density model (R^2=0.304), as can also be seen in the Figure S2. This supports the visual observation that the patterns rather repelled the here utilized cell-population and therefore the high density setup and model should be used for further analysis. The high density model confirmed that any dimension of nano-squares had the lowest pattern/smooth ratio, followed by grooves with R:G 1:3. The highest cell numbers were found on grooves with the reversed ridge to groove ratio of 3:1. In general, an increase in pitch size correlated with a decrease in cell number.

A first question that arises is how this numerical effect is established. One process that is influenced by cell - topography interaction, which could explain the here found differences, is proliferation [12, 13]. Yang et al. have studied the distribution behavior of cells in time on a non-uniform gradual microgrooved surface.[14] Fibroblasts seeded on the substrates were found heterogeneously distributed after 72 hours of culture, and concentrating on certain hotspots. These researchers concluded the differences in cell accumulations to be a result of variations in proliferation and not in migration. This is not in agreement with the current study, where more de novo DNA replicating cells were found on topographical fields. Since the cells did not increase in numbers on the nano-patterns, although proliferation was stimulated, the low cell-ratios can therefore only be explained by increased cell-migration away from the topography after division.

 Subsequently, a second underlying question is which intra- and extracellular mechanisms allow for a topographical influence on cell migration. Surface topographies are known to influence the formation and dissociation of focal adhesions that span through the cell-membrane and connect the intracellular compartments with the extracellular matrix.[15] Manipulation of the focal adhesions may lead to physical changes and reorganization of intracellular compartments, by means of mechanotransduction.[16, 17]

Such processes can in turn have influence on protein expression, protein interaction, local protein concentration, and intracellular signaling, such as in case of the focal adhesion kinase (FAK). FAK, which upon stimulation at the membrane can induce signal-transduction into the nucleus and gene expression,[15, 18, 19] is known to have strong effects on cell adhesion and migration.[20] Previous studies exploiting a similar "biochip"-setup in our group have indeed shown an effect of topographies on osteoblast focal adhesions.[21] All topographies were found to decrease the focal adhesion length. Consistent to our findings, squares and grooves with R:G of 1:3 decreased the focal adhesion length the strongest compared to cells on the smooth control. The short focal adhesions were correlating with the highest migration speed on the patterns. However, cells could attach and migrate on all topographies, meaning that the cell-repelling effect we observed in our experiment is not caused by cellular disability to remain on the topography in the first place, yet a result of cells actively avoiding or leaving such surfaces.

Another noticeable effect that can be connected to focal adhesion formation was observed at the edges of the topographical fields. Migration is dependent on the propagation of the leading edge filopodiae that are mainly driven by reorganization of the actin skeleton and formation of focal complexes/adhesions. Once focal adhesions are formed, they are used as an anchoring point for a mechanical shift of the cell in a certain direction (the actual migration). However, entering grooved surfaces filopodiae may follow the continuous ridges, on which focal adhesion are mainly formed,[22] without entering the grooves. On the squared patterns, which do not feature a topographical continuity in any direction, SEM showed filopodial propagation to be occurring at the shortest distance between the squares edges. However, the found cell-alignment bordering the squared area suggests that it is more favorable to evade that pattern than propagation and focal complex formation along the squares.

Although in our experiment cells preferred the smooth surface, it cannot be concluded that nano-topographies in general are cell-repelling. Especially as Fan et al. in a different experimental setup found neuronal cells migrating away from smooth silicon surface onto separated nanoroughness.[23] Such opposite behavior can occur by the difference in the used culturing

material (polystyrene vs. silicon), by difference in topography (isotropic vs. anisotropic), or by a cell-type specificity, as cells from separate lineages tend to differ in properties like size and protein (e.g. integrin) expression. For the organized development of cell-based tissue and organ constructs, it is therefore also interesting to utilize the herein developed set-up to compare the behavior of separate cell-types, which are known to differ in aspects such as size, migration speed or focal adhesion expression (e.g. normal vs. cancer cells), or to investigate preferential migration behavior between different types of biomaterials (e.g. polymer vs. titanium or ceramics).

Conclusion

In conclusion, the use of a multi-patterned biochip setup allows for enhanced evaluation of cell behavior, as compared to uniformly patterned setups. This work for the first time describes cellular ability to actively avoid surfaces featuring certain topographies on submicron and nanometric scale, which cannot be explained by disability of the cells to migrate on the surfaces, or by differences in proliferation. Cells were found to interact primarily with the surface ridges or pillars and rather not with the grooves or pits. Cell preference (e.g. nanogrooves with a ridge to groove ratio of 3:1 wider than 200 nm) and disfavor for certain nanotopographies (e.g. nanosquared surfaces) can be utilized for development and modification of biomaterials used for regenerative medicine approaches.

4

References

1. S.Anil, P.S.A., H. Alghamdi and J.A. Jansen, Dental Implant Surface Enhancement and Osseointegration, in Implant Dentistry - A Rapidly Evolving Practice, I. Turkyilmaz, Editor 2011, InTech. p. 83-108.

2. Svanborg, L.M., M. Andersson, and A. Wennerberg, Surface Characterization of Commercial Oral Implants on the Nanometer Level. Journal of Biomedical Materials Research Part B-Applied Biomaterials, 2010. 92B(2): p. 462-469.

3. Wennerberg, A. and T. Albrektsson, Effects of titanium surface topography on bone integration: a systematic review. Clinical Oral Implants Research, 2009. 20: p. 172-184.

4. Wennerberg, A. and T. Albrektsson, On Implant Surfaces: A Review of Current Knowledge and Opinions. International Journal of Oral & Maxillofacial Implants, 2010. 25(1): p. 63-74.

5. Klymov, A., et al., Understanding the role of nano-topography on the surface of a bone-implant. Biomaterials Science, 2013. 1(2): p. 135-151.

6. McMurray, R.J., et al., Nanoscale surfaces for the long-term maintenance of mesenchymal stem cell phenotype and multipotency. Nat Mater, 2011. 10(8): p. 637-44.

7. Meirelles, L.D.S., P.C. Chagastelles, and N.B. Nardi, Mesenchymal stem cells reside in virtually all post-natal organs and tissues. Journal of Cell Science, 2006. 119(11): p. 2204-2213.

8. van Delft, F.C.M.J.M., et al., Hydrogen silsesquioxane/novolak bilayer resist for high aspect ratio nanoscale electron-beam lithography. Journal of Vacuum Science & Technology B, 2000. 18(6): p. 3419-3423.

9. van Delft, F., et al., Manufacturing substrate nano-grooves for studying cell alignment and adhesion. Microelectronic Engineering, 2008. 85(5-6): p. 1362-1366.

10. van de Sande, F.H., et al., The influence of different restorative materials on secondary caries development in situ. J Dent, 2014.

11. Harrell, F.E., Regression modeling strategies : with applications to linear models, logistic regression, and survival analysis. Springer series in statistics2001, New York: Springer. xxii, 568 p.

12. Biggs, M.J., et al., The effects of nanoscale pits on primary human osteoblast adhesion formation and cellular spreading. J Mater Sci Mater Med, 2007. 18(2): p. 399-404.

13. Rebollar, E., et al., Proliferation of aligned mammalian cells on laser-nanostructured polystyrene. Biomaterials, 2008. 29(12): p. 1796-1806.

14. Yang, J., et al., A High-Throughput Assay of Cell-Surface Interactions using Topographical and Chemical Gradients. Advanced Materials, 2009. 21(3): p. 300-304.

15. Yang, K., et al., Nanotopographical Manipulation of Focal Adhesion Formation for Enhanced Differentiation of Human Neural Stem Cells. Acs Applied Materials & Interfaces, 2013. 5(21): p. 10529-10540.

16. McNamara, L.E., et al., The role of microtopography in cellular mechanotransduction. Biomaterials, 2012. 33(10): p. 2835-47.
17. Wang, N., J.D. Tytell, and D.E. Ingber, Mechanotransduction at a distance: mechanically coupling the extracellular matrix with the nucleus. Nature Reviews Molecular Cell Biology, 2009. 10(1): p. 75-82.
18. Lim, S.T., Nuclear FAK: a new mode of gene regulation from cellular adhesions. Mol Cells, 2013.
19. Teo, B.K., et al., Nanotopography Modulates Mechanotransduction of Stem Cells and Induces Differentiation through Focal Adhesion Kinase. ACS Nano, 2013.
20. Deramaudt, T.B., et al., Altering FAK-Paxillin Interactions Reduces Adhesion, Migration and Invasion Processes. PLoS One, 2014. 9(3).
21. Lamers, E., et al., The influence of nanoscale topographical cues on initial osteoblast morphology and migration. Eur Cell Mater, 2010. 20: p. 329-43.
22. Lamers, E., et al., The influence of nanoscale grooved substrates on osteoblast behavior and extracellular matrix deposition. Biomaterials, 2010. 31(12): p. 3307-16.
23. Fan, Y.W., et al., Culture of neural cells on silicon wafers with nano-scale surface topograph. Journal of Neuroscience Methods, 2002. 120(1): p. 17-23.

4

Supplementary information and data

Model building process

Models for low and high density were built separately. In all cases the adjusted R^2 was used to decide upon inclusion of independent variables in the model.

1. The type of **pattern** was decided to be required for the model. Using "Smooth" as the reference structure, which yielded four indicator variables for the other surface structures: Squared, grooved 3:1, grooved 1:1 and grooved 1:3.

2./3. The **feature** of the structure is related to four distances: pitch, square/ridge width, pit/groove width, and depth. By design of the study these four are highly correlated. Regression models estimate the effects of all its independent variables, corrected for all the other independent variables. This can be seen as the effect of "independent variable X_i" while keeping all the other independent variables constant. In case of highly correlated independent variables this is rather difficult. Therefore, one of the four dimensions was chosen for further modelling. To this end models with the shape parameters were extended with each of the four size parameters. Of these four **groove width** performed best and was included in further models.

4. Next **time** was tested for inclusion in the model. For low seeding observations with Time=4, 24, 48 and 72 were available. For high seeding only T=48 and T=72. For both situations T=72 was used as reference, leaving the other time points as indicator variables. As time conceptually was seen as one variable, the models with full inclusion of the indicator variables were compared to models without time. Both for low and high seeding, Time showed to improve the model.

5. The effect of the dimension is not necessarily the same for all shapes. Therefore it was tested whether a separate groove width size effect for each topographies (that is: **interaction** of **pattern** and **groove width**) did improve the model. This was the case both for low and high seeding.

6. It was tested whether **interaction** of **time** and **groove width** did improve the model. It was for high seeding, but not for low.

7. To allow for **non-linear shapes**, the square of the groove size was added to model. This was an improvement both for low and high seeding.

8. Last, it was tested if **interaction** of **pattern** and **square of groove width** was an improvement of the model. This was the case for both situations.

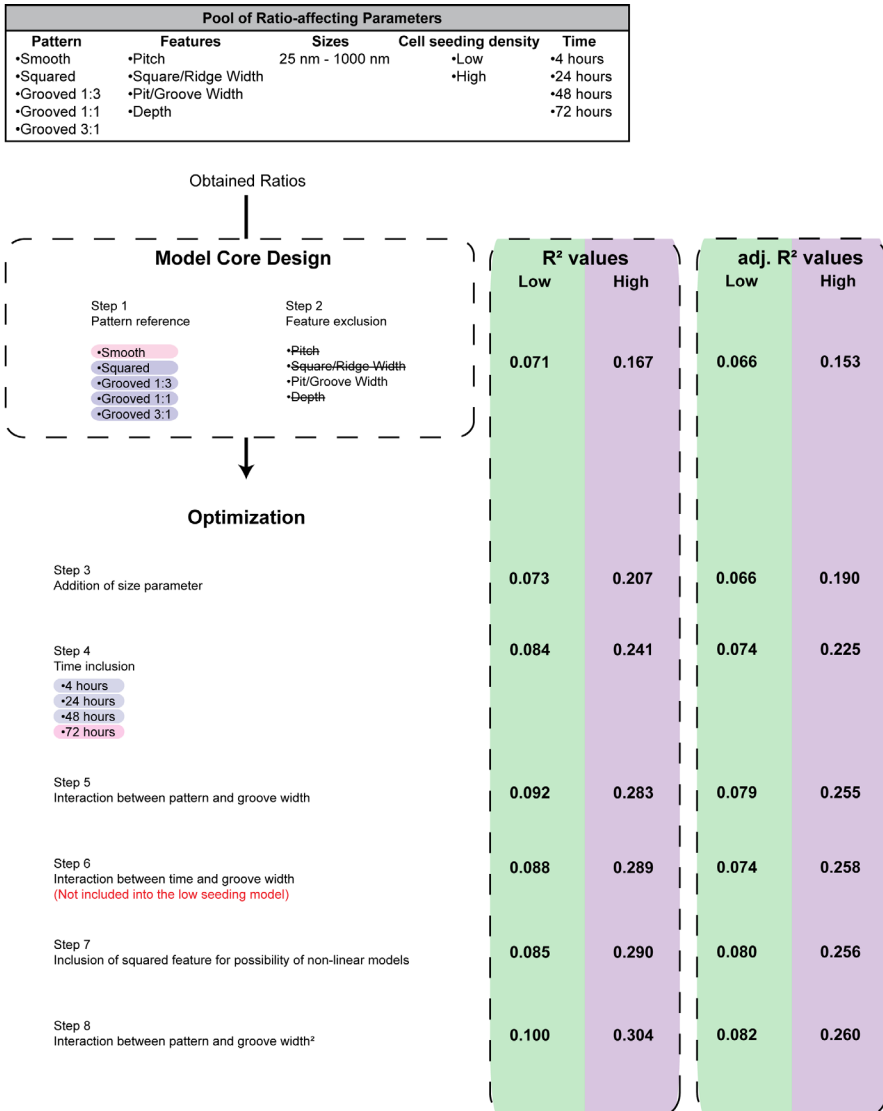| Pool of Ratio-affecting Parameters				
Pattern	**Features**	**Sizes**	**Cell seeding density**	**Time**
•Smooth	•Pitch	25 nm - 1000 nm	•Low	•4 hours
•Squared	•Square/Ridge Width		•High	•24 hours
•Grooved 1:3	•Pit/Groove Width			•48 hours
•Grooved 1:1	•Depth			•72 hours
•Grooved 3:1				

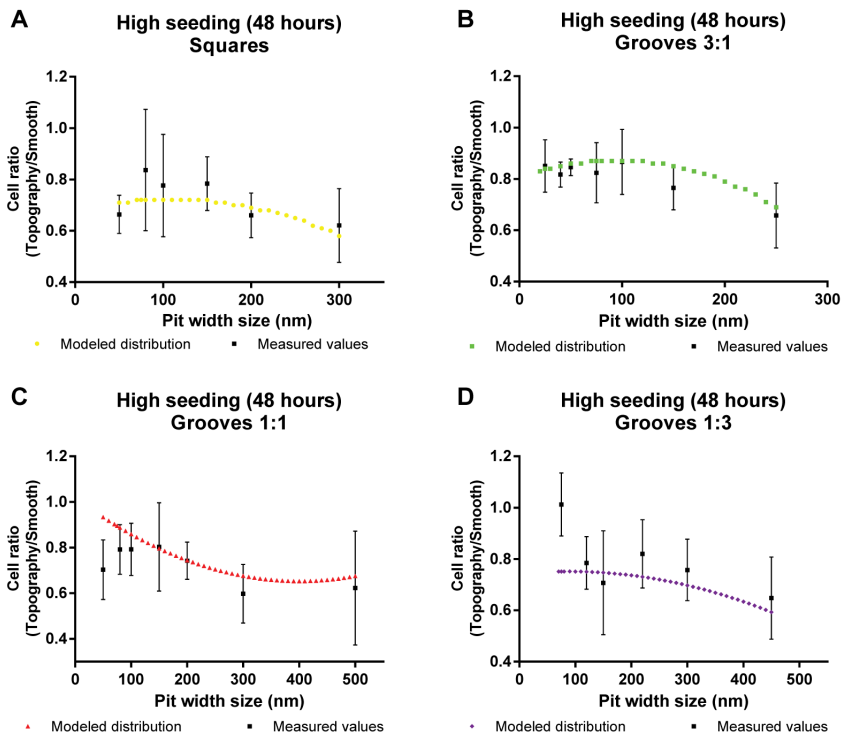**Figure S1: Flowchart of the decision process of the model design.**

Figure S2: The modeled ratios on different topographies as a function of the groove/pit width size in comparison to the experimentally measured values. A) The situation is compared for the low seeding density at 4 hours and B) the high seeding density at 48 hours.

Table S1: Regression analysis models describing cell migrational behavior between topographical fields and smooth surrounding.

Low density model	P	Effect	95,0% Confidence Interval for the Effect	
			Lower Bound	Upper Bound
Constant	0	0,961	0,912	1,01
Pattern (Reference = Smooth)				
Squares	0,089	-0,359	-0,773	0,055
Grooves 3:1	0,874	0,019	-0,218	0,256
Grooves 1:1	0,105	-0,196	-0,433	0,041
Grooves 1:3	0,731	-0,073	-0,487	0,342
Time (Reference = 72 Hours)				
4 Hours	0,243	0,035	-0,024	0,094
24 Hours	0,724	-0,011	-0,073	0,051
48 Hours	0,026	-0,095	-0,178	-0,011
Groove/Pit width				
Size x Squares	0,455	$1,915 \times 10^{-3}$	$-3,11 \times 10^{-3}$	$6,94 \times 10^{-3}$
Size x Grooves 3:1	0,429	$-1,675 \times 10^{-3}$	$-5,832 \times 10^{-3}$	$2,482 \times 10^{-3}$
Size x Grooves 1:1	0,089	$1,806 \times 10^{-3}$	$-0,273 \times 10^{-3}$	$3,884 \times 10^{-3}$
Size x Grooves 1:3	0,762	$-0,518 \times 10^{-3}$	$-3,868 \times 10^{-3}$	$2,832 \times 10^{-3}$
Size² x Square	0,336	$-6,374 \times 10^{-6}$	$-19,386 \times 10^{-6}$	$6,637 \times 10^{-6}$
Size² x Grooves 3:1	0,231	$8,556 \times 10^{-6}$	$-5,47 \times 10^{-6}$	$22,583 \times 10^{-6}$
Size² x Grooves 1:1	0,042	$-3,642 \times 10^{-6}$	$-7,149 \times 10^{-6}$	$-0,135 \times 10^{-6}$
Size² x Grooves 1:3	0,897	$0,383 \times 10^{-6}$	$-5,4 \times 10^{-6}$	$6,166 \times 10^{-6}$

$R^2 = 0,1$

High density model	P	Effect	95,0% Confidence Interval for the Effect	
			Lower Bound	Upper Bound
Constant	0	0,966	0,928	1,004
Pattern (Reference = Smooth)				
Squares	0,216	-0,214	-0,554	0,126
Grooves 3:1	0,385	-0,086	-0,281	0,109
Grooves 1:1	0,195	0,128	-0,066	0,323
Grooves 1:3	0,389	-0,149	-0,489	0,191
Time (Reference = 72 Hours)				
48 Hours	0,003	-0,075	-0,124	-0,026
Groove/Pit width				
Size x Squares	0,618	$1,047 \times 10^{-3}$	$-3,081 \times 10^{-3}$	$5,176 \times 10^{-3}$
Size x Grooves 3:1	0,346	$1,636 \times 10^{-3}$	$-1,781 \times 10^{-3}$	$5,052 \times 10^{-3}$
Size x Grooves 1:1	0,063	$-1,625 \times 10^{-3}$	$-3,338 \times 10^{-3}$	$0,088 \times 10^{-3}$
Size x Grooves 1:3	0,765	$0,418 \times 10^{-3}$	$-2,337 \times 10^{-3}$	$3,172 \times 10^{-3}$
Size x 48 Hours	0,181	$-0,204 \times 10^{-3}$	$-0,504 \times 10^{-3}$	$0,096 \times 10^{-3}$
Size² x Squares	0,477	$-3,86 \times 10^{-6}$	$-14,542 \times 10^{-6}$	$6,822 \times 10^{-6}$
Size² x Grooves 3:1	0,199	$-7,53 \times 10^{-6}$	$-19,045 \times 10^{-6}$	$3,986 \times 10^{-6}$
Size² x Grooves 1:1	0,12	$2,283 \times 10^{-6}$	$-0,596 \times 10^{-6}$	$5,161 \times 10^{-6}$
Size² x Grooves 1:3	0,616	$-1,209 \times 10^{-6}$	$-5,957 \times 10^{-6}$	$3,538 \times 10^{-6}$

$R^2 = 0,304$

5

Increased acellular and cellular surface mineralization induced by nanogrooves in combination with a calcium-phosphate coating

Alexey Klymov, Jiankang Song, Xinjie Cai, Joost te Riet, Sander Leeuwenburgh, John A Jansen and X Frank Walboomers

Introduction

To improve bone-anchoring of dental and orthopedic implants, manipulation of the material surface forms an essential target.[1-4] The use of dedicated topographies has been studied extensively and was found to influence the bone-to-implant response in *in vitro, in vivo* and clinical studies.[5-8] In addition to topography, changing the (bio-)chemical surface properties of the implant material significantly affects its interaction with the host-tissues.[9, 10] In this regard, calcium phosphate coatings are well-described, as they can result in the formation of natural bone-like apatite.[11] Multiple studies confirmed that such coatings significantly improve dental and orthopedic implant performance, by means of enhanced biocompatibility, osteoconduction, or even osteoinduction.[12-14]

The effect of implant surface-configuration on tissue-response starts at cellular and molecular levels,[15] and can be mediated by several mechanisms. For example, conventional surface roughness by grit-blasting might improve the implant function by stimulation of osteogenic differentiation and cellular mineralization, as suggested by an *in vitro* study of Wall et al..[16] The underlying topographical influence on cell-skeleton organization, focal adhesion formation, and associated signaling pathways has been found for features with sizes down to the nano-scale.[17] However, roughness is a rather abstract parameter, which is independent of the structure and form of the measured topography. As an alternative, defined organized topographies were utilized for *in vitro* setups and fine-tuning of cell behavior by variation of the feature shape and size.[18, 19] Especially topographies with features on the submicron and nano-sized scale were studied extensively during the past decade. Due to their dimensions, nanotopographies are thought to interact with cells in a more "natural" manner, resembling interaction with the fibrillar extracellular matrix (ECM).[20]

In addition to the effects of texture, the contribution of calcium-phosphate coatings on implant performance may be dual. On the one hand, CaP can facilitate cell-independent acellular surface mineralization.[21] On the other hand, chemical stimulation of cells can occur through calcium-sensing receptors (CasR), through which differentiation, ECM deposition, and mineralization can be induced.[22] Moreover, a combination of rough texture

5

together with the addition of biochemical cues was shown to synergistically affect cell-behavior.[23, 24]

Although various methods exist to apply a CaP coating onto a material surface, the combination of a coating with an organized uniform nanotopography remains challenging. Due to heterogeneity and thickness, many coating techniques cannot preserve complex nano-structures.[25] Therefore, the current study utilized a controlled "biomimetic" wet calcium-phosphate deposition technique to coat nanogrooved surfaces,[26] in order to evaluate the influence of combined topographical and biochemical cues on cellular mineralization behavior. We postulate (1) that with these thin coatings it will be possible to preserve the topographical structure on nanogrooved surfaces, allowing cellular recognition and adaptation to the topography, and (2) that a combination of topographical and biochemical cues will synergistically increase the mineralization of the surfaces by facilitation of the cellular and the acellular surface mineralization.

Materials and Methods

Substrate Production

Polystyrene solvent casting

A grooved pattern was introduced into a silicon master wafer by means of laser interference lithography as described before.[27] This wafer was then used as a mold for reproduction of the topography into tissue culture plastic by solvent casting. For this purpose, polystyrene (PS, Acros, Geel, Belgium) was dissolved in chloroform in a proportion of 1:6 (w/v) and casted on the silicon master. As controls, smooth surfaces were produced. After evaporation, the substrates were treated by radiofrequent glow-discharge (Harrick, Ossining, USA) in Argon gas for 5 minutes at an atmospheric pressure of about 10^{-2} mbar. Glow discharge treatment increased the wettability and sterilized the polystyrene surfaces. The substrates were used directly for cell culture, or were additionally coated with calcium-phosphate. For the experiments round-shaped substrates (smooth, grooved) with a diameter of 1.1 cm (A ≈ 1 cm²) were punched out.

Calcium Phosphate coating

A wet-chemical coating method was applied, as described previously.[26] In brief, the polystyrene replicates were immersed in a solution at 37°C, which contained 2 mM Na_2HPO_4 (Merck, Darmstadt, Germany), 147 mM NaCl (Merck), 2.5 mM $CaCl_2$ (Merck), and 100 mM urea (Invitrogen, Karlsruhe, Germany). Urease (type III from Jackbeans, U1500-20kU, Sigma-Aldrich, Taukirchen, Germany) was resuspended in a 200 mM Na_2HPO_4 (Merck) buffer solution to a concentration of 1 Unit / μL. Under continuous stirring, urease was added to the solution in a proportion of 1 Unit / mL (600 μl in 600 mL coating solution). After 60 minutes the substrates were washed in 100 % Ethanol and dried to air.

Substrate characterization

Atomic force microscopy (AFM)

An atomic force microscope (Catalyst, Bruker, Santa Barbara, CA, USA) was used to analyse substrates in tapping mode with a 118 μm long silicon cantilever (NW-AR5T-NCHR, NanoWorldAG, Wetzlar, Germany). This type of AFM probe has a nominal resonant frequency of 317 kHz and nominal spring constant of 30 N/m, and is equipped with a high aspect ratio (7:1) portion of the tip with a nominal length of >2 μm and a half-cone angle of <5°. The nominal radius of curvature of the AFM probe tip was less than 10 nm. Height images of each field/sample were captured in ambient air at 50% humidity. The analyzed field was scanned at a rate of 1.0 Hz and 512 scanning lines.

Scanning electron microscopy (SEM)

The substrates were lyophilized and sputter-coated with gold (10 nm thick layer). Surface topography was examined by scanning electron microscopy (JEOL 6310, Jeol, Japan).

Transmission electron microscopy (TEM)

To define the thickness and homogeneity of the coating, the substrates were embedded in Araldite epoxy resin (Huntsman Corporation, Salt Lake City, UT, USA). After polymerization, ultra-thin sections were made and

observed using the transmission electron microscope (JEOL JEM-1010). The thickness of the coating was defined by measuring the distances between the polystyrene and the border of the coating inside the groove, on the side of the walls and on top of the ridge (12 measurements/sample; 3 samples).

Cell-culture

The mouse derived MC3T3-E1 osteoblast-like cell line was proliferated in α Minimal Essential Medium without ascorbic acid (αMEM; Catalog Number A10490-01, Gibco, Invitrogen Corp., Paisley, Scotland) supplemented with 10% fetal calf serum (FCS; F7524; Sigma;), penicillin (100 U/mL) and streptomycin (10 µg/mL) (Gibco). For the experiments, cells were trypsinized (0.25 % w/v trypsin, 0.02 % EDTA; Sigma) and seeded onto the substrates at a density of 10 x 10^3 cells / cm². For the duration of the experiment the cells were maintained in osteogenic medium, i.e. αMEM supplemented with 10% FCS, penicillin (100 U/mL) and streptomycin (10 µg/mL), 200 µM L-ascorbic acid-2-phosphate (Sigma), 10 nM dexamethasone (Sigma) and 10 mM β-glycerophosphate (Sigma). The medium was refreshed twice per week.

Cell morphology, viability and proliferation

LIVE/DEAD assay

Possible cytotoxic effects induced by the coating were analyzed by the LIVE/DEAD assay according to the manufacturer's protocol (Molecular Probes, Leiden, The Netherlands). In short, 1 day after seeding cells on the different substrates (n=3) were incubated in 2 µM calcein acetoxymethyl ester (AM) and 4 µM ethidium homodimer (EthD-1) reagents in conditioned medium for 45 minutes. After incubation, the substrates were washed in fresh stain-free medium for additional 15 minutes. Washed substrates were mounted on a drop of phosphate buffered saline (PBS, Gibco) on microscope slides and were examined using a fluorescence microscope (Axio Imager Microscope Z1, Zeiss, Jena, Germany).

Cell morphology

To assess cellular morphology on the different substrates, cells were

cultured in a density of 1 x 10³ cells / cm² for 1 day (n=3), washed twice with PBS and fixed with 3.3 % paraformaldehyde in PBS for 15 minutes. After fixation the substrates were washed twice and placed in 1 mL PBS permeabilization buffer containing 0.25 % Triton-X 100 (Sigma) and 10% FCS for a period of 15 minutes. Subsequently the cells were washed twice and stained for actin-filaments with phalloidin conjugated with Alexa-568 (Molecular Probes) for two hours diluted (1:250) in PBS containing 10% FCS. After staining the specimens were washed and mounted with DAPI containing Mowiol 4-88 solution (Polysciences Europe GmbH, Eppelheim, Germany), and examined using the Axio Imager Z1 microscope.

Alamar Blue assay

Cell viability of cells cultured on the different substrates (n=4) was followed during the experiment until day 32, according to the manufacturer's protocol (Molecular Probes). In short, a 10% alamar Blue solution was prepared in differentiation medium and 1 mL was used per substrate during a 4 hours incubation period at 37°C. After incubation, the emission fluorescence was measured at a wavelength of 585 nm using a fluorescence microplate reader (Bio-Tek Instruments, Abcoude, The Netherlands).

Total DNA quantification

After 1, 4, 7, 14, 21, 28 and 35 days of culture, the substrates were washed twice with PBS and placed in 0.5 mL distilled water at -80°C. After all time-points were collected, the seeded samples were defrosted and one additional freeze-thaw cycle at -20°C was performed to allow cell-wall permeabilization by crystal formation. The lysate was collected and used for total DNA assay. Cell quantification (n=4) was performed using a double stranded DNA binding fluorophore method according to the manufacturer instructions (PicoGreen dsDNA quantification kit, Molecular Probes). Total DNA concentration was determined by measuring the PicoGreen emission intensity at a wavelenght of 530 nm using a fluorescence microplate reader. Cell osteogenic differentiation

Alkaline phosphatase (ALP) activity

 The expression of the early osteogenesis differentiation marker alkaline

Table 1: Primer sequences used for real-time PCR

Gene	Forward (5'→3')	Reverse (5'→3')
BMP2	CTCCTAAAGGTCGACCATGG	GCAGCCTCAACTCAAATTCG
OC	CCGGGAGCAGTGTGAGCTTA	TAGATGCGTTTGTAGGCGGTC
BSP	TTTATCCTCCTCTGAAACGGT	GTTTGAAGTCTCCTCTTCCTCC
COL I	GCATGGCCAAGAAGACATCC	CCTCGGGTTTCCACGTCTC
OPN	GATGAACAGTATCCTGATGCC	TTGGAATGCTCAAGTCTGTG
GAPDH	CATCAAGAAGGTGGTGAAGC	ATTGTCATACCAGGAAATGAGC

phosphatase (ALP) was measured in the lysates from days 1, 4, 7, 14, 21, 28 and 35, which were obtained as described above. ALP was quantified (n=4) as the turnover of ALP-substrate p-nitrophenyl phosphate into 4-nitrophenol. The concentration of the product after one hour of incubation was relative to the absorbance at a wavelength of 405 nm, which was measured in an ELISA microplate reader (Bio-Tek Instruments). For comparison, the ALP activity was normalized to the amount of DNA in each sample.

Gene expression analysis by quantitative real-time polymerase chain reaction (qPCR)

After 7 and 21 days of culture, samples were collected for gene expression quantification by means of real time polymerase chain reactions (RT-PCR). Osteogenesis-related gene marker expression was evaluated by qPCR. Primers were designed for bone morphogenetic protein 2 (*BMP2*), osteocalcin (*OC*), osteopontin (*OPN*), bone sialoprotein (*BSP*) and collagen type 1 (*COLI*) (Table 1). The specificity of the primers was confirmed separately before the real-time PCR reaction. Total RNA was isolated using the TRIzol method (Invitrogen, Breda, the Netherlands) according to the manufacturer's instruction. The RNA concentration was measured with a spectrophotometer (NanoDrop 2000, Thermal scientific, Wilmington, DE). After the RNA isolation, a reverse transcriptase reaction was performed using Superscript First-strand Synthesis System for RT-PCR (Invitrogen,

Breda, the Netherlands); according to the manufacturer's protocol. The cDNA was then amplified and specific gene expression was quantified using IQ SYBR Green Supermix PCR kit (BioRad, Hemel Hempstead, United Kingdom) in a real-time PCR (BioRad, CFX96™ real-time system) (n≥6). Some results were excluded from further analysis due to evaporation during the process. Relative gene expression was normalized to the expression of the household gene glycerinaldehyd-3-phosphat-dehydrogenase *(GAPDH)* and calculated via the $2^{-\Delta\Delta Ct}$ method.[28]

Mineralization

Calcium concentration quantification

To measure the acellular mineralization in time, non-cell seeded substrates (n=3) were made and treated in the same manner as the seeded substrates regarding incubation and medium refreshment. At days 1, 4, 7 and 14, these substrates were collected and washed twice with PBS and placed in empty 12 wells plates at -80°C until use. The post-lysis substrates that were collected on days 1, 4, 7, 14, 21, 28 and 35 were used for calcium quantification in the seeded situation. Seeded and non-cell seeded substrates were placed overnight in 0.5 mL 1M acetic acid to dissolve the mineral on the surface, thereby releasing Ca-ions. The calcium concentration was determined utilizing the ortho-cresolphthalein complexone (OCPC) method (Sigma). After 10 min of incubation at room temperature absorbance was measured at 570 nm in the ELISA microplate reader.

Visualization and quantification of calcified extracellular matrix area

For visualization of calcified extracellular matrix on the substrate surface, Alizarin Red staining was performed on substrates collected after visual onset of mineralization (Day 21, 28 and 35). The substrates were washed twice with PBS and fixed with 3.3 % paraformaldehyde in PBS for 15 minutes. After fixation the substrates were washed twice and placed in 1 mL of the staining solution (2% Alizarin Red S in PBS; Acros) for 10 minutes and washed with demineralized water allowing the non-specific stain to detach from the substrate. Finally, the substrates were collected and mounted with DAPI containing Mowiol 4-88 solution. The substrates were

5

observed by light and fluorescent microscopy using the Z1 microscope. The mineralization was quantified by measuring the Alizarin Red-positive area, in relation to the total substrate area (n=8).

Statistical analysis

Statistical analysis was performed between all of the four groups using two-way ANOVA with post-hoc Tukey multiple comparisons correction. Moreover, additional comparisons were performed between groups based either on coating or topography. In the graphs a "T" has been used to highlight the days with significant differences based on the topographies (namely smooth non-coated + smooth coated vs. grooved non-coated + smooth coated). Similarly a "C" was used for highlighting significant differences based on the coating (namely smooth non-coated + grooved non-coated vs. smooth coated + grooved coated). Calculations were performed in Prism 6 (GraphPad Software, Inc., La Jolla, CA). A p-value ≤ 0.05 was considered statistically significant.

Results
Substrates

The substrates were characterized and routinely checked for replication and coating quality by means of AFM and SEM (Figure 1 and Table 2). As depicted in the SEM micrographs, the coating consisted of nano-sized nodules, which by visual inspection were homogeneously spread on the polystyrene surface. Since drying of samples is necessary for scanning electron microscopy, the grooves appear wider on the SEM micrographs compared to the data obtained by AFM. AFM data showed that the coating significantly increased the nanoroughness of smooth substrates, as well as of the ridge and groove region of the patterned area. Although the coating did decrease the groove width, no significant changes were found for the pitch or groove depth dimensions. TEM analysis (Figure 2; Table 3) showed that coatings consisted of phases of either low or high electron density. Bright, globular particles of low electron density were surrounded by grey amorphous structures of higher electron density. Coating thickness was measured between 40 nm and 60 nm depending on the location. Still, a

continuous coating inside the grooves, on top of the ridge, as well as on the perpendicular walls was achieved.
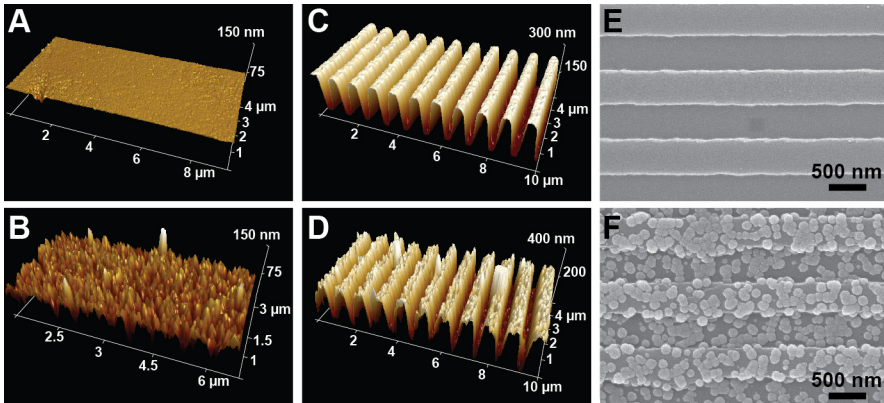

Figure 1: Surface characterization of the four experimental substrate groups. Atomic force micrographs of A) smooth polystyrene surface, B) nanosized grooves on polystyrene, C) calcium phosphate coated smooth surface, and D) grooved surface having the same coating. Scanning electron micrographs of E) grooved non coated and F) grooved coated substrates.

5

Table 2: Characterization of smooth and nanogrooved substrates by atomic force microscopy

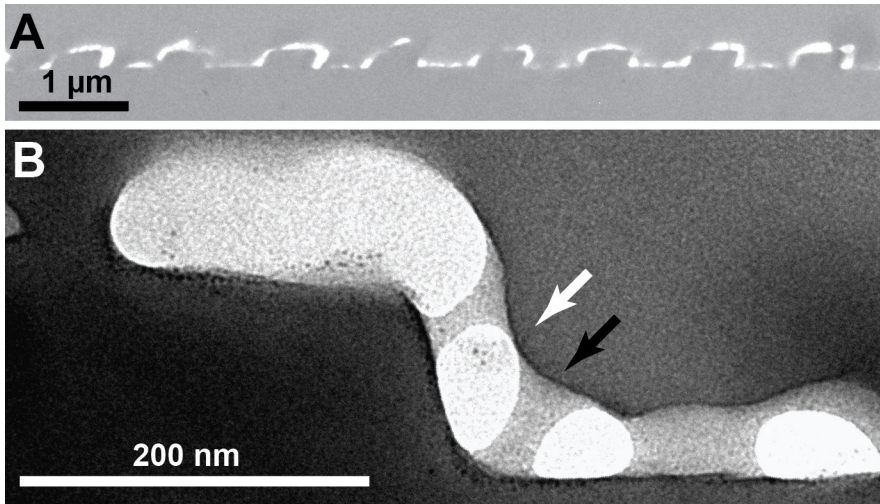|		Non-coated	Coated
Smooth			
	Rq (nm)	0,86 ± 0,2	26,08 ± 6,07
Patterned			
	Pitch (nm)	939 ± 3	943 ± 13
Ridge			
	Width (nm)	489 ± 16	602 ± 36
	Rq (nm)	8,69 ± 3,73	26,2 ± 6,05
Groove			
	Width (nm)	429 ± 21	292 ± 29
	Depth (nm)	186 ± 4	184 ± 7
	Rq (nm)	7,8 ± 3,07	27,73 ± 3,36

Figure 2: Transmission electron micrographs of coated grooved substrates in a cross-section. A) The calcium phosphate coating was found on all of the groove features, i.e. inside the groove, on the walls, as well as on the top of the ridges. B) At higher magnification differences in electron density could be observed, being either nodules of low electron density (white arrow), or amorphous layer of material having a higher electron density (dark arrow).

Table 3: Coating thickness as measured on the transmission electron micrographs

Location	Coating thickness (nm)
Ridge	43 ± 25
Groove	47 ± 35
Wall	65 ± 34

Cell morphology, viability and proliferation

On smooth and smooth coated substrates cells had no noticeable specific cell-body organization (Figure 3a). Contrary, cells on both grooved substrate types aligned parallel to the groove direction, and displayed a spindle-like morphology. No visual differences were found regarding cell spreading and orientation between non-coated and coated substrates.

No stress-related alterations in morphology, such as apoptotic or necrotic blebs, were observed by microscopy for cells cultured on the coated substrates. Cytocompatibility was confirmed by the LIVE/DEAD assay on day 1, which showed almost exclusively viable cells on all of the substrates (data not shown). Also DNA quantification and the Alamar Blue assay showed high cell numbers and metabolic activity, with no differences between all groups in the progress of the experiment (Figure 3b and 3c).

Osteogenic differentiation

Alkaline phosphatase activity

In general, a continuous increase in ALP activity could be measured in time for all of the experimental groups (Figure 4). However, the increase was less strong for the smooth coated substrates, as is evident from day 28. The non-coated topographies on their own were not influencing the ALP activity on any of the timepoints. Contrary, the combination of coating and nanogrooves significantly increased ALP activity compared to smooth coated and non-coated substrates on day 4, and to smooth coated substrates on days 21 and 28. Comparison between smooth and grooved surfaces, independent of the coating, showed significantly higher ALP activity on the grooved substrates on days 4, 21 and 28.

Gene expression analysis by quantitative real-time polymerase chain reaction

The expression of the tested genes on RNA level was measured relative to the smooth group at day 7 and day 21 (Figure 5). At day 7 OPN expression was 1.3-fold higher on grooved coated substrates compared to the smooth control. At day 21, both grooved coated and non-coated groups showed significantly higher expression levels of OC compared to the smooth group.
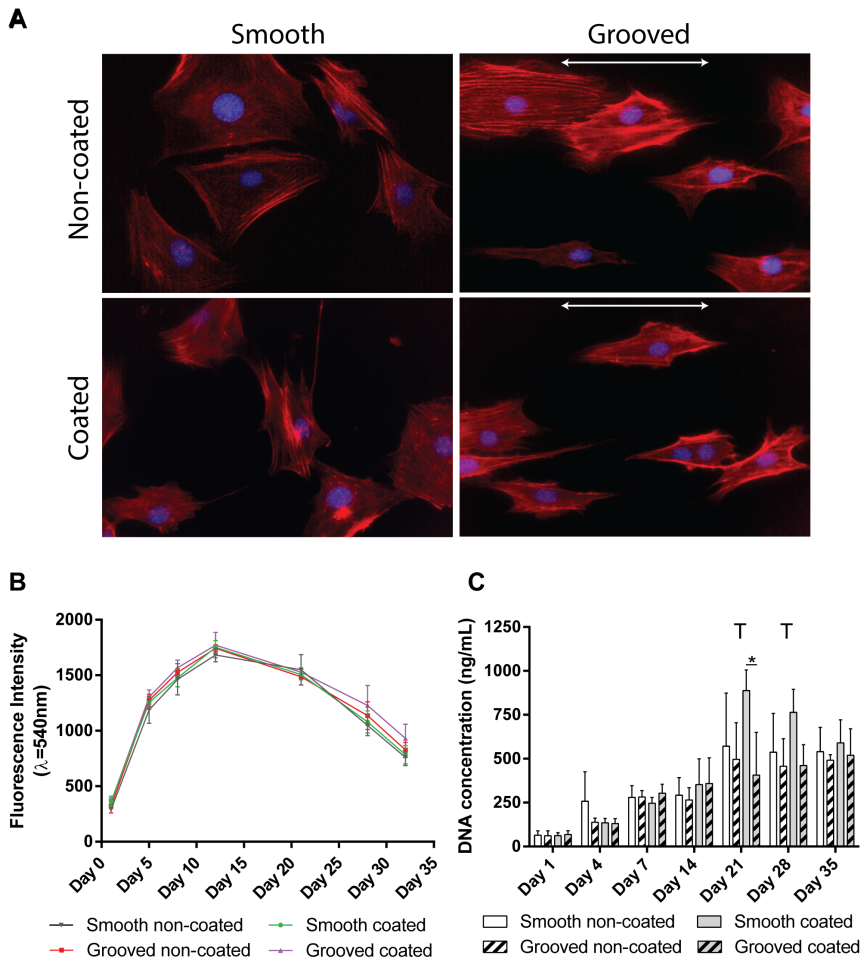
5

Figure 3: Cell morphology, viability and proliferation. A) Fluorescence micrographs of MC3T3 cells on the surface of the four types of substrates after 1 day of culture. The coating did not influence the topographical influence of the grooves (the arrow indicates the groove orientation) on the cell-alignment. B) Regarding viability, cells on the four different substrates behaved similarly, as shown by the Alamar Blue assay C) No differences were found for the total amount of DNA that has been measured on the four different substrates during the first 14 days of culture. Cells on smooth substrates proliferated longer than cells on grooved substrates, as seen at day 21 and 28 (* indicates $p \leq 0.05$; T indicates significance when samples were compared based on topography and independent of the coating; C indicates significance when samples were compared based on coating and independent of the topography).
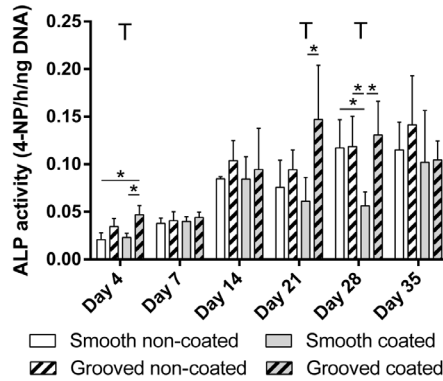
Figure 4: ALP activity as a marker for early osteogenetic differentiation. On day 4, 21 and 28 a significantly higher ALP activity was measured on grooved surfaces (non coated and coated). A synergetic increase in ALP activity was observed on day 4 on the combined nanogrooved and CaP coated substrates. (* indicates $p \leq 0.05$; T indicates significance when samples were compared based on topography and independent of the coating; C indicates significance when samples were compared based on coating and independent of the topography).
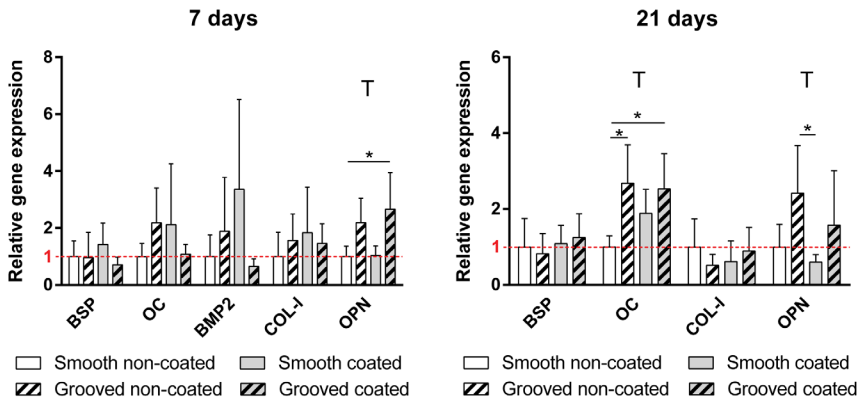

Figure 5: Gene expression at mRNA level as detected by means of qPCR. Bone sialoprotein (BSP), osteocalcin (OC), Bone morphogenic protein 2 (BMP2), Collagen Type 1 (COLI) and osteopontin (OPN), were evaluated at day 7 and day 21 of culture. The red dash line indicates the gene expression level of the reference group (Smooth non-coated). Grooved surfaces (non-coated and coated) significantly increased the expression of OPN on day 7 and day 21, and of OC on day 21. On day 7 a synergetic effect on the expression of OPN is found, which is increased significantly compared to the smooth control. (* indicates $p \leq 0.05$; T indicates significance when samples were compared based on topography and independent of the coating; C indicates significance when samples were compared based on coating and independent of the topography).

The expression level of OPN was significantly higher in the grooved group compared to the smooth coated group. BMP2 gene expression at day 21 was not detectable in all four groups. BSP and COLI gene expression was at a similar level for all groups at both time points.

Comparison of the effects induced by topography or by coating showed that grooves (non-coated and coated) significantly increased the expression of OPN on days 7 and 21, and the expression of OC on day 21. No effect was found for the coating.

Mineralization

Calcium concentration quantification

Acellular surface mineralization was evaluated on substrates that were incubated in osteogenic medium without cells during a period of 14 days (Figure 6a). At day 1 no significant differences were found between the non-coated and coated substrates, with all groups having Ca-concentrations lower than 2 µg/cm². No significant differences were observed also on days 4 and 7. However, between day 7 and day 14 obvious mineralization of the coated substrates has occurred. While the calcium amount on non-coated substrates remained beneath 2 µg/cm^2, the calcium measured on coated substrates increased significantly up to 35 times higher. Moreover, the measured concentration of 70 µg/cm^2 on the grooved coated substrates was significantly higher than the concentration of 40 µg/cm^2 on the smooth coated substrates.

After seeding cells capable of mineralization on the substrates, the cellular mineralization behavior differed considerably from the acellular testing conditions (Figure 6b). At 14 days, cellular mineralization was much less pronounced compared to acellular mineralization. Until day 21, all substrates contain between 1 and 2 µg/cm^2 calcium only. Between day 21 and 28 the cellular mineralization process started in all four groups, reaching average calcium amounts between 19 µg/cm² (smooth non-coated) to 49 µg/cm² (grooved coated). While no increase in total mineral was induced by solely having the topography or coating, on the combined coated and nanogrooved surface was significantly more calcium found compared to the non-coated smooth group on day 28. Independently of

the coating, grooved substrates had significantly higher Ca-concentration compared to the smooth substrates on day 28. At day 35, calcium levels on all substrates increased to an equal level, and no significance between groups could be found anymore.
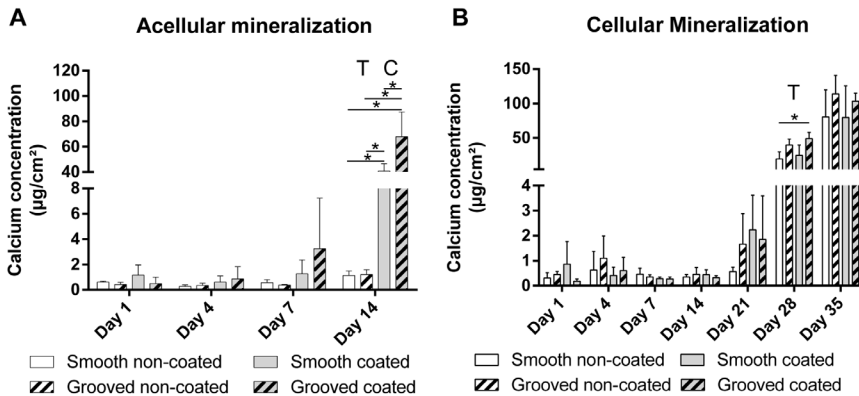

Figure 6: Calcium quantification on the surface of four different substrates. A) Acellular mineralization on non cell-seeded substrates showed a significant increase in calcium on calcium phosphate coated substrates. Synergistic effects were found for the grooved coated surfaces. B) Substrates seeded with MC3T3 cells showed a reduced mineralization capacity compared to the passive mineralization condition. Grooves (non-coated and coated) significantly increased the mineralization compared to smooth substrates at day 28. However, only grooved coated substrates increased the mineralization significantly to the smooth non-coated controls. (* indicates $p \leq 0.05$; T indicates significance when samples were compared based on topography and independent of the coating; C indicates significance when samples were compared based on coating and independent of the topography).

Visualization and area quantification of mineralization

Between 14 and 21 days of seeding, opaque precipitates on the surface of the substrates were formed. Alizarin red staining was used to confirm a calcified nature of the deposited material (Figure 7a). By visual observation, a larger area stained positive on the grooved substrates, compared to the smooth substrates. The staining on the smooth substrates showed slightly elongated mineralization following the direction of the wave-like cell organization that is known to be the result of strong confluence. Calcified deposits on the grooved substrates were clearly aligned in the direction of the grooves. The alignment was maintained until the last time point of 35
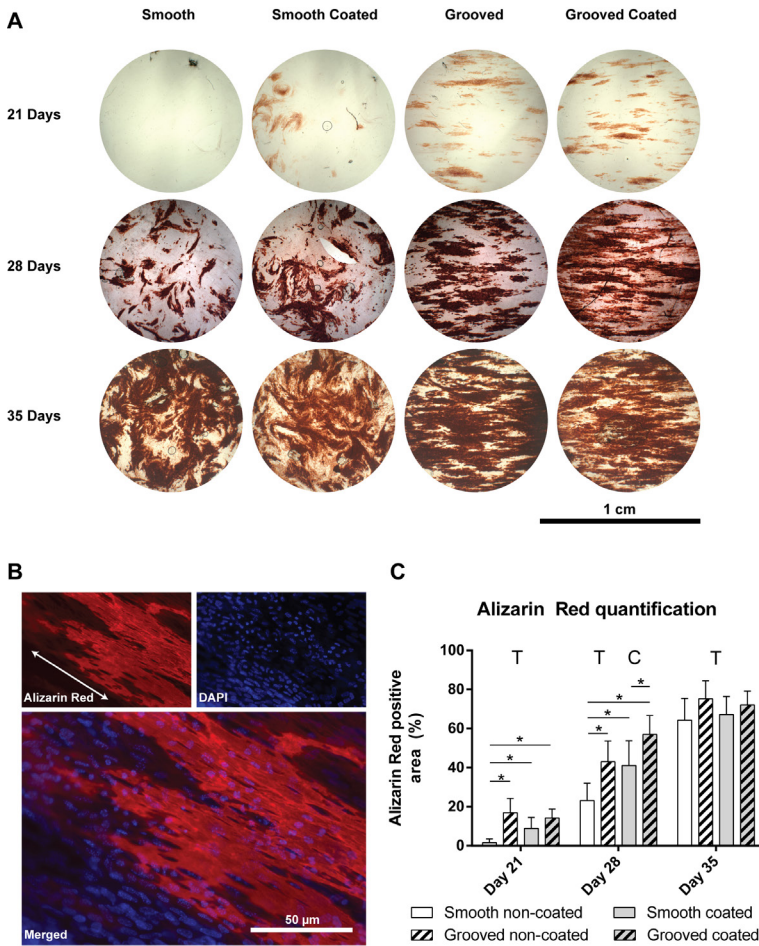
Figure 7: Calcium indicating Alizarin Red staining. A. Light micrographs of the four different substrates after 21, 28 and 35 days of culture. By visual observation the earlier onset of mineralization and alignment of the mineral in the direction of the grooves was found. **B.** Fluorescent micrographs of Alizarin Red stained coated grooved substrate after 28 days of osteoblast-like cells. The mineral (Red) was organized in the parallel direction with the grooves. Cell-nuclei that did not overlap with the mineral staining were elongated in the direction of the grooves. This alignment was lost for most of the cells that overlap with the Alizarin Red signal. **C.** Quantification of the Alizarin Red positive area confirmed the observation. On all observed timepoints the topography (grooves non-coated and coated) showed significantly more calcium staining, compared to the smooth (non-coated and coated) substrates. Additive effects of the coating and topography were found on day 28 on the grooved coated substrates. (* indicates $p \leq 0.05$; T indicates significance when samples were compared based on topography and independent of the coating; C indicates significance when samples were compared based on coating and independent of the topography).

days of culture. In contrast, no organization was found for the Alizarin Red stain on the surface of non-cell seeded substrates, but was homogeneously distributed (not shown). Fluorescent microscopy confirmed the Alizarin Red signal aligning on the microscopic level (Figure 7b). The DAPI stained nuclei were found evenly distributed on Alizarin Red negative and positive area.

The quantification of the complete substrate staining could confirm these observations (Figure 7c). The total Alizarin Red-positive area was significantly higher on the non-coated grooved and the two coated surfaces, compared to the smooth non-coated surfaces, on day 21. In time, the stained area increased on all groups, but also on day 28 the differences remained the same. In addition, significant differences were also found between the smooth coated and grooved coated substrates. After 35 days of culture, no significant differences could be observed anymore between groups. When taking only the topography into account, significance could be found between the smooth and the grooved groups at all time points. For coated versus non-coated groups, only significant difference could be found at day 28.

Discussion

Experimental design

Modern bone-implant are designed to interact with the patient's tissues already on the cellular level, due to the introduction of specific surface mechanical and chemical properties. In order to study such fundamental cell-surface interaction mechanisms and potentially optimize implant surfaces, anisotropic ordered topographies allow for screening studies under highly controlled, reproducible experimental conditions. However, combinations of such fine and complex nano-topographies with the majority of commercially available calcium phosphate coating techniques are difficult, as heterogeneous and thick calcium-phosphate layers may cause a complete loss of the pattern's spatial integrity. Herein, we utilized nano-topography fabrication methods and a wet calcium-phosphate deposition method allowing for the production of four different substrates differing in topographical and/or chemical surface composition. The

substrates were evaluated for their ability to influence the mineralization progress in time in absence, or in presence of mineralizing cells. The findings demonstrated that mineralization was positively influenced by nano-grooves, calcium phosphate coatings, and the combination thereof. However, the mechanisms behind acellular and cellular mineralization are different and seem not necessarily to contribute to a mutual outcome regarding surface mineralization.

 When looking at our setup, the applied urea/urease method produced a reproducible calcium phosphate layer deposition on the polystyrene grooved surfaces. Chemical analysis based on XRD and FTIR, as performed in previous studies employing the same coating method, showed spectra that are typical for crystalline, apatitic calcium phosphate layers.[26] The measured coating thickness was in the range of tens of nanometers, at which no cytotoxic or proliferation-affecting effects were observed. Moreover, during the optimization processes of the method it was found that the thickness of the coating can easily be adapted by slight variation of the protocol, such as urease concentration, steering speed, and coating time. This may allow for coating of surfaces with even more complexity and smaller size aspects than the utilized grooves in this study.

Osteogenic differentiation

Although only smaller effects were induced by the different substrates on proliferation, changes in differentiation behavior were evident. Topographical influence on gene expression was found for several osteogenic markers. Independent of the coating, grooved surfaces increased the ALP activity and the expression of osteocalcin and osteopontin mRNA on several timepoints. Coatings could only increase ALP activity on day 4 in combination with nanogrooves, but this effect appeared synergistic (i.e. larger than the individual contribution of texture and coating alone). Moreover, while free ionic calcium has been shown to increase osteopontin protein expression levels in MC3T3,[29] our coating increased expression only in combination with topography. This might be the result of a different mechanism of action, which is not solely based on the release of calcium-ions from the apatite coating. This observation indicates that the initially applied coating is still present, or has at least induced changes to cellular-

differentiation that can be measured after three weeks of culture.

The mechanisms behind the above-mentioned effects of the used substrates have still to be elucidated. Two separate mechanisms may be triggered by the topography and the coating; i.e. (1) a calcium-responsive pathway (e.g. CasR mediated signaling pathway), and (2) a mechanotransduction mediated pathway (e.g. FAK mediated signaling pathway). Synergistic effects can be caused by simultaneous activation of intracellular pathways targeting the same genes. Moreover, they can influence each other in a direct manner. It was shown that mechanical stimulation can directly activate the CasR and calcium signaling inside cells.[30, 31] Likely, the applied nanotopography acts as a form of "passive" mechanical stimulation, which in term allows a stronger response to the CaP coating.

Mineralization

Regarding the mineralization studies, especially the difference between the non-seeded and cell seeded situations were apparent. Acellular mineralization was shown to drastically increase in the non-seeded situation on coated surfaces, with grooved coated substrates reaching the highest measured calcium concentrations. While the coatings apparently stimulate further mineralization upon soaking in solutions containing calcium and phosphate ions,[32] grooves increase the total surface area. However, in the seeded situation the difference between coated and non-coated surfaces was strongly reduced. The formation of a cellular monolayer, which was formed already at the first day after seeding, may explain the observed phenomenon. The cellular sheets can separate the substrate-surface from the surrounding, thereby hampering the diffusion of calcium and phosphate ions towards the coating surface which ultimately resulted into reduced mineralization rates. This crucial finding allows further speculations about the relevance of the mineralization assessment in Kokubo's simulated body fluid (SBF). Although widely utilized and claimed to be related to *in vivo* bioactivity of a material, the relevance of this method has been questioned as well.[33] The discrepancy observed herein between the two tested situations suggests that the biological response to a material that is brought into a living system will be mainly regulated by cell-driven mechanisms, rather than by passive processes. However, in our

5

experiment coating was seen to contribute to the measured and visualized total calcium. Although the analysis showed that topography was the main property that controlled the calcium amount, a clear synergistic effect is found back for acellular and cellular mineralization.

From the results found in this (and in previous) studies, a hypothetical model can be made for the process occurring during osteogenic culture of cells on the substrates. While coatings actively increase the local calcium concentration, the grooves may function in a passive manner. On smooth surfaces the cell-monolayer seals the surface separating it from the medium. On grooved surfaces the situation is more complex. It has been shown that cells primarily interfere with the nanogrooved topography by focal adhesion formation on top of the ridges leaving out the grooves.[27, 34] This means that a spatial compartmentalization occurs, which separates not only the apical cell space from the medium, but also shields the grooves from each other. Consequently, a heterogeneity concerning the ionic concentrations can occur between separate grooves on the same substrate, after cells begin to secrete mineralization vesicles. This can lead to supersaturation localized inside isolated grooves as opposed to gradual equilibration of calcium on the entire smooth surface. Such a spatially organized mineralization inside nanosized grooves has been reported before by our group, where calcium nodules were found oriented inside the grooves after 8 days of culture [27]. Except explaining the increased mineralization, that observation may be the reason for mineral organization in the herein described experimental setup. Possibly, inside the grooves mineralization can mainly propagate along the grooves and interconnect with increasing mineral amount. Such a hypothesis should be confirmed in future, for instance in experiments making use of substrates with variable groove volume, which should be related to the speed of mineralization onset, and amount of mineral deposited.

Conclusion

Topography and coatings can serve as a fine-tuning method for the behavior of mineralizing cells on the surface of bone implants. Recapitulating, this study showed that a urea/urease controlled system can be used to deposit

thin calcium phosphate coatings onto polystyrene surfaces, preserving the topographical arrangement of an underlining nanostructure. The resulting materials could be used for combinatorial studies on the effect of nanotopography and biochemical cues on acellular and cellular mineralization-behavior. We found the coating to have a tremendous impact on acellular mineralization, which was further increased by the presence of nanogrooves. However, acellular mineralization results were not related to the cellular biological response, which was mainly influenced by the topographical component. In conclusion, the 430 nm groove nanopattern was shown to positively influence the differentiation and mineralization processes, which to some extent could be improved by additional presence of the CaP coating. Besides increasing surface-mineralization, nanogrooves further organized the mineral deposition morphologically. However, these observations should be validated in pre-clinical experimental studies.

5

References

1. Svanborg LM, Andersson M, Wennerberg A. Surface Characterization of Commercial Oral Implants on the Nanometer Level. J Biomed Mater Res B. 2010;92B:462-9.

2. Gaintantzopoulou M, Zinelis S, Silikas N, Eliades G. Micro-Raman spectroscopic analysis of TiO2 phases on the root surfaces of commercial dental implants. Dental materials : official publication of the Academy of Dental Materials. 2014;30:861-7.

3. Liu R, Lei T, Dusevich V, Yao X, Liu Y, Walker MP, et al. Surface characteristics and cell adhesion: a comparative study of four commercial dental implants. Journal of prosthodontics : official journal of the American College of Prosthodontists. 2013;22:641-51.

4. Gittens RA, Scheideler L, Rupp F, Hyzy SL, Geis-Gerstorfer J, Schwartz Z, et al. A review on the wettability of dental implant surfaces II: Biological and clinical aspects. Acta biomaterialia. 2014;10:2907-18.

5. Wennerberg A, Albrektsson T. Effects of titanium surface topography on bone integration: a systematic review. Clin Oral Implan Res. 2009;20:172-84.

6. Wennerberg A, Albrektsson T. On Implant Surfaces: A Review of Current Knowledge and Opinions. Int J Oral Max Impl. 2010;25:63-74.

7. Shalabi MM, Gortemaker A, Van't Hof MA, Jansen JA, Creugers NH. Implant surface roughness and bone healing: a systematic review. Journal of dental research. 2006;85:496-500.

8. Tabassum A, Walboomers F, Wolke JG, Meijer GJ, Jansen JA. The influence of surface roughness on the displacement of osteogenic bone particles during placement of titanium screw-type implants. Clinical implant dentistry and related research. 2011;13:269-78.

9. Forster Y, Rentsch C, Schneiders W, Bernhardt R, Simon JC, Worch H, et al. Surface modification of implants in long bone. Biomatter. 2012;2:149-57.

10. Surmenev RA, Surmeneva MA, Ivanova AA. Significance of calcium phosphate coatings for the enhancement of new bone osteogenesis--a review. Acta biomaterialia. 2014;10:557-79.

11. Habibovic P, Barrère F, Van Blitterswijk CA, de Groot K, Layrolle P. Biomimetic Hydroxyapatite Coating on Metal Implants. Journal of the American Ceramic Society. 2002;85:517-22.

12. Alghamdi HS, Cuijpers VM, Wolke JG, van den Beucken JJ, Jansen JA. Calcium-phosphate-coated oral implants promote osseointegration in osteoporosis. Journal of dental research. 2013;92:982-8.

13. Yokota S, Nishiwaki N, Ueda K, Narushima T, Kawamura H, Takahashi T. Evaluation of thin amorphous calcium phosphate coatings on titanium dental implants deposited using magnetron sputtering. Implant dentistry. 2014;23:343-50.

14. Vercaigne S, Wolke JG, Naert I, Jansen JA. A histological evaluation of TiO2-gritblasted and Ca-P magnetron sputter coated implants placed into the trabecular bone of the goat: Part 2. Clin Oral Implants Res. 2000;11:314-24.

15. Klymov A, Prodanov L, Lamers E, Jansen JA, Walboomers XF. Understanding the role of nano-topography on the surface of a bone-implant. Biomaterials Science. 2013;1:135-51.

16. Wall I, Donos N, Carlqvist K, Jones F, Brett P. Modified titanium surfaces promote accelerated osteogenic differentiation of mesenchymal stromal cells in vitro. Bone. 2009;45:17-26.

17. Teo BK, Wong ST, Lim CK, Kung TY, Yap CH, Ramagopal Y, et al. Nanotopography modulates mechanotransduction of stem cells and induces differentiation through focal adhesion kinase. ACS nano. 2013;7:4785-98.

18. de Peppo GM, Agheli H, Karlsson C, Ekstrom K, Brisby H, Lenneras M, et al. Osteogenic response of human mesenchymal stem cells to well-defined nanoscale topography in vitro. International journal of nanomedicine. 2014;9:2499-515.

19. Lovmand J, Justesen J, Foss M, Lauridsen RH, Lovmand M, Modin C, et al. The use of combinatorial topographical libraries for the screening of enhanced osteogenic expression and mineralization. Biomaterials. 2009;30:2015-22.

20. Kim J, Kim HN, Lim KT, Kim Y, Seonwoo H, Park SH, et al. Designing nanotopographical density of extracellular matrix for controlled morphology and function of human mesenchymal stem cells. Scientific reports. 2013;3:3552.

21. van der Wal E, Vredenberg AM, Ter Brugge PJ, Wolke JG, Jansen JA. The in vitro behavior of as-prepared and pre-immersed RF-sputtered calcium phosphate thin films in a rat bone marrow cell model. Biomaterials. 2006;27:1333-40.

22. Yamauchi M, Yamaguchi T, Kaji H, Sugimoto T, Chihara K. Involvement of calcium-sensing receptor in osteoblastic differentiation of mouse MC3T3-E1 cells. American journal of physiology Endocrinology and metabolism. 2005;288:E608-16.

23. Zhang W, Wang G, Liu Y, Zhao X, Zou D, Zhu C, et al. The synergistic effect of hierarchical micro/nano-topography and bioactive ions for enhanced osseointegration. Biomaterials. 2013;34:3184-95.

24. Liu J, Wang X, Jin Q, Jin T, Chang S, Zhang Z, et al. The stimulation of adipose-derived stem cell differentiation and mineralization by ordered rod-like fluorapatite coatings. Biomaterials. 2012;33:5036-46.

25. Yang Y, Kim KH, Ong JL. A review on calcium phosphate coatings produced using a sputtering process--an alternative to plasma spraying. Biomaterials. 2005;26:327-37.

26. Nijhuis AW, Nejadnik MR, Nudelman F, Walboomers XF, te Riet J, Habibovic P, et al. Enzymatic pH control for biomimetic deposition of calcium phosphate coatings. Acta Biomater. 2014;10:931-9.

5

27. Lamers E, Walboomers XF, Domanski M, te Riet J, van Delft FC, Luttge R, et al. The influence of nanoscale grooved substrates on osteoblast behavior and extracellular matrix deposition. Biomaterials. 2010;31:3307-16.

28. Livak KJ, Schmittgen TD. Analysis of relative gene expression data using real-time quantitative PCR and the 2(T)(-Delta Delta C) method. Methods. 2001;25:402-8.

29. Wu X, Itoh N, Taniguchi T, Nakanishi T, Tanaka K. Requirement of calcium and phosphate ions in expression of sodium-dependent vitamin C transporter 2 and osteopontin in MC3T3-E1 osteoblastic cells. Biochimica et biophysica acta. 2003;1641:65-70.

30. Walker LM, Publicover SJ, Preston MR, Ahmed MAAS, El Haj AJ. Calcium-channel activation and matrix protein upregulation in bone cells in response to mechanical strain. Journal of cellular biochemistry. 2000;79:648-61.

31. Sauer H, Hescheler J, Wartenberg M. Mechanical strain-induced Ca2+ waves are propagated via ATP release and purinergic receptor activation. Am J Physiol-Cell Ph. 2000;279:C295-C307.

32. Dey A, Bomans PH, Muller FA, Will J, Frederik PM, de With G, et al. The role of prenucleation clusters in surface-induced calcium phosphate crystallization. Nature materials. 2010;9:1010-4.

33. Bohner M, Lemaitre J. Can bioactivity be tested in vitro with SBF solution? Biomaterials. 2009;30:2175-9.

34. Lamers E, van Horssen R, te Riet J, van Delft FCMJM, Luttge R, Walboomers XF, et al. The Influence of Nanoscale Topographical Cues on Initial Osteoblast Morphology and Migration. European cells & materials. 2010;20:329-43.

6

Nanometer-grooved topography stimulates trabecular bone regeneration around a concave implant in a rat femoral medulla model

Alexey Klymov, Joost te Riet, Peter Mulders, Han Gardeniers, John A Jansen and X Frank Walboomers

Introduction

Musculoskeletal disorders belong to the most common disability conditions affecting more than 8% of the global population.[1] Annually, more than 50 million incidents occur worldwide of which around 10 million require operative procedures including fracture repair and the placement of metallic reconstructive devises.[2] In addition, about one million dental implants are placed worldwide yearly in edentulous patients.[3] While current survival rates of modern titanium implants reach numbers above 95% during a period of 5 years, the success in elderly and compromised patients is significantly lower.[4-6] Moreover, the chance for implant-failure is steadily increasing with the wearing time.[7, 8] As the aging of the western society continues, the healthcare systems will eventually be faced with the problem of reduced implant success rates. Therefore, next generation implants will need to last over a longer period of time and moreover, considering age related diseases like diabetes and osteoporosis, will need to be adapted to compromised situations. For this purpose, optimizing the interface between the implant and the patients' bone seems a promising strategy.

Especially the positive osseointegrative effects of surface topography have been widely recognized. Nearly all modern implants display some sort of surface roughness, which is usually introduced using common industrially applied implant manufacturing methods (i.e. grit-blasting, acid etching, machining).[9, 10] In general, surface topographies are thought to directly influence cell-behavior of bone-forming cells by mechanical stimulation and interaction with the intracellular signaling pathways mediated by focal adhesions.[11] However, a disadvantage of roughness is the difficulty of characterization, the identification of relevant features needed to induce certain cell-behavior, and therefore the optimization of these features. An improvement of this situation could be the utilization of strictly defined, organized and ordered topographies.

Multiple *in vitro* studies have shown the potential of ordered topographies to directly interact with bone-forming cells.[12-14] Especially grooves with submicron and nano-dimensions were found to be promising in inducing strong effects on osteogenic differentiation and increased mineral

6

deposition *in vitro*.[15-20] The same studies show that the magnitude of such an influence is directly related to the groove/ridge sizes. However, the translation of knowledge, obtained from these *in vitro* studies, to crucial pre-clinical studies occurs rarely. One study that has evaluated the effects of submicron and nano-sized grooves on bone regeneration *in vivo* was performed by Prodanov et al..[21] For the experiment, nanogrooves with groove widths between 75 nm and 500 nm were introduced into flat titanium discs by nanoimprint lithography, which were then compared to conventional grit-blasted/acid etched surfaces. The implants were installed onto the cortical bone of rabbit tibia and the bone-to-implant contact was evaluated 4 and 8 weeks after implantation. The authors found a significantly higher bone-to-implant contact on 225 nm wide grooves compared to the control at the early timepoint. However, as bone-implants are generally not planar, and for a major part in contact also with trabecular bone, the described experimental setup has only limited clinically relevance.

In order to mimic the clinical situation, the here presented study was aimed to produce cylindrical implants with nanosized topographies featured on the entire surface. The effects of clinically applied rough surfaces (Rq = 1.6 µm) were compared to nanogrooves (pitch/groove width/depth: 300/150/50 nm and 1000/200/60 nm) regarding their osseointegrative capacity. The implants were implanted in a rat femoral medulla model,[22] and evaluation of bone regeneration was performed after 4 and 8 weeks by histomorphometry.

Material and Methods

Implant production

Figure 1 shows the manufacturing method for the implants. Two silicon wafers were processed by means of laser interference lithography for the production of two different grooved patterns (ridge:groove; 150:150 nm and 800:200 nm), as described before.[23] For a control surface, a rough pattern was introduced in a titanium plate by grit-blasting. The wafers and the titanium plate were used as master-templates for reproduction of the surface topographies into a thin layer of silicone rubber Polydimethylsiloxane

(PDMS; Elastosil RT 601, Wacker-Chemie, München, Germany). Afterwards, the replicate was rolled up inside a tubular mold for the final production of cylindrical implants. Implants were then cast using a two-component epoxy resin (Araldite/Aradur; Huntsman Corporation, Salt Lake City, UT), resulting in a final dimension of 2,4 mm Ø x 5 mm. Implants were coated with a 20 nm thick titanium layer by using a 6 kW supersource electron-beam system (Temescal, Livermore, CA), at an evaporation speed of 250 picometer/sec. For sterilization the implants were gamma irradiated with a radiation dosage between 25 kGy and 50 kGy (Synergy Health, Ede, Netherlands).
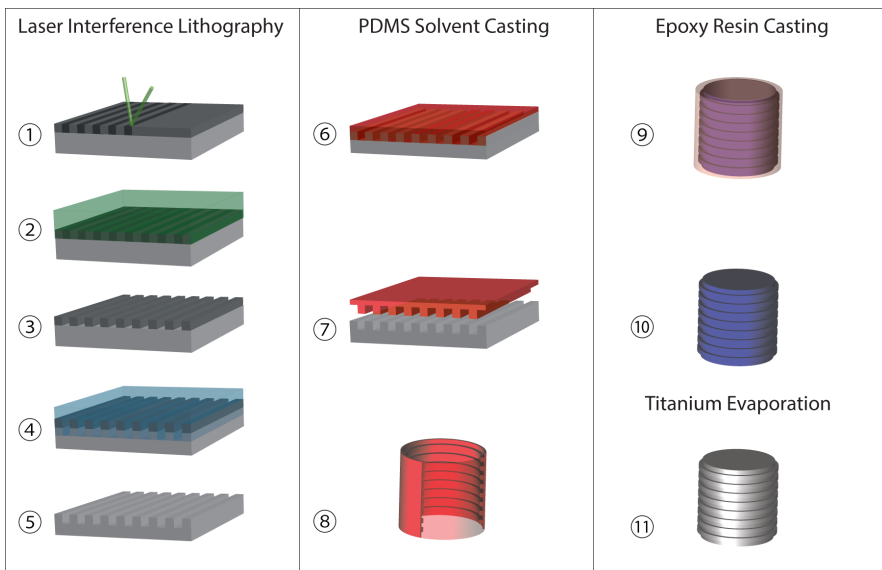

Figure 1: Schematic representation of the nanogrooved implant production. (1) A grooved pattern was written into a photoresist by interference of two laser-beams. (2) The reacted resist was removed. (3) The silicon wafer surface was exposed within the areas that were written into the resist. (4) The exposed silicon was etched to a desired depth. (5) After the remaining resist was removed, the silicon wafer featured the pattern of interest. (6) The wafer was used as a mold for replication of the topography into silicone rubber. (7) After polymerisation, the silicone rubber was be peeled off from the wafer. (8) The flexible PDMS replicate was introduced into a tube, delivering a curved nanogrooved hollow mold. (9) The mold was filled with an epoxy-resin. (10) After polymerization the rubber was peeled off, leaving the polymeric implant. (11) In the last step the implant was evaporated with a thin layer of titanium .

Implant characterization and quality control

The implants were characterized and quality control was performed by means of atomic force microscopy (AFM), electron microscopy and profilometry. For AFM (Catalyst, Bruker, Santa Barbara, CA, USA) the analysis was done in tapping mode with a 118 µm long silicon cantilever (NW-AR5T-NCHR, NanoWorldAG, Wetzlar, Germany) with average nominal resonant frequencies of 317 kHz and average nominal spring constants of 30 N/m. This AFM probe has a high aspect ratio (7:1) portion of the tip with a nominal length of >2 µm and a half-cone angle of <5°. Nominal radius of curvature of the AFM probe tip was less than 10 nm. The analyzed field was scanned at a rate of 1.0 Hz and 512 scanning lines.

For scanning electron microscopy (SEM) the substrates were sputter-coated with gold and surface topography was examined by a JEOL 6310 SEM (Jeol, Tokyo, Japan).

To examine the titanium layer, the substrates were embedded in araldite. After polymerization, ultrathin sections were made and observed by transmission electron microscopy (JEOL JEM-1010).

The roughness Rq of the control implants was assessed with the Universal Surface Tester (UST, INNOWEP GmbH, Würzburg, Germany).

Cytocompatibility test

Rat bone marrow cells (rBMCs) were obtained from femurs of 6 week-old male Wistar WU rats according to local ethical approval (RU DEC 2012-317). Femurs were washed three times in α Minimal Essential Medium (αMEM; Gibco, Invitrogen Corp., Paisley, Scotland) containing 0.5 mg/mL gentamycin (Gibco) and 3mg/mL fungizone (Gibco). The epiphyses were removed and cells were flushed out from the diaphyses using αMEM supplemented with 10 % fetal calf serum (FCS; Sigma F7524, Taukirchen, Germany), and penicillin (100 U/mL) and streptomycin (10 µg/mL) (Gibco). One day after incubation, non-adherent cells were removed and the medium was refreshed. Cells were allowed to proliferate for 6 days, were collected by trypsinization (trypsin/EDTA; 0.25% w/v trypsin, 0.02% EDTA; Sigma) and seeded onto the implants in a density of 5×10^3 cells/cm² in 24 wells plates. At day 1 after seeding LIVE/DEAD assay (Molecular Probes,

Leiden, The Netherlands) was performed according to the manufacturer's manual. After staining the cells were washed with PBS and evaluated without fixation using a Zeiss fluorescence microscope (Axio Imager Microscope Z1, Carl Zeiss Micro Imaging GmbH, Göttingen, Germany).

Animal experiment

The study was performed according to the guidelines for animal care in the Netherlands and was approved by the Radboud University Nijmegen Medical Center Animal Committee (DEC- 2013-121). Male Wistar rats with a pre-surgical weight of approximately 350 grams were used. All surgeries were performed under sterile conditions and general anesthesia (Isoflurane). To reduce post-operative pain, Rimadyl (5 mg/kg body weight) was administered subcutaneously before surgery and on day 2 and 3 after surgery. In addition, Temgesic (0.02 mg/kg body weight) was administered immediately after surgery. Bone implantation was performed as described before.[22, 24] In short, into the patella-femoral groove a cylindrical hole (diameter: 2.5 mm and depth: 7 mm) was drilled parallel to the long femoral axis. The wider dimension of the drilled cavity was chosen to avoid the destruction of the topography and titanium coating that can occur during a press fit implant insertion. The depth dimension chosen for implantation was to avoid direct implant - growth plate contact. The implants were placed into the trabecular bone of the femoral condyle protruding inside the medullar cavity and the wound was closed with sutures. The experiments were randomized and blinded. At 4 weeks and 8 weeks the rats were sacrificed by CO_2 suffocation, the femurs were retrieved and used further for fixation and histological staining.

Histological evaluation

The explanted femurs were fixed in a 10% formalin solution for a period of 1 week. After fixation the samples were dehydrated in ascending grades of alcohol from 70% to 100%, and embedded in poly(methyl methacrylate) resin. After polymerization, cross-sections were prepared with a thickness of approximately 10 µm parallel to the long axis of the implant. A series of at least three sections was made per substrate using a modified sawing

6

microtome technique, as described previously.[25] The sections were stained with Methylene Blue and Basic Fuchsin. Image acquisition was performed using a slide scanner (Pannoramic SCAN, 3DHISTECH Kft., Budapest, Hungary). Image analysis was performed with Image Pro Plus 6 (Media Cybernetics, Rockville, MD). For the analysis of the bone-volume around the implant, positively stained bone in the peri-implant distance of 100 μm was quantified. Quantification was performed individually for each slide on both patterned sides of the implant. Areas that were found to be in contact with cortical bone were excluded from further quantification. The means from multiple slides of the same sample were averaged and used for statistical analysis. Statistical analysis was performed using GraphPad Instat (GraphPad Software, San Diego, California, USA). Differences in bone volume were calculated using two-way ANOVA with post-hoc Tukey analysis. Significance was considered at $p < 0.05$. Values are presented as absolute means with standard deviations.

Results

Implant quality control

Since the surface topography caused breaking of the reflecting light, implants with a poorly transferred surface topography could immediately be recognized by visual inspection, and were removed (Figure 2). Further inspection by scanning electron micrographs revealed an excellent reproduction quality of the rough and grooved surfaces (Figure 3A-C). Transmission electron microscopy confirmed a continuous thin titanium layer of approximately 20 nm in thickness on the surface of the implants (Figure 3D). While gamma irradiation had no influence on surface topography, a change of the material color was observed from white transparent to yellow transparent. Figure 3E-G shows the atomic force microscope reconstruction of the three titanium coated surfaces. The topographical feature sizes as measured by AFM and UST are reported in Table 1.

Figure 2: The produced curved rods with topographies (from left to right: Rough, 150 nm grooves, 200 nm grooves). The light breaking effect of the patterns allowed a fast elimination of implants having not properly replicated topographies. In the next step the implants were shortened to the necessary dimensions.
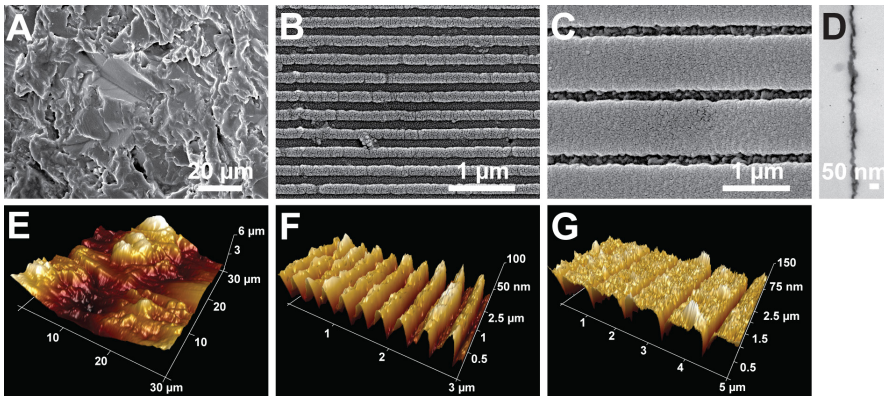

Figure 3: Characterization and quality control of the produced implants. Scanning electron micrographs of (A) Rough, (B) 150 nm, and (C) 200nm grooved implants. (D) The transmission electron micrograph analysis showed the thin titanium layer on the surface to be approximately 20nm in thickness. Atomic force microscopy was utilized to characterize the surface feature characteristics of (E) Rough, (F) 150 nm, and (G) 200 nm grooved implant surfaces.

Table 1: Characterization of titanium coated bone implants

	Rq	Pitch	Groove width	Groove depth
Topography				
Rough	1.6 ± 0.1 µm			
150 nm		302 ± 2 nm	150 ± 5 nm	47 ± 8.3 nm
200 nm		1003 ± 6 nm	205 ± 32 nm	67.7 ± 3.5 nm

In vitro cell viability and cell-implant interaction

LIVE/DEAD staining showed abundant green calcein staining, indicating all implants were cytocompatible. Figure 4 shows cells on rough and 200 nm grooved implants. The cells were strongly separated on rough implants, displaying small amorphous cell-bodies. Contrary, cells on the grooved implants were found more often interconnected, and featured a strongly spread morphology. No further assessment of cell morphology was performed, as this was the topic of previous *in vitro* reports.[23, 26]

General observations animal study

No visible complications could be observed after surgery concerning animal health or behavior. Wound closing occurred without complications. Also no signs of severe inflammation or other adverse tissue reactions were seen. Multiple samples were used for a biomechanical test to determine implant-bone fixation, which proved unsuccessful, and therefore was abandoned. This resulted in n = 6 to n = 10 for the subsequent histomorphometric evaluation.

Histological and histomorphometrical evaluation

Histological analysis confirmed that the implants were surrounded by trabecular bone. In between the voids of the bone trabeculae bone marrow was present. All implants were found to be intact. The trabecular bone was in direct contact with the implant surface without the presence of an intervening fibrous tissue layer. Subjectively, no major differences were seen between the various implant surfaces. During implantation time (4 vs. 8 weeks), the amount of bone at the implant surface appeared to increase (Figure 5).

Figure 6 shows the results from the quantification of osseointegration at a distance of 100 μm on the peri-implant area. The measured mean bone volume was found to be statistically equal between the various implant surfaces after 4 weeks of implantation, i.e.39 % (SD = 11) for the rough, 44% (SD = 10) for the 150 nm grooved patterned and 47% (SD = 12) for the 200 nm grooved surfaces. The histomorphometric evaluation confirmed that a significantly higher bone content was present after 8 weeks (44%; SD
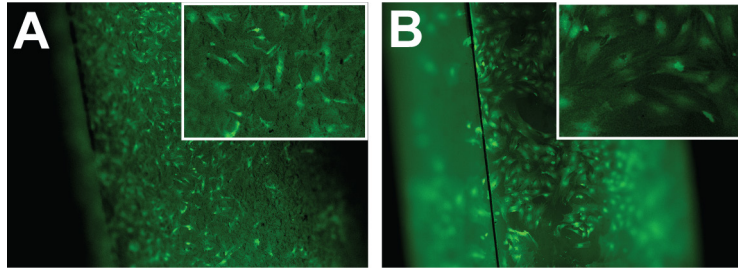
Figure 4: Calcein-AM staining of rat bone marrow derived cells showing cytocompatibility after 1 day of culture on (A) Rough and (B) 200 nm grooved implants. Also note that cells on the rough surface were strongly separated and displayed amorphous cell-body organization, while cells on the grooved implants were found grouped and spread-out.
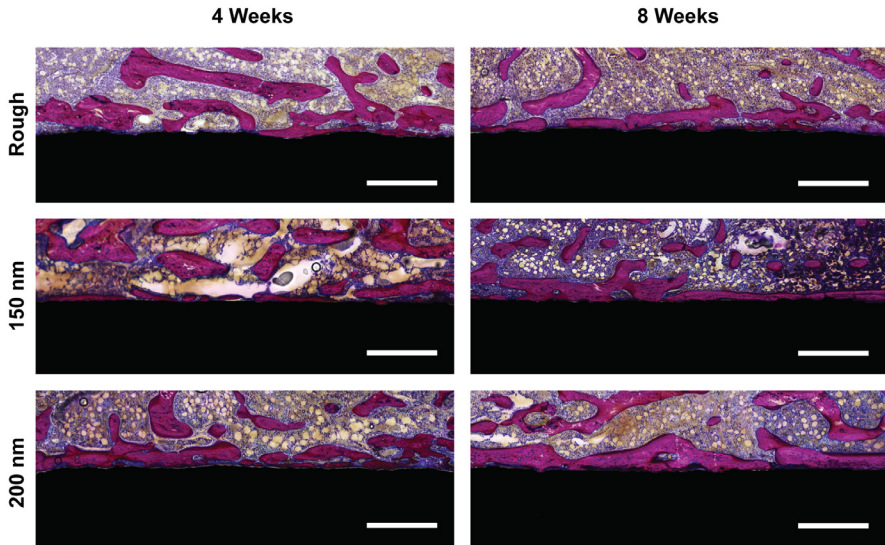

Figure 5: Trabecular bone response to implants 4 and 8 weeks after implantation. Methylene blue and basic fuchsine staining showed in general trabecular bone making direct contact with the implant surfaces and an overall increase in total bone volume around the implants between 4 and 8 weeks (Implants are blacked out). The scale bar represents a distance of 500 μm.

= 11) compared to 4 weeks (57%; SD = 13) (pooled data, p=0,0006). Further analysis of the separate data revealed that only for the 200 nm grooved pattern the increase in bone between 4 weeks (47%; SD = 12) and 8 weeks (65%; SD = 7) was significant. In addition, comparison of the 8 week data showed the presence of a significantly higher bone volume around the 200 nm surface (65%; SD = 7), compared to the rough control (49%; SD = 15).
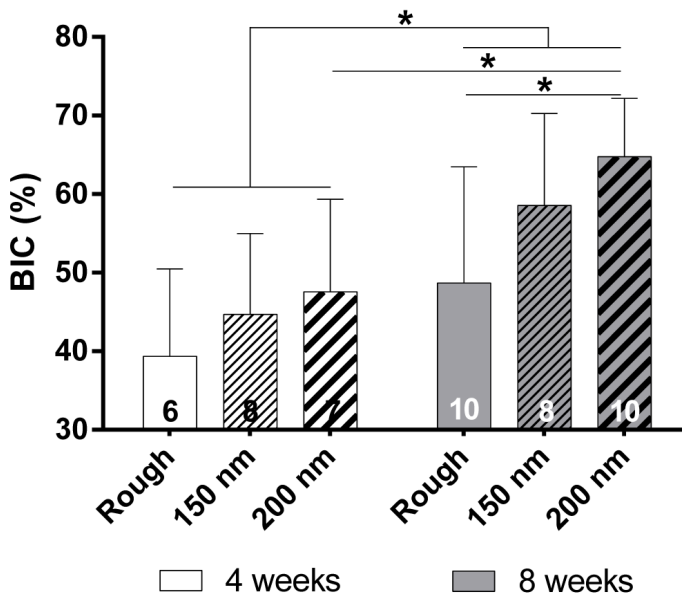
Figure 6: Representation of the obtained trabecular bone-positive area, in the peri-implant area of 100 μm. In general the bone to implant contact increased between 4 and 8 weeks. A significant difference between grooves and the control rough surface was only observed for the 200 nm pitch pattern at week 8. Moreover, the 200 nm pitch pattern is the only one significantly increasing the bone-positive area between week 4 and week 8.

Discussion

While modern clinically available implants still mostly feature low-tech rough surfaces, research evidences the potential of organized nanogrooves to outperform random roughness regarding stimulation of bone-regeneration relevant cell-behavior. However, the limitations of introducing nanotopographies into complex titanium surfaces, such as used in implantology (e.g. circular implants), make production of samples for pre-clinical evaluation rather difficult. In the present study, we used an epoxy resin that was polymerized in a circular nano-patterned mold, resulting in a round-shaped implant. The implants were coated with a thin titanium layer, and were evaluated for their osseointegrative potential in a rat-femoral medulla model. We found that one of the nanogrooved implants was able to outperform rough implants regarding the quantified trabecular bone volume around the implants.

Considering our experimental setup, several remarks can be made. As stated above, in the current study no bulk titanium was used for the production of the implant core. Araldite was chosen, as it is an excellent material for reproduction of surface topographies, while being found compatible in *in vitro* and *in vivo* setups.[27, 28] Moreover, it is known that nanotopographies have the potential to influence signaling and activity of inflammatory cells, which may interfere during the osteointegrative process.[29] However, high cytocompatibility of the material was confirmed by the DEAD/ALIVE assay in our experiments on all patterns. Moreover, in order to study biocompatibility implants were also brought in direct contact with soft tissues, by implanting them into subcutaneous pockets (data not shown). After 4 weeks of implantation, all implants were found covered with a fibrous capsule with a thickness of approximately 50 μm. No signs of chronic inflammation were found in histologically stained sections. The findings suggest excellent soft tissue biocompatibility of the topographies and the polymeric/titanium material.

In general, the production method was highly reliable and resulted in implants of uniform size and shape. The used resin for the production of implants has excellent reproductive properties and probably can be used for the replication of structures that are smaller than the here described.

6

However, Araldite implants are not clinically relevant, as this resin is not used for clinical applications as bone implants. Therefore, Araldite implants were deposition with a thin titanium layer. Although such manufacturing pathway allows for a fast production of a wide range of patterns on complex curved objects, also the production methods of actual clinically applicable implants should be developed further. The methods would need to allow for manufacturing of nanotexture over large surface areas of metals under strongly controlled conditions. Recently the laser-shock nanoimprinting method was presented that might allow the introduction of ordered nano-topographies directly into metals.[30] Utilizing this technique for the production of patterned implants made from bulk titanium in the form of conventional implants, would allow a setup more comparable to the clinical situation for future studies. This would also avoid the possibility of delamination of the titanium coating. Although we found no evidence of such an event, we can also not prove the presence and stability of the titanium coating after implantation in the current model.

 While clinical implants are mostly placed using the standard undersized technique (drilled cavity undersized in the relation the implant diameter), in the current study we were placing the implants in a wider cavity to avoid destruction of the topography and coating by the extremely dense cortex. Such variation of the implantation protocol might eventually induce a different bone-response. However, having an entirely titanium made implant will allow the application of the regular technique, with reduced chances of damaging the fine surface features. It should also be considered that eventually the topographies have to be manufactured on surfaces of implants that are designed for specific treatments. For example for dental applications screw-type implants are usually used, as to date they have proven to provide an optimal implant fixation.

In addition to being more clinically relevant, titanium would be more practical during histomorphometric analysis. In general, quantification of the bone-to-implant contact (BIC) should be considered optimal for studies that are interested in the effects of the substrate-surfaces on bone-regeneration. However, as BIC is representing a single line between the implant and the bone tissue, such method was unpractical for our sections, as due to the transparent nature of the resin the exact border of the implant was often

difficult to define. However, also the quantification of the bone volume in the peri-implant area of up to 500 µm is often performed in bone implant optimization studies. Since surface patterns are known to trigger cell-signaling, which can influence cellular behavior also on longer distances,[29] quantification of the bone volume would be a rational parameter to assess also in our study. However, due to the proximity of the cortex to the medulla region, it is impossible to reliably measure the trabecular bone volume including such distant areas. Therefore, a smaller distance of 100 µm was chosen at which the volume of trabecular bone could be reliably measured. For future experiments should be noted that when using the here utilized medulla model, a shorter or smaller diameter implant size should be considered to avoid possible cortical osteoconduction artefacts. Eventually, a monocortical model (e.g. condyle, jaw) could be utilized.

The current investigation proved that osseointegration of bone implants can be manipulated and even improved by the utilization of a predefined nano-size topography. Histomorphometry showed a significantly higher bone volume around the 200 nm grooved implants, compared to the rough controls. Moreover, the increased bone volume around the implants was significantly higher only for the 200 nm grooved pattern at a comparison between 4 and 8 weeks. Also the *in vivo* study by Prodanov et al. showed that bone-regeneration is dependent on the groove widths.[21] The authors report that from the tested groove widths between 75 nm and 500 nm, only the 225 nm wide grooves could induce stronger cortical bone formation at the implant surface. However, contrary to our study the ridge width was 75 nm, while in our experiment the ridge was approximately 800 nm. Combined, these findings suggest that grooves with widths of about 200 nm have the potential to increase cortical and trabecular bone at the implant-bone interface. However, additional studies are necessary to further evaluate and potentially optimize the manner in which patterns influence bone formation. For example the influence of the ridge dimension should be addressed in more detail in future experiments. Moreover, the influence of same patterns should be tested in models that can combine cortical and trabecular bone evaluation, as they might be influenced differently by the same topography.

6

Conclusion

In this study a method was developed to produce a curved implant equipped with a nanotextured surface. The implants were placed in a rat femoral medulla model and bone regeneration on the implant surfaces was evaluated after 4 and 8 weeks by histomorphometry. Compared to industrially utilized micro-roughness, a significantly higher bone volume around 200 nm grooved implants was found. Moreover, the 200 nm grooved implants were found to significantly increase in amount of bone between the 4 and 8 weeks. In conclusion, 200 nm wide nanogrooves can positively influence the osseointegration of implants.

References

1.   Vos T, Flaxman AD, Naghavi M, Lozano R, Michaud C, Ezzati M, et al. Years lived with disability (YLDs) for 1160 sequelae of 289 diseases and injuries 1990–2010: a systematic analysis for the Global Burden of Disease Study 2010. The Lancet. 2012;380:2163-96.

2.   The Orthopaedic Industry Annual Report. Orthoworld Inc.; 2014.

3.   Pye AD, Lockhart DE, Dawson MP, Murray CA, Smith AJ. A review of dental implants and infection. The Journal of hospital infection. 2009;72:104-10.

4.   Jung RE, Pjetursson BE, Glauser R, Zembic A, Zwahlen M, Lang NP. A systematic review of the 5-year survival and complication rates of implant-supported single crowns. Clinical oral implants research. 2008;19:119-30.

5.   Diz P, Scully C, Sanz M. Dental implants in the medically compromised patient. J Dent. 2013;41:195-206.

6.   Total hip replacement and resurfacing arthroplasty for end-stage arthritis of the hip. NICE technology appraisal guidance; Feb. 2014.

7.   Pjetursson BE, Thoma D, Jung R, Zwahlen M, Zembic A. A systematic review of the survival and complication rates of implant-supported fixed dental prostheses (FDPs) after a mean observation period of at least 5 years. Clinical oral implants research. 2012;23 Suppl 6:22-38.

8.   Bozini T, Petridis H, Garefis K, Garefis P. A meta-analysis of prosthodontic complication rates of implant-supported fixed dental prostheses in edentulous patients after an observation period of at least 5 years. The International journal of oral & maxillofacial implants. 2011;26:304-18.

9.   Liu R, Lei T, Dusevich V, Yao X, Liu Y, Walker MP, et al. Surface characteristics and cell adhesion: a comparative study of four commercial dental implants. Journal of prosthodontics : official journal of the American College of Prosthodontists. 2013;22:641-51.

10. Svanborg LM, Andersson M, Wennerberg A. Surface characterization of commercial oral implants on the nanometer level. Journal of biomedical materials research Part B, Applied biomaterials. 2010;92:462-9.

11. Dalby MJ. Cellular response to low adhesion nanotopographies. International journal of nanomedicine. 2007;2:373-81.

12. Klymov A, Prodanov L, Lamers E, Jansen JA, Walboomers XF. Understanding the role of nano-topography on the surface of a bone-implant. Biomater Sci-Uk. 2013;1:135-51.

13. Lovmand J, Justesen J, Foss M, Lauridsen RH, Lovmand M, Modin C, et al. The use of combinatorial topographical libraries for the screening of enhanced osteogenic expression and mineralization. Biomaterials. 2009;30:2015-22.

14. de Peppo GM, Agheli H, Karlsson C, Ekstrom K, Brisby H, Lenneras M, et al. Osteogenic response of human mesenchymal stem cells to well-defined nanoscale topography in vitro. International journal of nanomedicine. 2014;9:2499-515.

6

15. Wittenbrink I, Hausmann A, Schickle K, Lauria I, Davtalab R, Foss M, et al. Low-aspect ratio nanopatterns on bioinert alumina influence the response and morphology of osteoblast-like cells. Biomaterials. 2015;62:58-65.

16. Kim J, Kim HN, Lim KT, Kim Y, Seonwoo H, Park SH, et al. Designing nanotopographical density of extracellular matrix for controlled morphology and function of human mesenchymal stem cells. Scientific reports. 2013;3:3552.

17. Kim J, Kim HN, Lim KT, Kim Y, Pandey S, Garg P, et al. Synergistic effects of nanotopography and co-culture with endothelial cells on osteogenesis of mesenchymal stem cells. Biomaterials. 2013;34:7257-68.

18. You MH, Kwak MK, Kim DH, Kim K, Levchenko A, Kim DY, et al. Synergistically enhanced osteogenic differentiation of human mesenchymal stem cells by culture on nanostructured surfaces with induction media. Biomacromolecules. 2010;11:1856-62.

19. Wang PY, Li WT, Yu JS, Tsai WB. Modulation of osteogenic, adipogenic and myogenic differentiation of mesenchymal stem cells by submicron grooved topography. J Mater Sci-Mater M. 2012;23:3015-28.

20. Watari S, Hayashi K, Wood JA, Russell P, Nealey PF, Murphy CJ, et al. Modulation of osteogenic differentiation in hMSCs cells by submicron topographically-patterned ridges and grooves. Biomaterials. 2012;33:128-36.

21. Prodanov L, Lamers E, Domanski M, Luttge R, Jansen JA, Walboomers XF. The effect of nanometric surface texture on bone contact to titanium implants in rabbit tibia. Biomaterials. 2013;34:2920-7.

22. Alghamdi HS, Bosco R, van den Beucken JJJP, Walboomers XF, Jansen JA. Osteogenicity of titanium implants coated with calcium phosphate or collagen type-I in osteoporotic rats. Biomaterials. 2013;34:3747-57.

23. Lamers E, Walboomers XF, Domanski M, te Riet J, van Delft FC, Luttge R, et al. The influence of nanoscale grooved substrates on osteoblast behavior and extracellular matrix deposition. Biomaterials. 2010;31:3307-16.

24. Alghamdi HS, Cuijpers VMJI, Wolke JGC, van den Beucken JJJP, Jansen JA. Calcium-phosphate-coated Oral Implants Promote Osseointegration in Osteoporosis. J Dent Res. 2013;92:982-8.

25. van der Lubbe HB, Klein CP, de Groot K. A simple method for preparing thin (10 microM) histological sections of undecalcified plastic embedded bone with implants. Stain technology. 1988;63:171-6.

26. Lamers E, van Horssen R, te Riet J, van Delft FCMJM, Luttge R, Walboomers XF, et al. The Influence of Nanoscale Topographical Cues on Initial Osteoblast Morphology and Migration. European cells & materials. 2010;20:329-43.

27. Chehroudi B, Gould TR, Brunette DM. Effects of a Grooved Epoxy Substratum on Epithelial-Cell Behavior Invitro and Invivo. J Biomed Mater Res. 1988;22:459-73.

28. Schuler M, Kunzler TP, de Wild M, Sprecher CM, Trentin D, Brunette DM, et al. Fabrication of TiO2-coated epoxy replicas with identical dual-type surface topographies used in cell culture assays. Journal of Biomedical Materials Research Part A. 2009;88A:12-22.

29. Lamers E, Walboomers XF, Domanski M, Prodanov L, Melis J, Luttge R, et al. In vitro and in vivo evaluation of the inflammatory response to nanoscale grooved substrates. Nanomed-Nanotechnol. 2012;8:308-17.

30. Gao H, Hu YW, Xuan Y, Li J, Yang YL, Martinez RV, et al. Large-scale nanoshaping of ultrasmooth 3D crystalline metallic structures. Science. 2014;346:1352-6.

6

7

Mineralization and bone regeneration using a bioactive elastin-like recombinamer membrane

Esther Tejeda-Montes, Alexey Klymov, M Reza Nejadnik, Matilde Alonso, J Carlos Rodriguez-Cabello, X Frank Walboomers, Alvaro Mata

Introduction

Bone grafts are extensively used in bone healing therapies that require significant osteoconductive and osteoinductive enhancement. Despite a number of well-known negative consequences, autogenous cancelous bone continues to be the preferred bone graft option and a major target to replace.[1] Scaffolds based on collagen,[2] hyaluronic acid,[3] chitosan,[4] biological composites,[5] and self-assembling materials [6] have been and continue to be investigated as three-dimensional bone graft alternatives.

In an attempt to further enhance bone regeneration therapies, and taking advantage of the benefits of the periosteum, the use of periosteal grafts has emerged as an attractive strategy.[7] An ideal periosteal graft would not only provide a physical structure that facilitates osteoconduction, but also osteoinductive signals that stimulate osteogenesis and ultimately promote biomineralization.[8] Membranes made of amniotic tissue,[9] chitosan-silica [10] or silk fibroin nanofibers [11] have been reported to induce osteoblastic differentiation *in vitro.* Also, a variety of *in vitro* mineralizing membranes based on chitosan/bioactive glass nanoparticles,[12] platelet-rich fibrin functionalized with alkaline phosphatase (ALK),[13] polycaprolactone fibers incorporating nano-apatite particles [14] or forsterite nanopowder,[14] and collagen [16] have been developed. In addition, the capacity of membranes to enhance bone regeneration *in vivo* has been reported. Examples include membranes based on a modified polylactide/polyglycolide acid polymer,[17] collagen membranes combined with a porous titanium membrane,[18] or chitosan bioelectric membranes capable of accelerating bone fracture healing by electric stimulation.[19] However, the success of periosteal grafts has been restricted by limitations associated with the lack of biocompatibility, absence of bioactivity, poor mechanical properties, or early degradation.[20] A possible alternative to overcome these limitations may be found in the use of molecularly designed materials made from peptides and proteins. This approach offers a much higher level of tuneability, spatio-temporal control, bioactivity, and stimulation of bone formation. Towards this goal, phosphorylated serine [S(P)],[6] MLPHHGA heptapeptide,[21] the bone sialoprotein sequence E7PRGDT,[22] or the statherin-derived protein sequence DDDEEKFLRRIGRFG [23] have been used and reported to promote

7

mineralization *in vitro*. Elastin-like recombinamers (ELRs), genetically engineered protein-based polymers inspired by the extracellular matrix protein elastin, are especially attractive due to their molecular versatility, biomimetic character, biocompatibility, good mechanical properties, and biodegradability.[24] These molecules are mainly composed of the repeating pentapeptide domain VPGXG (where X could be any amino acid apart from proline) and can be designed to contain additional bioactive sites such as RGDS or REDV.[25]

In an effort to bioengineer a bioactive membrane for bone regeneration that takes advantage of the potential benefits of these biomolecular sequences, we have recently reported on a couple of strategies based on peptide and protein-based materials [26] and [27]. In particular, we have described the fabrication and characterization of thin robust ELR membranes comprising the bioactive epitope DDDEEKFLRRIGRFG, and their capacity to promote osteogenesis *in vitro*.[27] The present work provides further evidence of the potential use of these membranes for bone regeneration applications. First, we describe the *in vitro* mineralization and osteogenic properties of the bioactive ELR membranes tested under biomimetic conditions in both static and dynamic culture settings. Then, we report on the bone regeneration capacity of these membranes using an orthotopic critical-size rat calvarial defect model.

Materials and methods

ELR molecules

Four ELRs molecules were supplied by Technical Proteins NBT S.L. (Valladolid, Spain). The materials consisted of repeating pentapeptide domains of VPGIG and VPGKG to provide structural integrity including the amino acid lysine (K) to serve as a cross-linking point (IK), that incorporated the peptide RGDS for mesenchymal stem cell adhesion (RGDS), the peptide DDDEEKFLRRIGRFG for nucleation of mineralization (HAP) and an ELR that combined the later and the RGDS sequence (HAP-RGDS) (Table 1).

ELR Material	ELR sequence (**bioactive sequence**)	Bioactivity	ELR Con. (%)	ELR : Cross-linker ratio
IK	(VPGIG VPGIG VPGKG VPGIG VPGIG)$_{24}$	Control	4	1 : 0.75
RGDS	[[(VPGIG)$_2$(VPGKG)(VPGIG)$_2$]$_2$AVT G**RGDS**PASS[(VPGIG)$_2$(VP GKG)(VPGIG)$_2$]$_2$]$_6$	Cell Adhesion	3.5	1 : 0.50
HAP	[[(VPGIG)$_2$(VPGKG)(VPGIG)$_2$]$_2$ **DDDEEKFLRRIGRFG** [(VPGIG)$_2$(VPGKG)(VPGIG)$_2$]$_2$]$_3$	Mineralization	5	1 : 3
HAP-RGDS	[[(VPGIG)$_2$(VPGKG)(VPGIG)$_2$]$_2$**DDDEEKFLRRIGRFG**[(VPGIG)$_2$(VPGKG)(VPGIG)$_2$]$_2$]$_4$ [[(VPGIG)$_2$(VPGKG)(VPGIG)$_2$]$_2$AVTG**RGDS**PASS [(VPGIG)$_2$ (VPGKG) (VPGIG)$_2$]$_2$]$_4$	Mineralization and cell adhesion		1 : 3

Table 1: Sequence, functionality (bioactivity), concentration, and ELR:Cross-linker ratio of the ELR materials.

7

Membrane fabrication

Membranes were fabricated according to a recently reported method [25] and [27] (Figure 1 a–c). The ELR molecules were dissolved in anhydrous dimethylformamide (DMF) (Sigma–Aldrich, Taufkirchen, Germany) at room temperature, and then mixed with hexamethyl diisocyanate (HDI) (Sigma–Aldrich, Taufkirchen, Germany) (Table 1). Four ELR membranes were fabricated from the different ELR molecules, containing either one of the bioactive sequences (RGDS, HAP, and HAP-RGDS) or without any bioactivity (IK).
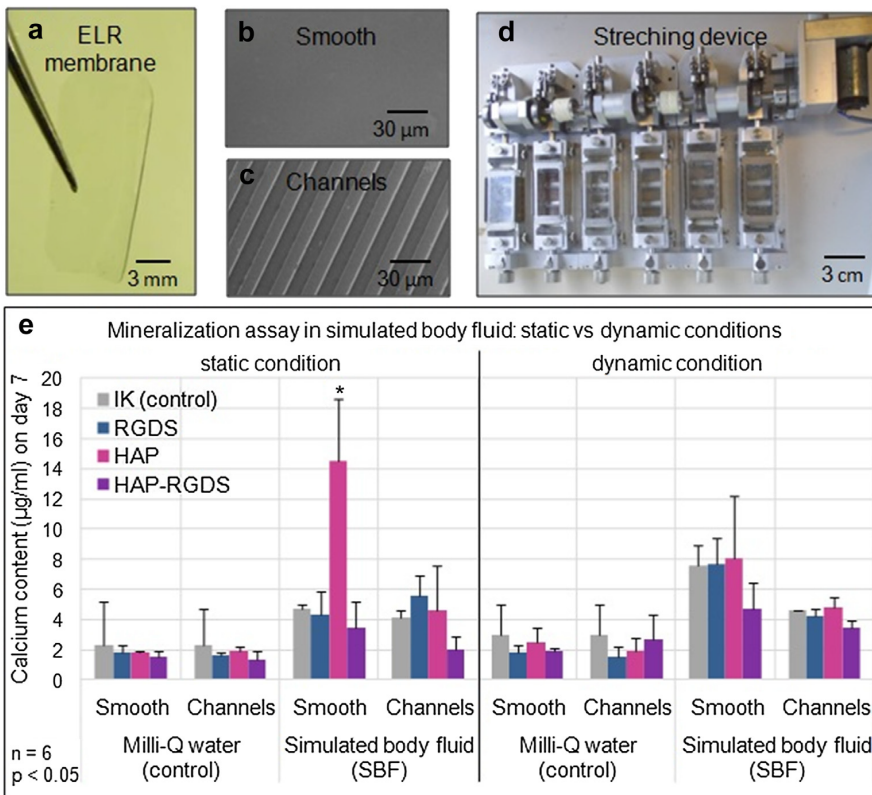

Figure 1: A) ELR membranes fabricated by drop-casting approach C) exhibiting or B) not channel topographies were tested in dynamic condition in a D) custom-made stretching device used to apply uniform, cyclic, and uniaxial strain of 8%. E) Smooth HAP membranes incubated in simulated body fluid (SBF) exhibited the highest amount of deposited calcium compared to all other membranes in either static or dynamic conditions.

Fabrication and characterization of topographically patterned ELR membranes

In order to fabricate topographically patterned ELR membranes, a patterned PDMS mould was fabricated by soft lithography techniques as previously reported.[27] The features consisted of channels that were 7 μm high, 10 μm wide, and separated by 10 μm wide ridges (Channels) (Figure 1c). Membrane fabrication and pattern reproducibility were analyzed by qualitative observations using scanning electron microscopy (SEM) and profilometry.

Mechanical stimulation

A custom-made stretching device [28] was used in this study (Figure 1d). The system applied uniform, cyclic, uniaxial strain to elastic silicone dishes that had 18 cm^2 surface growth areas, in which the ELR membranes were immobilized. A cyclic stretching magnitude of 8% at 1 Hz frequency with intermittent stretch duration of 15 min stretch/15 min rest for 16 h, followed by 8 h of rest was applied. This process was defined as dynamic condition throughout the document. All experiments were performed inside of a cell culture incubator controlling temperature and CO_2 level (37 °C and 5% CO_2). The static condition was used as control. This procedure was applied in Sections "Membrane mineralization in simulated body fluid" and "*In vitro* cell differentiation"

Membrane mineralization in simulated body fluid

Membranes made of IK, RGDS, HAP and HAP-RGDS ELR molecules, comprising or not microtopographical channels in a rectangular shape (7.5 × 15 mm^2) were analyzed in this study. The experiment was performed applying a mechanical stimulation described in "Mechanical stimulation", while the samples were incubated in 3 ml of simulated body fluid (SBF) which was replaced daily for 7 days. ELR membranes incubated in milli-Q water in static conditions were used as control. SBF was prepared following a previously reported protocol.[29] The SBF solution was prepared using 50 mM Tris($CH_2OH)_3CNH_2$, 136.8 mM NaCl, 3 mM KCl, 1.5 mM $MgCl_2 6H_2O$, 2.5 mM $CaCl_2 H_2O$, 1 mM K_2HPO_4, 4.15 mM $NaHCO_3$,

7

and 0.5 mM $Na_2SO_410H_2O$. In order to prevent the unwanted deposition of calcium phosphate minerals during the storage of SBF, two stock solutions were prepared. The first stock solution was made with the reagents $Tris(CH_2OH)_3CNH_2$, NaCl, KCl, K_2HPO_4, $NaHCO_3$, $Na_2SO_410H_2O$ and the second stock solution with the reagents $Tris(CH_2OH)_3CNH_2$, NaCl, $MgCl_2 6H2O$, $CaCl_2H_2O$. After adjusting the pH of the stock solutions to 7.4, they were stored at 4 °C. Prior to the mineralization experiments, the stock solutions were mixed and diluted with milli-Q water to obtain the SBF concentration of the reagents. The resulting SBF solution was filtered using a surfactant-free cellulose acetate filter unit (pore size 0.2 µm) to eliminate impurities and used in the mineralization experiments. In order to assess the mineralization potential of the ELR membranes, *in vitro* mineralization in SBF was investigated using different techniques. Each sample was assayed in triplicate and the experiment was repeated twice.

Calcium content

ELR membranes were rinsed twice with milli-Q water after 7 days of incubation in SBF solution. Then, 100 µl of 0.5 M acetic acid was added in each membrane. The samples were maintained under agitation overnight at room temperature. The supernatant was recollected and calcium content was determined using an orthocresolphthalein complexone method.[30] The calcium content was measured on a fluorescence microplate reader (Bio-Tek Instruments Inc., Winooski, VT, USA) at 570 nm, and determined by extrapolating known values from a standard curve. All samples were assayed twice.

Mineral characterization

The mineral on Smooth HAP membranes incubated in SBF for 7 days in static condition was characterized by time-of-flight secondary ion mass spectroscopy (TOF-SIMS) and scanning electron microscopy fitted with an energy dispersive spectrometer (SEM-EDS). Smooth HAP membranes incubated in milli-Q water were used as control.

Membranes analyzed by TOF-SIMS were rinsed twice with milli-Q water, frozen at −80 °C overnight and freeze-dried for 24 h. The TOF-SIMS (TOF-

SIMS IV, ION-TOF, Germany) operated at a pressure of 5×10^{-9} mbar. Samples were bombarded with a pulsed Bismuth liquid metal ion source (Bi^{3+}), at energy of 25 keV. The gun was operated with a 20 ns pulse width, 0.3 pA pulsed ion current for a dosage lower than 5×10^{11} ions/cm^2(below the threshold level of 1×10^{13} ions/cm^2 generally accepted for static SIMS conditions). Charge neutralization was achieved with a low energy (20 eV) electron flood gun. The secondary ions were detected with a reflector time-of-flight analyzer, a multichannel plate (MCPs), and a time-to-digital converter (TDC). Measurements were performed with a typical acquisition time of 20 s at a TDC time resolution of 200 ps and 128 × 128 pixel image size. Secondary ion spectra were acquired from areas of 400 × 400 μm^2 within the sample's surface. Mass spectral acquisition and image analysis were performed within the IonSpec software (version 4.1, ION-TOF, Germany) and Ion image software (version 3.1, ION-TOF, Germany), respectively. Each spectrum was normalized to the total intensity.[31]

Membranes analyzed by SEM-EDS were frozen at −80 °C overnight after washing twice with milli-Q water. After 24 h membranes were freeze-dried, and finally they were coated with a 10 nm layer of gold–platinum. The mineral morphology and chemical composition were imaged and analyzed by SEM (JSM-7100F, JEOL, Germany) fitted with an energy dispersive X-ray microanalyzer (Oxford Inca 350, Oxford instruments, UK) at 20 kV.

Membrane Young's modulus

The stiffness of ELR membranes was measured by the Young's modulus. A tensile test was performed under wet conditions in milli-Q water at 37 °C. ELR Membranes were fabricated in rectangular shape (8 × 15 mm^2). The thickness of the membranes was measured with a micrometer having a precision of 0.01 mm. Mechanical tests were performed with a BOSE® ElectroForce® BioDynamicTM bioreactor (BOSE, Friedrichsdorf, Germany) with an orthopedic chamber, equipped with a 22 N load-cell at a speed of 1 mm/min, and forces were recorded using Win Test® software (BOSE, Friedrichsdorf, Germany). The Young's modulus was calculated as the slope of the straight line portion of the stress–strain curve. Membranes incubated in milli-Q water were used as control.

7

In vitro cell differentiation

Rat MSCs obtained following a procedure described previously,[38] were cultured on membranes made of IK and HAP ELR molecules comprising or not channels topographies. Cells were incubated overnight prior the application of the mechanical stimulation (Section "Membrane mineralization in simulated body fluid") for 2 days. Membranes were sterilized for 20 min under ultraviolet (UV) inside the cell culture hood, and then immobilized over the silicone dishes of the stretching device. The silicone dishes were prepared by combining Elastosil component A with Elastosil component B (Elastosil RT 601; Wacker-Chemie, Germany) at a 10:1 ratio, respectively. The elastomer was mixed, poured into the dish mould and, allowed to sit at room temperature overnight. The silicone dishes were then removed, cleaned with a 1% Liqui-nox liquid detergent (Alconox Inc., White Plains, NY) in milli-Q water solution, rinsed in milli-Q water, air-dried, and autoclaved at 121 °C for 15 min.

Cells were cultured in osteogenic differentiation medium (OM+) in tissue culture plastic (TCP+) as positive control, or without dexamethasone (OM−) on ELR membranes and tissue culture plastic (TCP−) as negative control. As an additional control, ELR membranes were cultured in OM− in static conditions. OM+ was prepared with 15 ml α-Eagle minimum essential medium (αMEM, Gibco-Invitrogen, Scotland) supplemented with 10% fetal bovine serum (FBS, Sigma–Aldrich, Taufkirchen, Germany), 50 mM ascorbic acid (Sigma, St. Louis, MO), 50 µg/ml gentamycin (Sigma, St. Louis, MO), 10 mM sodium-β-glycerophosphate (Sigma, St. Louis, MO), and 10^{-8} M dexamethasone (Sigma, St. Louis, MO). Rat MSCs of passage 3–6 were diluted in serum-free DMEM and seeded at 10,500 cells/cm^2 onto the substrates. After 2 h of culture, all the medium was replaced with DMEM containing 10% FBS for subsequent culture. Each sample was assayed in triplicate and the experiment was repeated twice.

Osteoblastic differentiation and mineralization assays

In order to analysis *in vitro* cell differentiation DNA content, alkaline phosphatase (ALK) activity and calcium content assays were performed on day 5 and 10. The culture media was removed and cells were rinsed

in phosphate-buffered saline (PBS). Then, 500 µl of filter milli-Q water was added to each sample. The cell suspension was transferred to an eppendorf, sonicated for 20 min, and the supernatant was collected and frozen at −20 °C overnight. The cell suspension was thawed and frozen two times more. This cell suspension was used in the following assays.

100 µl of the cell suspension was used to analyze the DNA concentration using the picogreen assay (Molecular Probes, The Netherlands) according to the manufacturer's instructions. The DNA content (µg/ml) of the samples was read in a microplate reader (BioRad 450, Bio-Rad Laboratories, Hercules, CA) at 480 nm and determined from a DNA standard curve. Second, in order to analyze ALK activity 100 µl of the cell suspension was added to 100 µl of working reagent consisting of 0.5 M 2S-amino-2methyl-l-propenyl (Sigma, St. Louis, MO), 5 mM p-nitro-phenol phosphate (Sigma, St. Louis, MO), and 5 mM magnesium chloride (1:1:1) (Sigma, St. Louis, MO). The reaction was stopped using 100 µl of sodium hydroxide (Sigma, St. Louis, MO), and the final absorbance was read at 405 nm using a microplate reader (BioRad 450, Bio-Rad Laboratories, Hercules, CA). A standard curve was generated by making serial dilutions of 4-nitrophenol, and sample measurements were extrapolated from known concentration values of the curve. ALK activity (nmol) was normalized to DNA concentration (µg/ml). Finally, information about the mineralized matrix formation on the ELR membranes was obtained by the calcium content assay using 20 µl of the cell suspension. The calcium content (µg/ml) was determined using the protocol described in Section "Calcium content", and normalized to DNA concentration (µg/ml).

Scanning electron microscopy characterization

Cells cultured on ELR membranes were rinsed twice with filtered PBS, fixed with 2% glutaraldehyde (Sigma, St. Louis, MO) in cacodylate (Sigma, St. Louis, MO) buffer for 5 min, and rinsed twice with 0.1 M sodium cacodylate buffer for 5 min. Then, the samples were dehydrated in a series of 70%, 80%, 90%, 96%, and 100% ethanol solution. Finally, two drops of tetramethylsilane (Sigma, St. Louis, MO) were added to each sample followed by air-dried for 5–10 min. The samples were coated with a 10 nm layer of gold.

In vivo characterization

The bioactivity of Smooth HAP ELR membrane scaffolds was tested in a 5 mm critical-size rat calvarial defect model.[32] The rats were treated with HAP membranes to evaluate the effect of the bioactive sequence, IK membranes to evaluate the effect of non-bioactive sequence and without treated to evaluate the healing in the empty defect. Membranes were sterilized in UV for 20 min and hydrated in physiological saline, previously to fill the calvarial defect.

A total of 21 male Sprague–Dawley rats (12-week-old, 425–475 g) were obtained from Janvier Lab Animal (France) (7 rats per group). The animals were housed singly and received food and water ad libitum. All animals' research protocols were approved by the Ethical Committee of Animal Experimentation (CEEA) of the University of Barcelona (Spain) and the Ministry of Agriculture, Livestock, Fisheries, Food, and the Environment of the Government Institution of Catalonia (Spain).

Surgical procedure

The surgery was performed in the Laboratory Animal Applied Research Platform at Parc Cientific Barcelona (PCB, Spain). The animals were anaesthetized using isoflurane (Sigma–Aldrich, Spain) inhalation anesthesia (5% induction; 3% maintenance). All animals prior to the surgical intervention received an intraperitoneal injection of buprenorphine (0.05 mg/kg) for postoperative analgesia, and its administration was repeated 12–16 h after the surgery. The animals were positioned onto a heating pad (37 °C) during all the surgery process. The skin that covered the skull was shaved and disinfected with iodopovidone solution. A midline incision of 2 cm was performed with a surgical blade. The skin was then reflected bilaterally to expose the calvarial bone surface. A 5 mm-diameter trephine bur (Fine Science tools, Heidelberg, Germany) mounted on a dental hand piece (Foredom, Bethel, New York, USA) was used to drill a round, segmental defect in the right parietal bone. During the drilling, the area was continuously irrigated with sterile saline solution, and subsequently the calvarial disk was carefully removed and extracted using tweezers. The defect was rinsed with physiological saline and the hydrated ELR membrane (7.5 × 7.5 mm) was

implanted covering the defect. The extreme of the membrane was fixed to the bone applying a drop of cyanoacrylate. The skin was closed over in layers with 4.0 Nylon sutures and was applied iodopovidone solution to prevent infections. Animals were monitored daily until euthanasia for any complications or abnormal behavior and were sacrificed 36 days after surgery by carbon dioxide inhalation.

High-resolution micro-computed tomography analysis

Immediately after rats were sacrificed, a high-resolution micro-computed tomography (microCT) analysis was performed using the Skyscan 1172 computed microtomographic system (Kontich, Belgium). The parameters of the scan were voltage source 81 kV, current source 124 µA, image pixel size 9 µm, an aluminum filter of 0.5 mm, a tomographic rotation of 180° and a sample rotation step of 0.8°. The reconstruction was carried out with NRecon (v1.6.2.0) software using a specific post-alignment per each sample and applying a medium intensity ring artefact correction. Microtomographic 3D analysis was analyzed with CTAn (v.1.10.1.3) software, using a global threshold of 50–255. A cylindrical volume of interest (VOI) was used to quantify the bone volume and bone mineral density corresponding with the size of the defect.

Histological analysis

The calvarias were extracted from the skull and fixed in 4% paraformaldehyde (Panreac, Spain) at pH = 7.2 for 2 days followed by bone decalcification with Surgipath Decalcifier II (Leica biosystems, Spain) for 4 h. Next, the calvarias were embedding in paraffin and 3 µm sections were made using a microtome. The histological sections were stained with H&E and Trichrome Goldner and observed with a microscope Zeiss AxioScope A (Carl Zeiss, Madrid, Spain) incorporating a Zeiss AxioCam MRc5 camera (Carl Zeiss, Madrid, Spain) for qualitative and semiquantitative evaluation. A score system was assigned (0, absent; 1, scarcely present; 2, slightly present 3, present; 4, intensively present) to the new ossified tissue (osteoblasts embedded in osteoid matrix) observed on the edge and in the middle of the defect allowing a numerical comparison.

7

Statistics

Data were reported as mean ± standard error of the mean. Statistical analysis was performed by one-way analysis of variance using ANOVA and student *t*-test. The non-parametric Krusskall–Wallis test was carried out to compare the histological semiquantitative results among groups for the *in vivo* experiment. Finally, *p*-values < 0.05 were considered significant.

Results

ELR membrane fabrication

Membranes were fabricated as previously reported [25] and [27] from either ELR materials comprising a bioactive sequence (RGDS, HAP or HAP-RGDS) or a non-bioactive ELR material (IK) used as control (Table 1). The quality and reproducibility of the membranes exhibiting topographical channels were verified by profilometry and SEM observations. These results confirmed topographical patterns with well-defined features that closely resembled those of the PDMS molds.

In vitro membrane mineralization

ELR membrane mineralization *in vitro* was assessed using a variety of techniques. First, the calcium (Ca) content assay revealed the highest amount of deposited Ca on Smooth HAP membranes tested in static condition (14.49 ± 4.19 μg/ml) compared to all other membranes in either static or dynamic conditions (Figure 1e). Second, TOF-SIMS analysis confirmed the presence of calcium phosphate (CaP) mineral on these membranes. As expected, positive TOF-SIMS peaks demonstrated the presence of CH_4N^+ (blue) on all ELR membranes, which corresponds to the common amino acid sequence of all ELRs tested. However, only HAP membranes exhibited peaks for Ca^{2+} (green) and $CaOH^+$(red) (Figure 2c–d), which corroborate the results of the Ca content assay. Similarly, negative TOF-SIMS peaks also revealed signals for CN^- and CNO^- on all ELR membranes, which again correspond to the common amino acid sequence of all tested ELRs, while signals for PO_2^- and PO_3^- were only observed on Smooth HAP membranes (Figure 2e–f). The presence of CaP was also

confirmed by chemical images that indicated strong PO_2^- and PO_3^- signals only on Smooth HAP membranes (Figure 2g–h). Furthermore, the total ion image revealed a homogenous distribution of the deposition of mineral within the ELR membrane surface. Finally, SEM examination (Figure 2a–b) and EDS analysis (Figure 2i–j) confirmed the presence of mineral on Smooth HAP membranes with a Ca/P ratio of 1.78.

Young's modulus

Tensile tests were conducted to investigate the effect of mineralization on the mechanical properties of the different membranes. Smooth HAP membranes were incubated in SBF for 7 days in static condition displayed the highest Young's modulus (E) (2081 ± 315 kPa) compared to all other tested membranes (Figure 2k), which exhibited moduli ranging between 362 ± 74 and 600 ± 249 kPa.

In vitro cell differentiation

Given the observed mineralizing nature of the Smooth HAP membranes, osteoblastic differentiation of rMSCs was investigated in both static and dynamic conditions by measuring ALK and Ca deposition. On day 5 and 10, the highest ALK/DNA expression was observed on cells growing on Smooth HAP membranes in non-osteogenic differentiation medium (0.23 ± 0.13), which was statistically similar to that expressed by cells growing on tissue culture plastic in osteogenic differentiation medium (TCP+) (0.28 ± 0.02) (Figure 3a). Furthermore, cells on these membranes growing in non-osteogenic differentiation medium also exhibited the highest Ca deposition on both day 5 and 10 compared to cells on any other membrane or control substrate growing in osteogenic differentiation medium (Figure 3b). SEM observations confirmed the presence of mineralized extracellular matrix formation on cells cultured on Smooth HAP membranes on day 10 (Figure 3c). Finally, there were no significant differences in ALK activity and Ca deposition between cells growing on membranes tested in static or dynamic culture conditions (Figure 3d–e).
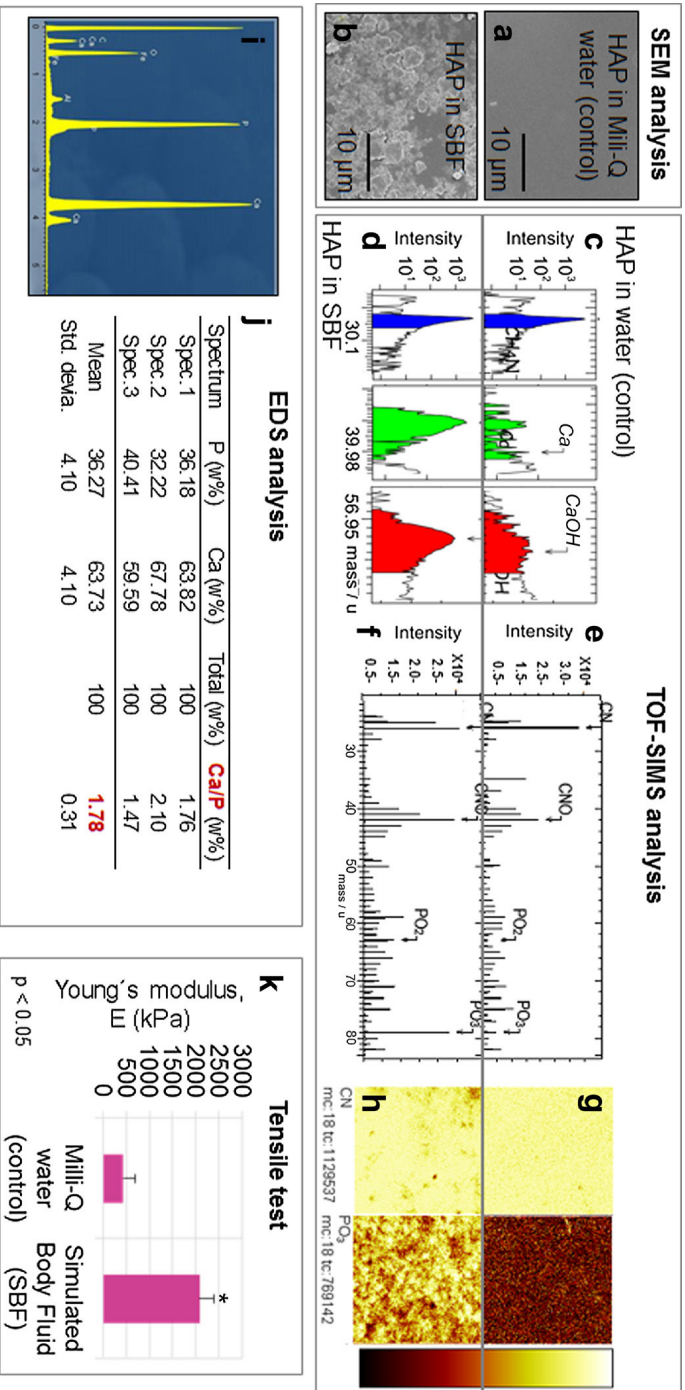
7

Figure 2: Presence of mineral was observed by SEM examination on A) Smooth HAP membrane incubated in SBF in static conditions compared with A) the control in mili-Q water. C) TOF-SIMS revealed in both cases peaks of CH_4N^+ and CN corresponding with amino acid from ELR molecules. While peaks of Ca_2^+ (green), $CaOH^+$ (red), PO_2^- and $PO3^-$ correspond with the mineral observed on Smooth HAP membranes incubated in SBF compared with the control in milli-Q water. D) EDS analysis confirmed that the mineral exhibited on Smooth HAP membranes displayed a Ca/P proportion of 1.78. E) Additionally, the highest value of Young modulus was observed on these membranes incubated in SBF.
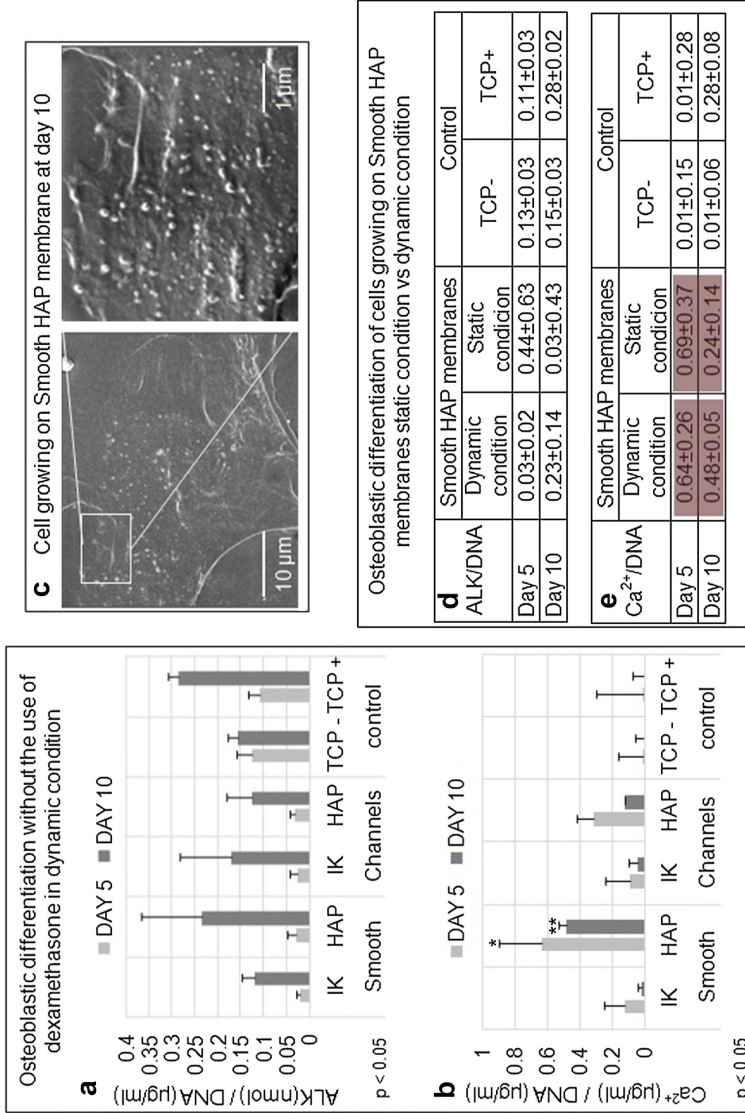
Osteoblastic differentiation of cells growing on Smooth HAP membranes static condition vs dynamic condition

d

ALK/DNA	Smooth HAP membranes		Control	
	Dynamic condition	Static condition	TCP-	TCP+
Day 5	0.03±0.02	0.44±0.63	0.13±0.03	0.11±0.03
Day 10	0.23±0.14	0.03±0.43	0.15±0.03	0.28±0.02

e

Ca^{2+}/DNA	Smooth HAP membranes		Control	
	Dynamic condition	Static condition	TCP-	TCP+
Day 5	0.64±0.26	0.69±0.37	0.01±0.15	0.01±0.28
Day 10	0.48±0.05	0.24±0.14	0.01±0.06	0.28±0.08

Figure 3: A) The highest ALK/DNA expression and B) Ca deposition was observed on rMSCs growing on Smooth HAP membranes in non-osteogenic differentiation medium, compared to cells on any other membrane or control substrate growing in osteogenic differentiation medium. C) SEM observations confirmed the presence of this mineral on cells cultured on Smooth HAP membranes on day 10. ALK activity D) and Ca deposition E) between cell growth on membranes tested in static or dynamic culture conditions were not significantly different.

Localization of ELR membranes within the defect site

In order to confirm that the ELR membranes were stable and positioned within the defect site, three animals were implanted with ELR membranes and sacrificed on day 7. In all three animals, the membranes were observed to be positioned within the defect site in the same location as they were placed during implantation (Figure 4c).

Quantification of bone formation by microCT

The microCT analysis demonstrated that the animals implanted with the HAP membranes presented the highest mean volume of ossified tissue within the defect (12.6 ± 2.4 mm^3) (Figure 4d, f) compared to animals receiving the non-bioactive IK membranes (9.2 ± 2.6 mm^3) Figure 4g) and those left untreated (9.0 ± 1.4 mm^3) (Figure 4h). While some regeneration was observed on all tested groups along the rim area of the defect, only animals implanted with the HAP membrane exhibited ossified tissue towards the center of the defect tending to breach the critical-size gap. These results were confirmed by histological analysis. MicroCT data was also used to quantify bone mineral density within the defect. In this case, there was greater variation between samples and no significant differences were observed between the three tested groups (Figure 4e).

Quantification of bone formation by histological analysis

Histological sections stained with H&E indicated greater ossification on animals treated with the HAP membranes both around the rim and in the middle of the defect (Figure 5a). Within these regions, Trichrome Goldner staining (Figure 5b) demonstrated the presence of both immature (osteoid) and mature bone as well as a layer of active osteoblasts (Figure 5c) embedded within an osteoid matrix located on the growth front along the developing bone around the rim of the defect (Figure 5d). In contrast, animals that were implanted with the IK membranes and animals that were not treated with any membrane only exhibited bone formation around the edge of the defect. In addition, in accordance with the MicroCT results, semi-quantitative analysis of histological sections also verified the presence of more regeneration in animals implanted with the HAP membranes compared to the other groups (Figure 5e).

In vivo characterization

Given the observed *in vitro* mineralizing nature and enhancement of osteoblastic differentiation of Smooth HAP membranes, experiments were conducted to analyze their bone regeneration capacity *in vivo* using an orthotopic critical-size rat calvarial defect model (Figure 4a–b).

Localization of ELR membranes within the defect site

In order to confirm that the ELR membranes were stable and positioned within the defect site, three animals were implanted with ELR membranes and sacrificed on day 7. In all three animals, the membranes were observed to be positioned within the defect site in the same location as they were placed during implantation (Figure 4c).

Quantification of bone formation by microCT

The microCT analysis demonstrated that the animals implanted with the HAP membranes presented the highest mean volume of ossified tissue within the defect (12.6 ± 2.4 mm^3) (Figure 4d, f) compared to animals receiving the non-bioactive IK membranes (9.2 ± 2.6 mm^3) Figure 4g) and those left untreated (9.0 ± 1.4 mm^3) (Figure 4h). While some regeneration was observed on all tested groups along the rim area of the defect, only animals implanted with the HAP membrane exhibited ossified tissue towards the center of the defect tending to breach the critical-size gap. These results were confirmed by histological analysis. MicroCT data was also used to quantify bone mineral density within the defect. In this case, there was greater variation between samples and no significant differences were observed between the three tested groups (Figure 4e).

Quantification of bone formation by histological analysis

Histological sections stained with H&E indicated greater ossification on animals treated with the HAP membranes both around the rim and in the middle of the defect (Figure 5a). Within these regions, Trichrome Goldner staining (Figure 5b) demonstrated the presence of both immature (osteoid) and mature bone as well as a layer of active osteoblasts (Figure 5c) embedded within an osteoid matrix located on the growth front along
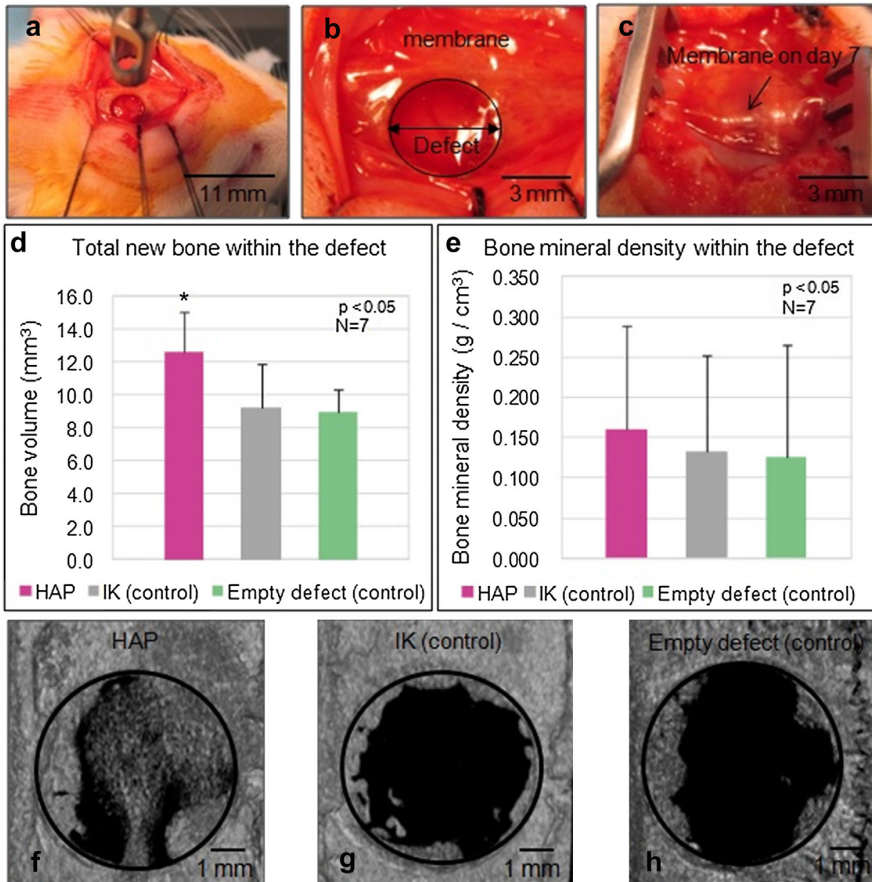
7

Figure 4: A) An orthotopic critical-size rat calvarial defect model was used to analyze the bone regeneration capacity of B) Smooth HAP membranes. C) Membranes were observed to be positioned within the defect site in the same location as they were placed during implantation on day 7. The microCT analysis demonstrated that animals implanted with the D) HAP membranes presented the highest mean volume of ossified tissue F) within the defect compared to animals receiving the G) non bioactive IK membranes and H) those left untreated. E) MicroCT analysis of bone mineral density within the defect revealed no significant differences between the tested groups.
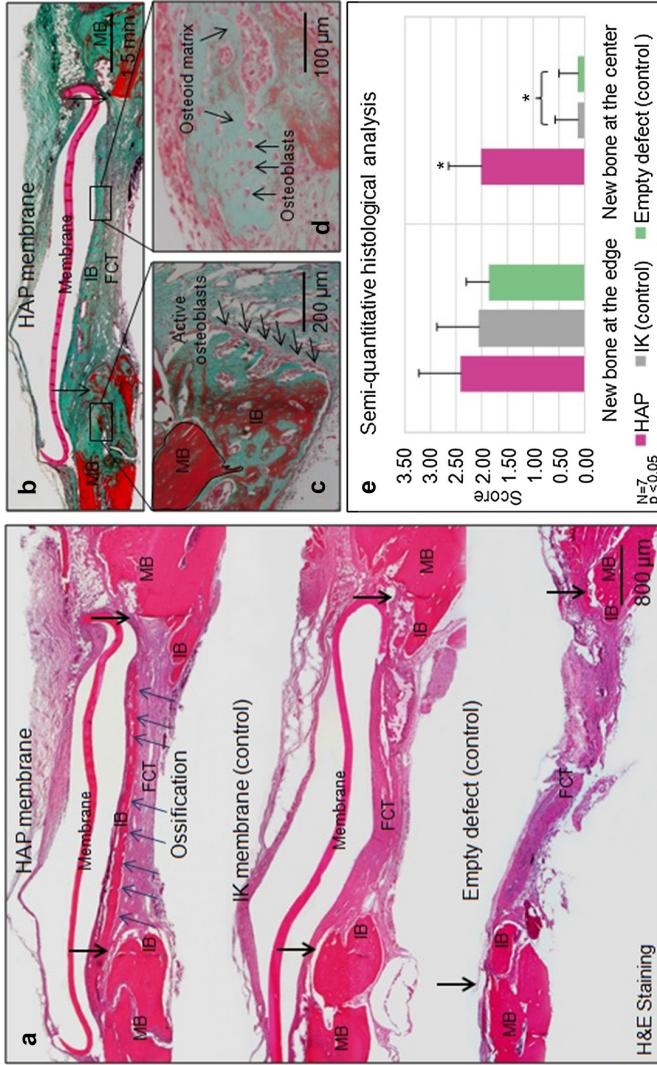
Figure 5: A) Histological sections stained with H&E indicated greater ossification on animals treated with the Smooth HAP membranes (blue arrows) both around the rim and in the middle of the defect compared to animals receiving the non-bioactive IK membranes and those left untreated. B) Histological sections stained with Trichrome Goldner of rats treated with Smooth HAP membranes demonstrated C) the presence of immature (osteoid) and mature bone as well as D) a layer of active osteoblasts embedded within an osteoid matrix located on the growth front along the developing bone around the rim of the defect. E) Semi-quantitative analysis of histological sections verified the presence of more regeneration in animals implanted with the HAP membranes compared to the other groups (P=0.03. (FCT: fibrous connective tissue, MB: mature bone, IB: immature bone).

7

the developing bone around the rim of the defect (Figure 5d). In contrast, animals that were implanted with the IK membranes and animals that were not treated with any membrane only exhibited bone formation around the edge of the defect. In addition, in accordance with the MicroCT results, semi-quantitative analysis of histological sections also verified the presence of more regeneration in animals implanted with the HAP membranes compared to the other groups (Figure 5e).

Discussion

Many proteins found in bone have the capacity to modulate or inhibit mineralization *in vivo*.[32] The possibility to fabricate materials using proteins as both structural and functional building-blocks may provide an effective tool to improve bone regeneration with high efficiency and control. In previous work, we developed a fabrication process to reproducibly create robust and tunable ELR membranes that exhibit specific physical and biomolecular signals [27] and the capacity to promote osteoblastic differentiation *in vitro*.[25] The main objective of the present study was to determine the *in vitro* mineralization and *in vivo* bone regeneration potential of bioactive ELR membranes in an animal model. In particular, the focus was to assess the bioactivity of ELR membranes containing the amino acid sequence DDDEEKFLRRIGRFG (HAP). This segment corresponds to SN_A15, an analog of the SN15 fragment of statherin in which aspartate (D) residues substitute the original phosphoserines and whose bioactivity is equivalent to the SN15 fragment of statherin.[33] Statherin is a protein found in saliva, a supersaturated metastable solution compound of ions, proteins, and water, which plays a role in the nucleation and growth of hydroxyapatite in the oral environment.[34] The N-terminal of the SN15 segment of statherin is formed by a sequence of negatively charged residues such as aspartic acid (D), glutamic acid (E) and phosphorylated-serine (S(P)).[33] This region is responsible for binding calcium ions present in the oral environment and stabilizing the growth and critical size of the CaP cluster required for precipitation and transformation into a crystalline phase of hydroxyapatite.[35] Upon a pH decrease next to the enamel due to the presence of metabolic products secreted by bacteria, statherin releases

the CaP ions on the surface of the tooth and enables their use to promote remineralization.[36] Our hypothesis was that the use of ELRs exhibiting this SN_A15 peptide sequence, which is known to modulate mineralization in enamel as described above, may be used to enhance mineralization in bone. In order to further enhance membrane bioactivity, we also designed and used ELRs with an additional RGDS sequence (HAP-RGDS) in order to promote integrin-mediated cell adhesion.

Mineralization experiments, with and without cells, were conducted in simulated body fluid (SBF) [29] in both static and dynamic experimental conditions since some studies have reported an increase of cell-mediated mineralization under applied strain.[30] In this work, Smooth HAP membranes tested under static conditions reproducibly and significantly increased their mineralization compared to all other tested membranes as revealed by the calcium content assay (Figure 1e), SEM observations (Figure 2a, b), TOF-SIMS analysis (Figure 2c, d), and EDS measurements (Figure 2i, j). These HAP membranes also exhibited a significant increase in Young's modulus compared to all other tested membranes (Figure 2k), an expected result given the presence of the observed mineral layer. These results are consistent with studies demonstrating the affinity of the SN_A15 fragment to adsorb to hydroxyapatite surfaces by chelation with surface calcium ions *in vitro*.[37] This affinity depends on the number and close vicinity of the negatively charged residues in the N-terminal domain, as demonstrated by studies using the individual SN_A15 sequence [33] and within our HAP ELR molecule on titanium surfaces.[38] Therefore, it is possible that the mineralization observed on our HAP membranes was produced by the high density of negative charges present on the N-terminal segment of the SN_A15 fragment of our HAP-containing ELRs. This hypothesis would explain the lower mineralization observed on HAP-RGDS membranes, since these membranes contain a lower density of the SN_A15 sequence compared to HAP membranes.[25]

Despite the strong mineralization on Smooth HAP membranes in static conditions, HAP membranes with Channel topographies and Smooth HAP membranes in dynamic conditions exhibited lower CaP deposition. While the reason for this decrease is not yet clear, it is possible that the 8% uniaxial strain used in this study may have assisted the release of

7

the mineral from the membranes due to mechanical deformation. An alternative explanation might be related with the decrease of mineralization as a result of a decrease in wettability [39] due to the presence of the channel microtopographies. Further studies will have to be performed in order to confirm this hypothesis.

Remarkably, in both static and dynamic conditions, rMSCs growing on HAP membranes in non-osteogenic differentiation medium exhibited similar levels of ALK/DNA expression and higher Ca deposition compared to cells growing in osteogenic differentiation medium on tissue culture plastic (TCP+). These results are in accordance with our previous finding that the amino acid sequence of the SN_A15 fragment significantly upregulates the early osteoblastic marker osterix *in vitro* even in the absence of osteogenic differentiation medium.[25] Previous studies have reported that the application of cyclic uniaxial strain on MSCs increased the production of matrix mineralization.[40] However, in our study mineralization of the membrane in the presence of cells was similar for both static and dynamic culture conditions. It is possible that the mineralizing effect expected to arise from the applied strain was masked by the strong mineralizing effect of the SN_A15 fragment present in HAP membranes.

Due to the strong osteoblastic differentiation and mineralization observed in the Smooth HAP membranes *in vitro*, they were subsequently implanted and assessed in a critical-size rat calvarial model. At day 7, membrane localization were assessed and confirmed to be within the defect in the same place as they were positioned at the time of implantation. This stability results from the distinctive strength and ease of manipulation exhibited by our ELR membranes, which contrast the inherent weakness of other peptide and protein-based scaffolds. With respect to membrane bioactivity, animals implanted with HAP membranes had the highest mean volume of ossified tissue exhibiting an osteoid matrix with active osteoblasts within the defect and in cases even bridging across the critical-size defect (Figure 4 and Figure 5d). Bone mineral density was also measured by microCT although the results exhibited a high variability and did not demonstrate significant differences. This high variability may have resulted because the values of bone mineral density obtained for all samples were lower than the selected range of the accuracy of the equipment. Nonetheless,

altogether the results are consistent with events normally observed in natural intramembranous ossification [41] and in accordance with studies that have demonstrated bone regeneration using other peptide-based materials with mineralization-promoting signals.[6] Both our *in vitro* data and *in vivo* results suggest that the presence of the SN$_A$15 sequence of HAP ELRs may promote early biomineralization and potentially lead to cellular signaling that stimulates progenitor cells and enhances the growth of osteoblasts *in vivo*.

The main design feature of the present study was the generation of ELR building-blocks that offer both mechanical stability through the elastin-like sequences and molecular signaling leading to mineral formation and osteogenesis through the SN$_A$15 segment. ELR-based materials have been found non-cytotoxic and bioactive [42] when used in ostechondral [43] and vascular [44] defects. To our knowledge, this is the first study that demonstrates enhanced bone regeneration using ELRs and the use of a statherin analog known to modulate mineralization in enamel for bone regeneration. A potential explanation for this finding may lie in the fact that statherin found in saliva and proteins found in bone, all of which regulate the growth of CaP, descend from a set of genes that have a common ancestor.[45] This relation may help explain why the SN$_A$15 fragment found to control enamel mineralization,[36] is also efficiently promoting bone formation as observed in this study. The use of non-collagenous proteins known to regulate the remarkable mineral formation found in enamel in order to design materials to improve mineralization and bone regeneration is an exciting possibility.

Conclusions

We report on the enhanced mineralization, osteogenesis and *in vivo* bone regeneration properties of molecularly designed ELR membranes. Smooth membranes, containing an analog of the SN15 fragments of statherin (DDEEKFLRRIGRFG), exhibited the highest quantity of calcium phosphate (Ca/P in 1.78) deposition with and without cells compared to all other tested membranes. Furthermore, these membranes displayed the highest production of alkaline phosphatase (ALK) on day 10 even in the presence of non-osteogenic media. This strong bioactivity was further

7

demonstrated *in vivo* as animals implanted with theses membranes exhibited the highest bone volume within the defect. This study validates the ability of generating ELR molecules that can serve as structural and functional building blocks to create robust biomaterials capable of orchestrating biological responses. Thin robust membranes made completely from molecularly designed ELRs that are capable to promote osteogenesis and enhance mineralization could serve as effective periosteal grafts capable of enhancing bone regeneration.

References

1. Lienemann P, Lutolf M, Ehrbar M. Biomimetic hydrogels for controlled biomolecule delivery to augment bone regeneration. Adv Drug Deliv Rev 2012;64:1078e89.
2. Brown R. Direct collagen-material engineering for tissue fabrication. Tissue Eng Part A 2013;19:1495e8.
3. Collins M, Birkinshaw C. Hyaluronic acid based scaffolds for tissue engineeringea review. Carbohydr Polym 2013;92:1262e79.
4. Ana MM, Catarina MA, Kasper FK, Antonios GM, Rui LR. Responsive and in situ-forming chitosan scaffolds for bone tissue engineering applications: an overview of the last decade. J Mater Chem 2010;20:1638e45.
5. Mobini S, Hoyer B, Solati-Hashjin M, Lode A, Nosoudi N, Samadikuchaksaraei A, et al. Fabrication and characterization of regenerated
6. silk scaffolds reinforced with natural silk fibers for bone tissue engineering. J Biomed Mater Res A 2013;101:2392e404.
7. Mata A, Geng Y, Henrikson K, Aparicio C, Stock S, Satcher R, et al. Bone regeneration mediated by biomimetic mineralization of a nanofiber matrix. Biomaterials 2010;31:6004e12.
8. Zhang X, Awad H, O'Keefe R, Guldberg R, Schwarz E. A perspective: engineering periosteum for structural bone graft healing. Clin Orthop Relat Res 2008;466:1777e87.
9. Gkioni K, Leeuwenburgh S, Douglas T, Mikos A, Jansen J. Mineralization of hydrogels for bone regeneration. Tissue Eng Part B Rev 2010;16:577e85.
10. Chen Y-J, Chung M-C, Jane Yao C-C, Huang C-H, Chang H-H, Jeng J-H, et al. The effects of acellular amniotic membrane matrix on osteogenic differentiation and ERK1/2 signaling in human dental apical papilla cells. Biomaterials 2012;33:455e63.
11. Lee E-J, Shin D-S, Kim H-E, Kim H-W, Koh Y-H, Jang J-H. Membrane of hybrid chitosan-silica xerogel for guided bone regeneration. Biomaterials 2009;30:
12. 743e50.
13. Kim K-H, Jeong L, Park H-N, Shin S-Y, Park W-H, Lee S-C, et al. Biological efficacy of silk fibroin nanofiber membranes for guided bone regeneration. J Biotechnol 2005;120:327e39.
14. Mota J, Yu N, Caridade S, Luz G, Gomes M, Reis R, et al. Chitosan/bioactive glass nanoparticle composite membranes for periodontal regeneration. Acta Biomater 2012;8:4173e80.
15. Douglas T, Gassling V, Declercq H, Purcz N, Pamula E, Haugen H, et al. Enzymatically induced mineralization of platelet-rich fibrin. J Biomed Mater Res A 2012;100:1335e46.
16. Yang F, Both S, Yang X, Walboomers X, Jansen J. Development of an electrospun nano-apatite/PCL composite membrane for GTR/GBR application. Acta Biomater 2009;5:3295e304.

7

17. Kharaziha M, Fathi M, Edris H. Development of novel aligned nanofibrous composite membranes for guided bone regeneration. J Mech Behav Biomed Mater 2013;24:9e20.
18. Benedetto M, Chiara EG, Jake EB, Showan NN. Collagen gel fibrillar density dictates the extent of mineralization in vitro. Soft Matter 2011;7:9898e907.
19. Schneider D, Weber F, Grunder U, Andreoni C, Burkhardt R, Jung R. A randomized controlled clinical multicenter trial comparing the clinical and histological performance of a new, modified polylactide-co-glycolide acid membrane to an expanded polytetrafluorethylene membrane in guided bone regeneration procedures. Clin Oral Implants Res 2014;25(2):150e9.
20. Shin S-I, Herr Y, Kwon Y-H, Chung J-H. Effect of a collagen membrane combined with a porous titanium membrane on exophytic new bone formation in a rabbit calvarial model. J Periodontol 2013;84:110e6.
21. Wang Y, Shi R, Gong P, Li J, Li J, Ao D, et al. Bioelectric effect of a chitosan bioelectret membrane on bone regeneration in rabbit cranial defects. J Bioact Compat Polym 2012;27(2):122e32.
22. Gentile P, Chiono V, Tonda-Turo C, Ferreira A, Ciardelli G. Polymeric membranes for guided bone regeneration. Biotechnol J 2011;6:1187e97.
23. Gungormus M, Branco M, Fong H, Schneider J, Tamerler C, Sarikaya M. Self assembled bi-functional peptide hydrogels with biomineralization-directing peptides. Biomaterials 2010;31:7266e74.
24. Sílvia G, Isabel BL, Jo~ao FM, Rui LR, David LK. Spider silk-bone sialoprotein fusion proteins for bone tissue engineering. Soft Matter 2011;7:4964e73.
25. Joaquim SB, Artur R, Ana MT, Matilde A, Francisco JA, Jos_e CR-C, et al. Development of biomimetic chitosan-based hydrogels using an elastin-like Polymer. Adv Eng Mater 2010;12:37e44.
26. Girotti A, Reguera J, Rodríguez-Cabello J, Arias F, Alonso M, Matestera A. Design and bioproduction of a recombinant multi(bio)functional elastin-like protein polymer containing cell adhesion sequences for tissue engineering purposes. J Mater Sci Mater Med 2004;15:479e84.
27. Tejeda-Montes E, Smith K, Rebollo E, G_omez R, Alonso M, Rodríguez-Cabello J, et al. Bioactive membranes for bone regeneration applications: effect of physical and biomolecular signals on mesenchymal stem cell behaviour. Acta Biomater 2014;10:134e41.
28. Ana CM, Katherine HS, Esther T-M, Elisabeth E, Rui LR, Helena SA, et al. Co-Assembled and microfabricated bioactive membranes. Adv Funct Mater 2013;23:430e8.
29. Tejeda-Montes E, Smith K, Poch M, L_opez-Bosque M, Martín L, Alonso M, et al. Engineering membrane scaffolds with both physical and biomolecular signaling. Acta Biomater 2012;8:998e1009.
30. Prodanov L, te Riet J, Lamers E, Domanski M, Luttge R, van Loon J, et al. The interaction between nanoscale surface features and mechanical loading and its effect on osteoblast-like cells behavior. Biomaterials 2010;31:7758e65.

31. Kokubo T, Takadama H. How useful is SBF in predicting in vivo bone bioactivity? Biomaterials 2006;27:2907e15.
32. Winter L, Walboomers X, Bumgardner J, Jansen J. Intermittent versus continuous stretching effects on osteoblast-like cells in vitro. J Biomed Mater Res A 2003;67:1269e75.
33. Sebasti_an M, Perez R, Egido J. Use of TOF-SIMS in vascular biology. In: Vivanco F, editor. Vascular proteomics: methods and protocols. Methods in molecular biology, New York, vol. 1000; 2013. pp. 33e43. chapter 3.
34. Benesch J, Mano J, Reis R. Proteins and their peptide motifs in acellular apatite mineralization of scaffolds for tissue engineering. Tissue Eng Part B Rev 2008;14:433e45.
35. Raj P, Johnsson M, Levine M, Nancollas G. Salivary statherin. Dependence on sequence, charge, hydrogen bonding potency, and helical conformation for adsorption to hydroxyapatite and inhibition of mineralization. J Biol Chem 1992;267:5968e76.
36. Stayton P, Drobny G, Shaw W, Long J, Gilbert M. Molecular recognition at the protein-hydroxyapatite interface. Crit Rev Oral Biol Med 2003;14:370e6.
37. Hay DI, Moreno EC. Statherin and the acidic proline-rich proteins. In: Tenovuo J, editor. human saliva: clinical chemistry and microbiology. Boca Raton, FL: CRC Press; 1989. pp. 131e50.
38. García-Godoy F, Hicks MJ. Maintaining the integrity of the enamel surface: the role of dental biofilm, saliva and preventive agents in enamel demineralization and remineralization. J Am Dent Assoc 2008;139:25Se34S.
39. Johnsson M, Levine M, Nancollas G. Hydroxyapatite binding domains in salivary proteins. Crit Rev Oral Biol Med 1993;4:371e8.
40. Li Y, Chen X, Ribeiro A, Jensen E, Holmberg K, Rodriguez-Cabello J, et al. Hybrid nanotopographical surfaces obtained by biomimetic mineralization of statherin-inspired elastin-like recombinamers. Adv Healthc Mater 2014: 1e10. http://dx.doi.org/10.1002/adhm.201400015.
41. Liao H, Andersson A-S, Sutherland D, Petronis S, Kasemo B, Thomsen P. Response of rat osteoblast-like cells to microstructured model surfaces in vitro. Biomaterials 2003;24:649e54.
42. Yan H, Xufeng N, Wei S, Changdong G, Qingling F, Yubo F. Combined effects of mechanical strain and hydroxyapatite/collagen composite on osteogenic differentiation of rat bone marrow derived mesenchymal stem cells. J Nanomater 2013;2013.
43. Dimitriou R, Tsiridis E, Giannoudis PV. Current concepts of molecular aspects of bone healing. Injury 2005;36:1392e404.
44. Sallach R, Cui W, Wen J, Martinez A, Conticello V, Chaikof E. Elastin-mimetic protein polymers capable of physical and chemical crosslinking. Biomaterials 2009;30:409e22.
45. Hrabchak C, Rouleau J, Moss I, Woodhouse K, Akens M, Bellingham C, et al. Assessment of biocompatibility and initial evaluation of genipin cross-linked

7

46. elastin-like polypeptides in the treatment of an osteochondral knee defect in rabbits. Acta Biomater 2010;6:2108e15.
47. Kumar V, Caves J, Haller C, Dai E, Liu L, Grainger S, et al. Acellular vascular grafts generated from collagen and elastin analogs. Acta Biomater 2013;9: 8067e74.
48. Kawasaki K, Weiss K. Mineralized tissue and vertebrate evolution: the secretory calcium-binding phosphoprotein gene cluster. Proc Natl Acad Sci U. S. A. 2003;100:4060e5.

7

8

Summary, Closing Remarks and Future Perspectives

Summary

The work performed in the field of tissue engineering during the past decades was full of breakthroughs and discoveries, which led to many innovations for improved health care. Nonetheless, our abilities to factually "engineer a tissue" are still limited and far away from growing a fully functional organ in the lab. The reason (despite the fact that a vast part of research is focused on trial-and-error improvement of clinically utilized materials), is that we do not entirely understand how the subunits of a multi-cellular system are interacting with each other, and with the materials that are brought inside the systems. Evolution has created and fine-tuned various cellular mechanisms that made multicellular life possible and efficient. Single cells are equipped with tools that allow them to perform coordinated processes such as organization, interaction, and migration, but also rejection and shielding of the organism from foreign materials. Only when we know every aspect of such cellular function in our bodies, we will have a chance to engineer tissues from scratch. However, at the moment we have the ability to improve available tissue engineering related applications, by designing materials that are based on involving the interaction with the patients' cells, and which can manipulate certain mechanisms of cell behavior.

 Although our abilities to control cell processes in a 3D environment are still limited, the manipulation on material surfaces is frequently performed. Surface roughness is an evident example of improvement of material performance in living systems, by application of surface topographies. Designed uniform patterns deliver an excellent opportunity to study and fine-tune the cell-behavior as a response to the interaction with the topography. In fact, recent research has shown that such topographies have the ability to outperform the rough surfaces regarding control of the cell-functions, such as change of cell morphology, migration, proliferation, differentiation, protein-expression, and extracellular matrix deposition and mineralization. While requiring only a small additional step in the production of many clinically used bio-materials, topographies have the potential to drastically improve the performance of many materials and devices. This thesis describes some aspects of how surface topographies can interact with cells and to which extent cellular behavior can be manipulated and

8

changed. This summary briefly described the main findings of the research questions that were addressed in the first chapter.

1. Which technologies can be used to manipulate solid matter to produce designed strictly organized topographies, and how can the cellular response to such substrates be assessed?

Bone-implant material development is proceeding at a high pace, and has shifted from straightforward biomaterial testing to more advanced cell-targeted approaches for surface modification and design. It has been long known that cells can recognize and respond to topographical features by changing their morphology and behavior. The progress in surface analytical devices, as well as in techniques for production of topographical features on the nanometer scale allow for the characterization of natural tissues and the reproduction of biomimetic nanofeatures in material surfaces. In **chapter 2**, some of the most common surface-characterization and surface-manufacturing techniques will be addressed and results from *in vitro* and *in vivo* studies will be presented. Knowledge on biomaterial nanotopography can be exploited for active stimulation and control of cellular behavior like attachment, migration, spreading, gene expression, proliferation, differentiation and secretion of matrix components.

2. To which extent can neuronal cells and their neurite extensions react and interact with nanosized grooves?

Modulation of a materials surface topography can be used to steer various aspects of adherent cell behaviour, such as cell directional organization. Especially nanometric sized topographies, featuring sizes similar to for instance the axons of the spiral ganglion cells, are interesting for such purpose. In **chapter 3**, we utilized nanosized grooves in the range of 75–500 nm, depth of 30–150 nm, and pitches between 150 nm and 1000 nm for cell culture of neuron-like PC12 cells. The organizational behaviour was evaluated after 7 days of culture by bright field and scanning electron microscopy. Nanotopographies were shown to induce aligned cell-body/axon orientation and an increased axonal outgrowth. Our findings suggest

that a threshold for cell body alignment of neuronal cells exists on grooved topographies with a groove width of 130 nm, depth of 70 nm and pitch of 300 nm, while axon alignment can already be induced by grooves with 135 nm width, 52 nm depth and 200 nm pitch. However, no threshold has been found for axonal outgrowth, as all of the used patterns increased outgrowth of PC12-axons. In conclusion, surface nanopatterns have the potential to be utilized as an electrode modification for a stronger separation of cells, and can be used to direct cells towards the electrode contacts of cochlear implants.

3. To which extent can cells recognize and preferentially migrate on patterned surfaces?

In **chapter 4**, we investigated whether cells have an intrinsic ability to recognize nanopatterns, which could lead to their accumulation or diminution on a biomaterial. A multi-patterned "biochip" was made, containing 36 differently designed surfaces, including squares and grooves varying in feature sizes between 10 and 1000 nm. The grooved patterns could additionally be subdivided into three groups having ridge to groove ratios of 1:1, 1:3 and 3:1. These substrates were used for culture of rat bone marrow derived mesenchymal cells. In time cells should accumulate on patterns of preference, while migrating away from patterns of disfavor. A regression analysis model was designed for the analysis of the obtained data. Results showed that strong differences existed between the tested patterns regarding the cellular affinity. All sizes of squares showed strong cell-repelling capacity, with the biggest sized squares displaying up to 40% less cells compared to the smooth surface. Among the nano-grooved patterns cell repelling was seen for the grooves with the ridge to groove ratio of 1:3, while grooves with the ridge to groove ratio of 3:1 partially showed cell attraction. Such effects were shown to be based on selective migration rather than proliferation. In conclusion, the use of a multi-patterned biochip setup allows for enhanced evaluation of cell behavior, as compared to uniformly patterned setups. Cells exhibit the ability to actively avoid or migrate to surfaces featuring certain topographies on nanometric scale. Such phenomena may be utilized for the development

8

of biomaterials in regenerative medicine.

4. Can a calcium-phosphate based coating change the response of mineralizing cells to nanosized grooves, regarding organization, proliferation, differentiation and mineralization?

In **chapter 5**, we evaluated the influence of nanoscale surface-topographies in combination with a calcium phosphate (CaP) coating on passive and cell-driven surface mineralization. Four groups of substrates were produced, including smooth, grooved (940 nm pitch, 430 nm groove width, 185 nm depth), smooth coated, and grooved coated. The substrates were characterized by scanning/transmission electron microscopy and atomic force microscopy. Osteoblast-like MC3T3 cells were cultured on the substrates for a period up to 35 days under osteogenic conditions. Differentiation was observed by alkaline phosphatase assay and PCR of collagen I (COLI), osteopontin (OPN), osteocalcin (OC), bone-morphogenic protein 2 (BMP2), and bone sialoprotein (BSP). Mineralization was quantified by a calcium assay and Alizarin Red staining. In addition, passive mineralization was determined after incubation of substrates in just cell culture medium without cells. Results showed that a reproducible nano-metric (~50 nm) CaP-layer could be applied on the substrates, without losing the integrity of the topographical features. While no relevant differences were found for cell viability, cells on smooth surfaces proliferated for a longer period than cells on grooved substrates. Also differentiation was affected by topographies, as indicated by an increased expression of OC, OPN and ALP activity. Deposition of a CaP coating significantly increased the passive calcification of smooth as well grooved substrate-surfaces. However, this mineralizing effect was strongly reduced in the presence of cells. In the cell seeded situation, mineralization was significantly increased by the substrate topography, while only a minor additive effect of the coating was observed. In conclusion, the here presented model can be exploited for experimental evaluation of cell-surface interaction processes and optimization of bone-anchoring capability of implants. The model showed that a combination of nanogrooves with a CaP coating can have a better outcome on *in vitro* mineralization processes, compared with the

separate surface cues and the smooth control. However, our results also indicated that passive mineralization assays are not necessary predictive for biological results.

5. Can nanosized grooves on the surface of spherical implants influence the regeneration of trabecular bone in an animal model?

Multiple *in vitro* studies have confirmed the promotion of bone forming cell activity on nano-patterned surfaces. However, there is a lack of translation of the *in vitro* knowledge into pre-clinical *in vivo* trials. In **chapter 6**, we developed a method to reproduce two nanogrooved patterns (groove width 150/200 nm, groove depth 50/70 nm and pitches of 300/1000 nm respectively) into cylindrical epoxy resin implants, which were subsequently coated with 20 nm of titanium. Also, epoxy implants with a conventional surface roughness (Rq = 1.6 μm) were produced. After cytocompatibility analysis of the produced surfaces, implants were installed into the femoral condyle of rats for 4 and 8 weeks. After retrieval histological and histomorphometrical analysis was performed, including the measurement of the bone volume in a 100 μm wide zone close the implant surface. Statistical testing showed that only for the implants provided with 200 nm wide grooves the amount of bone increased significantly between 4 and 8 weeks of implantation. In addition, at the late timepoint only implants with the 200 nm pattern revealed a significantly higher bone volume compared to the rough controls. In conclusion, the 200 nm grooved pattern can positively influence the osseointegration of implants, and should be evaluated and optimized in further (pre-)clinical studies.

6. Can microsized grooves on the surface of bioactive elastin-like recombinamer membrane influence the biological response, including differentiation and mineralization?

The search for alternative therapies to improve bone regeneration continues to be a major challenge for the medical community. In **chapter 7**, we report on the enhanced mineralization, osteogenesis, and *in vivo* bone regeneration properties of a bioactive elastin-like recombinamer

8

(ELR) membrane. Three bioactive ELRs exhibiting epitopes designed to promote mesenchymal stem cell adhesion (RGDS), mineralization (DDDEEKFLRRIGRFG), and both cell adhesion and mineralization were synthesized using standard recombinant protein techniques. The ELR materials were then used to fabricate membranes comprising either a smooth surface (Smooth) or channel microtopographies (Channels). Mineralization and osteoblastic differentiation of primary rat mesenchymal stem cells (rMSCs) were analyzed in both static and dynamic (uniaxial strain of 8% at 1 Hz frequency) conditions. Smooth mineralization membranes in static condition exhibited the highest quantity of calcium phosphate (Ca/P of 1.78) deposition with and without the presence of cells, the highest Young's modulus, and the highest production of alkaline phosphatase on day 10 in the presence of cells growing in non-osteogenic differentiation medium. These membranes were tested in a 5 mm-diameter critical-size rat calvarial defect model and analyzed for bone formation on day 36 after implantation. Animals treated with the mineralization membranes exhibited the highest bone volume within the defect as measured by micro-computed tomography and histology with no significant increase in inflammation. This study demonstrates the possibility of using bioactive ELR membranes for bone regeneration applications.

Closing remarks and future perspectives

In this thesis surface topographical features were utilized as a method for cellular manipulation. We studied how cells change their morphology, migration, and mineralization relevant behavior in response to the experienced topography in *in vitro* and *in vivo* setups. Our findings indicate that despite the minor changes to the material, surface patterns can dramatically influence cellular fate. Applying this strategy on the surfaces of implantable materials for tissue engineering approaches might improve the final outcome of clinical applications. However, different treatments need specific designs of the substrate surfaces. While for a cochlear implant the pure alignment that has been found in **chapter 3** would sufficiently improve the quality of the device, the situation for bone implants is more complicated. The implant surface should attract a specific subset of cells, promote osteogenic differentiation, and mineralization

during a time-period of several weeks. This shows the difficulty that implant manufacturers will face during the designing process. As stated above, events like the initial interaction with the body fluids, binding of proteins and cells, are substrate-dependent. Individually, these processes can be reliably studied *in vitro*. However, the system under study is highly dynamic from the materials and cell perspective. In time material surface properties will undergo changes such as (1) change of the topography and the topographic feature dimensions by degradation of the material or massive deposition of the extracellular matrix, (2) changes of the protein profile at the surface, (3) changes of the cell-types at the surface. That means that upon differentiation a different cell-type will be in contact with the substrate, which might react to the topographies in a different manner. Surfaces that might attract stem cells and facilitate differentiation, might repel osteoblasts. The situation becomes even more complicated in a living system, as factors such as dynamic flow, mechanical load and the interaction of hundreds of different cell-types will occur. Therefore, extrapolation of data from *in vitro* studies is risky, but might give insight in the fundamental processes and mechanisms. *In vivo* models more and more will become of importance for evaluation of materials, but need proper design and evaluation.

While failing of an *in vitro* designed pattern in an *in vivo* situation might be a huge problem for an implant manufacturer, several other concerns should be mentioned regarding topography influence in living systems. Research from various fields, such as toxicology, physiology, behavioral biology, and many others, shows that animal models are often not close enough to the situation in humans. Indeed, a vertebrate organism, including tissue composition, organ development and structure, physiological properties, but also cell types and sizes, is strongly variable between species. The development and optimization of a pattern for implant surface modification might dramatically diverge between different animal models and the final utilization inside a human body. Moreover, similar to drug development, a strong variation should also be expected between the responses to a pattern between individuals. The idea of "personalized medicine" should also be regarded in future implant studies on surface topography.

 Regarding the dramatic influence that topographies can have on living

8

cells, another critical question arises. In our studies, quantification and characterization methods were used to study desirable aspects of cell behavior. But if a pattern has the ability to reprogram the cell fate; how sure can we be that such a powerful mechanism is not inducing also unwanted changes to the organism. One can argue that we are introducing topographies into our bodies since decades, on for example the surfaces of bone implants. But while many studies were performed on the osseointegration and lifetime of the implants, no research was done on what the implants are changing and manipulating inside the patient that is not related to osseointegration. Biological safety studies are becoming an issue of increasing importance in the entire field of nanotechnology. The final safety of nanometrically patterned devices should also be studied in this regard.

Recapitulating it can be said that the possibility of adverse effects of nanotechnology in implantology should be considered and experimentally evaluated. However, on basis of the studies described in this thesis it should be concluded that topographies are a powerful tool that can be utilized for the study of strongly fundamental cellular mechanisms. Finally, these mechanisms can be exploited for the design and optimization of implants and tissue engineered devices.

9

Samenvatting, Sluitopmerkingen en Toekomstperspectieven

Samenvatting

De afgelopen decennia zijn er vele doorbraken geweest op het gebied van weefsel regeneratie ('*tissue engineering*'). Zulke vernieuwingen leiden tot een hogere kwaliteit van de geboden gezondheidszorg. Niettemin zijn onze mogelijkheden om feitelijk een weefsel te genereren beperkt, en zijn we nog steeds ver verwijderd van de mogelijkheid tot het kweken van een volledig functioneel orgaan in het lab. De reden (naast het feit dat een groot deel van het onderzoek naar de verbetering van klinisch gebruikte materialen gebaseerd is op '*trial-and-error*'), is dat we niet volledig begrijpen hoe de losse eenheden van een multi-cellulair systeem interactie met elkaar aangaan, en met de materialen die in het systeem worden gebracht. De evolutie heeft verschillende cellulaire mechanismen gecreëerd en verfijnd, die meercellig leven mogelijk en efficiënt maken. Cellen zijn uitgerust met gereedschappen die hen in staat stellen om gecoördineerde processen zoals organisatie, interactie, en migratie, maar ook afstoting en afscherming van vreemde materialen uit het organisme te bewerkstelligen. Pas wanneer we elk aspect van deze cellulaire functies in ons lichaam kennen, zullen we in staat zijn om weefsels in een petrischaal te genereren. Op dit moment beschikken wij alleen over de mogelijkheid om reeds beschikbare weefselregeneratie toepassingen verder te verbeteren, door het ontwerpen van materialen die een directe interactie met de cellen van de patiënt aan kunnen gaan, waardoor bepaalde aspecten van het celgedrag worden gestuurd.

Hoewel onze mogelijkheden om cellulaire processen in een 3D-omgeving te controleren nog steeds beperkt zijn, wordt oppervlakte modificatie van materialen regelmatig toegepast. Het aanbrengen van ruwheid of een specifieke oppervlakte topografie is een duidelijk voorbeeld van de verbetering van het materiaal voor de toepassing in een levend systeem. Door de mens ontworpen uniforme patronen zijn zeer geschikt om het celgedrag als reactie op een topografie te bestuderen en verder te verfijnen. Recent onderzoek heeft aangetoond dat dergelijke topografieën zeer goed in staat zijn om celfuncties te sturen, zoals het wijzigen van de celmorfologie, migratie, proliferatie, differentiatie, proteïne-expressie, de afzetting van extracellulaire matrix, en de mineralisatie; en dit ook beter

9

kunnen dan simpelweg opgeruwde oppervlakten. Hoewel het slechts een kleine extra stap zou zijn tijdens de productie van veel klinisch gebruikte biomaterialen, heeft het toepassen van een topografie potentieel om het gedrag van die materialen drastisch te verbeteren. Dit proefschrift beschrijft enkele aspecten van de interactie tussen oppervlakte topografie en cellen, en in hoeverre het cellulaire gedrag daadwerkelijk kan worden gemanipuleerd. Deze samenvatting zal in het kort de belangrijkste bevindingen bij de onderzoeksvragen uit het eerste hoofdstuk beschrijven.

1. Welke technologieën kunnen worden gebruikt om georganiseerde topografieën op vaste materialen te vervaardigen, en hoe kan de cellulaire respons op dergelijke substraten worden bestudeerd?

Bot implantatie materiaal worden in hoog tempo ontwikkeld, en innovaties verschuiven daarbij van een ongecompliceerde materiaalkundige aanpak tot aan zeer geavanceerde oppervlakte modificaties gericht op cellen. Het is al lang bekend dat cellen topografische kenmerken kunnen herkennen en hier op kunnen reageren door te veranderen van morfologie en van gedrag. Oppervlakte analyse technieken, en technieken voor de productie van topografie op nanometerschaal zijn ver vooruit gegaan. Dit maakt het mogelijk om natuurlijke weefsels te karakteriseren, en de zo gevonden bio-mimetische nano eigenschappen op een materiaal oppervlak te reproduceren. In **hoofdstuk 2**, wordt een aantal van de meest voorkomende oppervlakte karakterisering en -fabricage technieken besproken; en worden de resultaten van *in vitro* en *in vivo* studies gepresenteerd. Kennis over nanotopografie op biomaterialen kan worden benut voor actieve stimulering van het cellulaire gedrag. Eigenschappen zoals aanhechting, migratie, spreiding, genexpressie, proliferatie, differentiatie en de secretie van matrix componenten, kunnen door topografie gecontroleerd worden.

2. In welke mate kunnen neuronale cellen en hun extensies reageren op nanogroeven?

Modulatie van de oppervlakte topografie van een materiaal kan worden gebruikt om verschillende aspecten van hechtende cellen te sturen,

bijvoorbeeld de cel oriëntatie. Vooral nanometrische topografieën, qua afmetingen vergelijkbaar aan de axonen van spiraal ganglion cellen, zijn interessant voor een dergelijk doel. In **hoofdstuk 3**, werden nanogroeven gebruikt met afmetingen van 75-500 nm, een diepte van 30-150 nm, en een onderlinge afstand van tussen de 150 nm en 1000 nm, in een celkweek van neuron-achtige PC12 cellen. De organisatie van de cellen werd na 7 dagen geëvalueerd, door middel van licht- en scanning elektronenmicroscopie. De toegepaste nanotopografieën bleken de oriëntatie van cellichamen en van de axonen te beïnvloeden, en daarnaast axonale uitgroei te veroorzaken. Onze bevindingen suggereren dat een drempelwaarde voor de uitrichting van neuronale cellichamen bestaat bij een minimale groefbreedte van 130 nm, diepte van 70 nm en afstand van 300 nm; dit terwijl axonen al kunnen worden beïnvloed door kleinere groeven van 135 nm breed, 52 nm diep, en een afstand van 200 nm. Er is echter geen minimale drempel waarde gevonden voor axonale uitgroei, aangezien alle gebruikte patronen de uitgroei van PC12-axonen verhoogden. In conclusie kan gezegd worden dat oppervlakte nanopatronen potentieel gebruikt kunnen worden ter modificatie van elektrodecontacten van cochleaire implantaten, voor een betere onderlinge scheiding en uitlijning van cellen.

3. In welke mate kunnen cellen nanotopografieën op het oppervlak herkennen, en bestaat er een voorkeursmigratie tussen patronen?

In **hoofdstuk 4** is onderzocht of cellen het intrinsieke vermogen hebben om nanopatronen te herkennen, wat kan leiden tot de aantrekking, of juist tot de vermijding van die cellen ten opzichte van een gestructureerd biomateriaal. Er werd een "biochip" gemaakt, met 36 verschillend ontworpen nanopatronen aan het oppervlak, zoals vierkantjes en groeven variërend in afmeting tussen 10 en 1000 nm. Bovendien, werden de gegroefde patronen onderverdeeld in drie groepen met groef-richel verhouding van 1: 1, 1: 3 of 3: 1. De substraten werden gebruikt voor kweek van ratten beenmerg mesenchymale cellen. De onderliggende gedachte was dat de cellen zich op termijn zouden ophopen op patronen van voorkeur, terwijl ze weg zouden migreren van minder aantrekkelijke patronen. Er werd een regressieanalyse model ontwikkeld voor het bestuderen van de verkregen

9

gegevens. De resultaten toonden aan dat er grote verschillen bestaan tussen de geteste patronen wat betreft de cellulaire affiniteit. Alle maten vierkantjes vertoonden een sterk cel-afstotend vermogen, op de grootste vierkantjes waren zelfs tot 40% minder cellen aanwezig vergeleken met een glad controle oppervlak. Bij de nanogroefpatronen werd cel afstoting gezien voor de groeven met een verhouding van 1: 3, terwijl de groeven met een verhouding van 3: 1 gedeeltelijk cel attractie vertoonden. Dergelijke effecten bleken te zijn gebaseerd op selectieve migratie , en niet op proliferatie. Concluderend, is het gebruik van een multi- patroon biochip beter geschikt voor de evaluatie van celgedrag, vergeleken met studies waarin maar een enkel oppervlakte patroon wordt gebruikt. Cellen vertonen het vermogen om bepaalde naotopografieën actief te vermijden of om juist naar oppervlakken toe te migreren. Dergelijke fenomenen kunnen worden gebruikt voor de ontwikkeling van biomaterialen voor regeneratieve geneeskunde.

4. Kan een calciumfosfaat coating de respons van mineraliserende cellen op nanogroeven veranderen, wat betreft proliferatie, differentiatie en mineralisatie?

In **hoofdstuk 5** werd de invloed van oppervlakte nanotopografieën, in combinatie met een calciumfosfaat (CaP) coating, bestudeerd op passieve en cel-gedreven mineralisatie. Vier groepen substraten werden geproduceerd, nl. glad, gegroefd (940 nm groefafstand, 430 nm groefbreedte, 185 nm diepte), glad gecoat, en gegroefd gecoat. De substraten werden gekarakteriseerd met scanning- en transmissie elektronen microscopie, en door middel van atomic force microscopie. Daarna werden osteoblast-achtige MC3T3 cellen op de substraten gekweekt gedurende maximaal 35 dagen onder osteogene condities. De mineralisatie werd gekwantificeerd met behulp van een calcium assay en alizarine rood kleuring. Het differentiatie proces werd gevolgd door middel van een alkalische fosfatase activiteitsmeting, en door de mRNA genexpressie te kwantificeren voor collageen I (COLI), osteopontine (OPN), osteocalcine (OC), bot-morfogeen eiwit 2 (BMP2), en bot sialoproteïne (BSP). Uit de resultaten van de substraat karakterisering bleek dat een goed reproduceerbare nanometrische (~ 50

nm) CaP-laag kon worden aangebracht op de substraten, zonder dat de integriteit van de topografische kenmerken werd verstoord. De calcium test toonde aan dat coatings een sterke toename van passieve verkalking op het substraatoppervlak veroorzaakten. Echter, in aanwezigheid van een monolaag van cellen, werd het passieve mineralisatieproces sterk verlaagd. Hier werd gezien dat de toename van calcium op het substraat oppervlak juist hoofdzakelijk werd veroorzaakt door de topografie, terwijl de combinatie met de coating additionele, of zelfs synergetische effecten op mineralisatie opleverde. Een vergelijkbaar synergetisch effect werd ook gevonden bij de expressie van een aantal van de genen specifiek voor osteogene differentiatie. Ten slotte kon geconcludeerd worden dat het gebruikte model benut kan worden voor experimentele evaluatie van interactie tussen cellen en het oppervlak, en de optimalisatie van het botverankerend vermogen van implantaten.

5. Hebben nanogroeven op het oppervlak van sferische implantaten invloed op de regeneratie van het trabeculair bot in een diermodel?

Het is door verschillende onderzoeksgroepen in verschillende *in vitro* studies bevestigd, dat nanogroeven op het oppervlakte botvormende cellen kunnen stimuleren. Tegelijkertijd is er echter een gebrek aan translatie van zulke *in vitro* kennis, in de vorm van de noodzakelijke pre-klinische *in vivo* studies. In **hoofdstuk 6**, werd daarom een methode ontwikkeld waarbij twee nanopatronen (groefbreedte 150/200 nm, diepte resp. 50/70 nm en onderlinge afstand resp. 300/1000 nm) werden gereproduceerd vanaf vlakke silicium wafers naar cilindrische implantaten gemaakt uit epoxyhars. Deze implantaten werden bedekt met een dunne titaniumlaag (20 nm), en vergeleken met opgeruwde implantaten (Ra = 1,6 µm) in een *in vivo* rattenmodel. Mogelijke ontstekingsreacties werden geëvalueerd door het implantaat subcutaan te plaatsen voor een periode van 4 weken. Er werden daarbij geen verschillen gevonden tussen de groepen; overal werd slecht een minimale ontstekingsreactie en vreemd lichaam reactie gevonden. Daarna werd de osteointegratie van de topografieën bestudeerd door implantatie in de femorale medulla, gedurende 4 of 8 weken. De implantaten die voorzien waren van 200 nm groeven bleken

9

significant meer bot rondom het implantaat te vertonen, ten opzichte van het ruwe oppervlak na 8 weken in het experiment, en zij waren tevens de enige groep waarbij het omringende bot verhoogd aanwezig was bij een vergelijking tussen 4 en 8 weken.

6. Kunnen microgroeven op het oppervlak van bioactieve elastine-achtige recombinameer membranen de biologische respons, zoals differentiatie en mineralisatie, beïnvloeden?
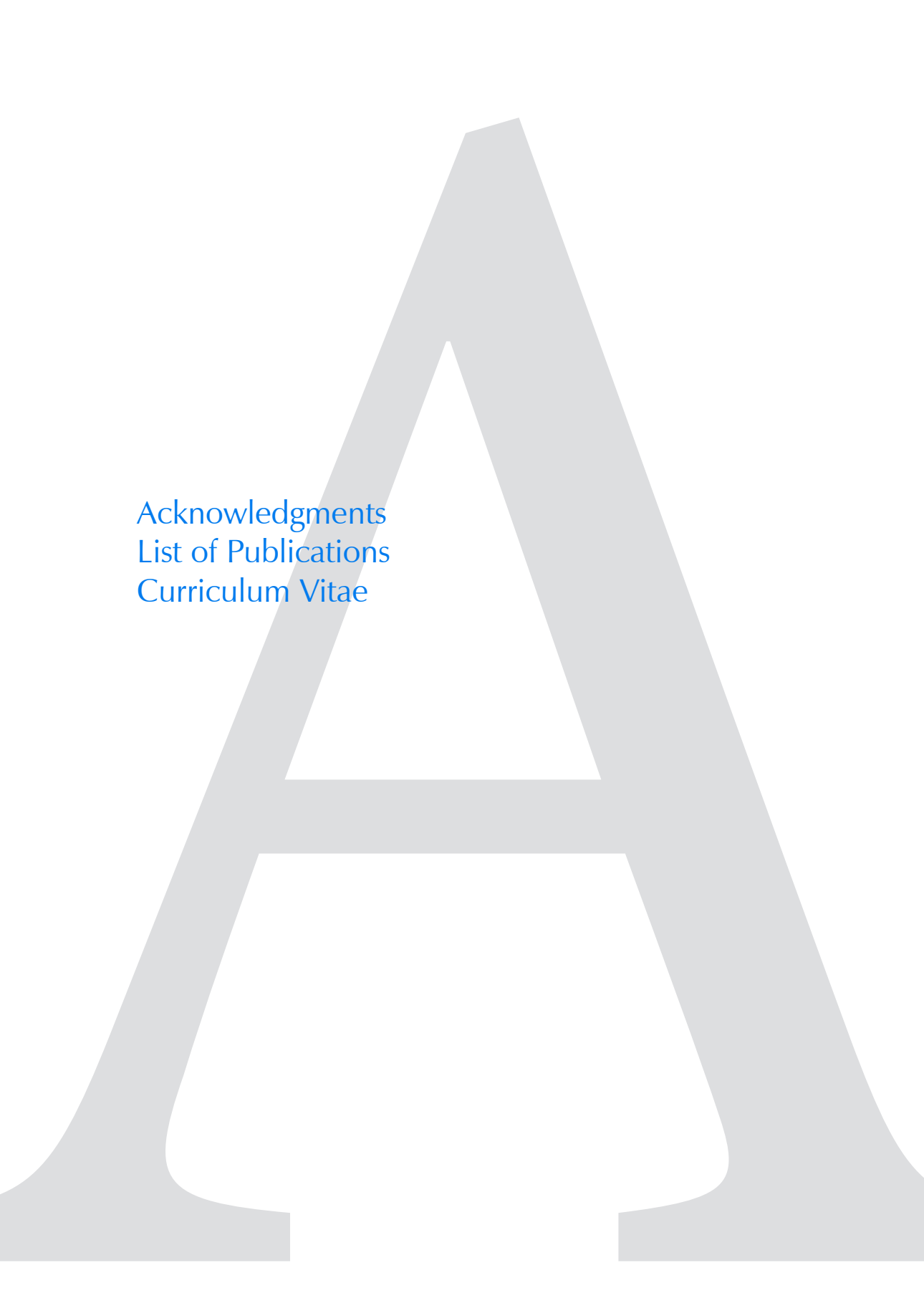
De zoektocht naar betere therapieën voor botherstel blijft een grote uitdaging voor de medische gemeenschap. In **hoofdstuk 7** werd een verbeterde mineralisatie, osteogenese, en *in vivo* botregeneratie aangetoond van van een bioactieve elastine-achtige recombinameer (ELR) membraan. Drie bioactieve ELRs werden gesynthetiseerd, die door middel van standaard recombinant eiwit technieken over epitopen beschikten die in staat waren mesenchymale stamcel adhesie (RGDS) te bevorderen, mineralisatie te verhogen (DDDEEKFLRRIGRFG), of zowel celadhesie als mineralisatie te verhogen. Deze drie ELR materialen werden vervolgens gebruikt om membranen met een glad oppervlak, of juist met microtopografie te fabriceren. Daarna werd de mineralisatie en osteoblast differentiatie van primaire rat mesenchymale stamcellen (rMSCs) geanalyseerd onder zowel statische als dynamische (unidirectionele rek van 8% met een frequentie van 1 Hz) omstandigheden. De gladde mineralisatie membranen vertoonden in rusttoestand de hoogste hoeveelheid calciumfosfaat (Ca / P van 1,78), zowel met als zonder de aanwezigheid van cellen, de hoogste Young's modulus, en de hoogste productie van alkalische fosfatase op dag 10 in de aanwezigheid van cellen in differentiatie medium. Deze membranen werden dan ook verder getest in een kritisch defect defect van 5 mm in diameter in het calvarium van ratten. Op dag 36 werd de botvorming onderzocht. De dieren die waren geïmplanteerd met de mineralisatie-bevorderende membranen vertoonden het hoogste botvolume in het defect, gemeten met micro-computertomografie en histologie, zonder een significante toename van de ontstekingsreactie. Deze studie toont dus aan dat het mogelijk is om bioactieve ELR membranen voor botregeneratie toepassingen te gebruiken.

Slotopmerkingen en toekomstperspectieven

In dit proefschrift werd oppervlakte topografie gebruikt, als een methode voor de manipulatie van cellulair gedraag. Er werd bestudeerd hoe cellen hun morfologie, migratie en mineralisatie gedrag kunnen veranderden, als reactie op de ondervonden topografie in zowel *in vitro* als *in vivo* experimenten. De bevindingen wijzen erop dat, ondanks de kleine veranderingen aan het materiaal, oppervlak patronen het lot van cellen drastisch kunnen beïnvloeden. Het toepassen van deze strategie op het oppervlak van implanteerbare materialen voor weefsel regeneratie, zou het uiteindelijke resultaat bij klinische toepassingen kunnen verbeteren. Het is echter duidelijk dat er voor verschillende behandelingen telkens specifieke ontwerpen van het substraatoppervlak nodig zijn. Terwijl bij de toepassing op een cochleair implantaat, zoals beschreven in **hoofdstuk 3**, het voldoende zou zijn om uitlijning te verkrijgen om de kwaliteit van het implantaat te verbeteren, is de situatie bij botimplantaten veel ingewikkelder. Het implantaatoppervlak moet daar een specifieke sub-set van cellen aantrekken, osteogene differentiatie induceren, en het mineralisatie vermogen verhogen gedurende een tijdsperiode van meerdere weken. Dit toont aan hoe moeilijk het ontwerpproces zal zijn voor de implantaat fabrikanten. Zoals hierboven beschreven, zijn fenomenen zoals de initiële interactie met de lichaamsvloeistoffen, de binding van eiwitten en de aanhechting van cellen substraat afhankelijk. Individueel kunnen deze processen weliswaar betrouwbaar worden bestudeerd in *in vitro* situaties. Het systeem als geheel is echter zeer dynamisch vanuit het perspectief van materialen en cellen. Over de tijd zullen materiaaloppervlak eigenschappen gewoonweg veranderen, bijvoorbeeld (1) de topografie en de afmetingen van topografische kenmerken kunnen veranderen door afbraak van het materiaal of door de afzetting van extracellulaire matrix, (2) het eiwit profiel aan het oppervlak kan veranderen, (3) de cel-types aan het oppervlak kunnen veranderen. Dat betekent, dat na differentiatie een andere celtype in contact zal zijn met het substraat, wat dus ook weer op een andere manier op de topografie zal reageren. Oppervlakken die stamcellen kunnen aantrekken en differentiatie kunnen induceren, zouden wellicht de gedifferentieerde osteoblasten weer kunnen afstoten. De situatie

9

wordt nog ingewikkelder in een levend systeem, waarbij factoren zoals dynamische vloeistof stroming, mechanische belasting en de interactie van honderden verschillende celtypen optreden. Daarom is een rechtstreekse extrapolatie van de *in vitro* verkregen gegevens onbetrouwbaar en riskant. Desondanks kunnen dergelijke studies wel inzicht in geven de fundamentele processen en mechanismen. *In vivo* modellen zullen echter meer en meer van belang worden voor de evaluatie van materialen.Naast de mogelijkheid dat een patroon, welke ontworpen is vanuit een vitro situatie, niet tot het gewenste *in vivo* resultaat hoeft te leiden, moet er ook nog met een aantal andere problemen rekening gehouden worden. Uit onderzoek vanuit verschillende wetenschapsgebieden, zoals toxicologie, fysiologie, gedragsbiologie etc. blijkt, dat diermodellen vaak niet dicht genoeg bij de situatie in de mens komen. Gewervelde organismen zijn sterk variabel tussen verschillende species, wat betreft de samenstelling van hun weefsels, de ontwikkeling en structuur van de organen, de fysiologische eigenschappen, en zelfs de soorten en afmetingen van de cellen. De ontwikkeling en optimalisatie van een patroon voor implantaat oppervlaktemodificatie kan dus drastisch verschillen tussen verschillende proefdiermodellen en het uiteindelijke gebruik in een menselijk lichaam. Bovendien kan, vergelijkbaar bij de ontwikkeling van geneesmiddelen, een sterke variatie worden verwacht tussen de respons op een patroon tussen verschillende individuen. Het idee van "gepersonaliseerde geneeskunde" moet ook in de toekomst voor oppervlaktetopografie implantaat studies worden beschouwd.De sterke invloed die topografieën op levende cellen kunnen hebben, levert ook nog een andere kritische vraag op. In onze studies, werden alleen voor ons zelf interessante aspecten van het celgedrag gekwantificeerd en gekarakteriseerd. Maar als een patroon het vermogen heeft om het lot van een cel te herprogrammeren; hoe zeker kunnen we dan zijn dat zo'n krachtig mechanisme niet ook ongewenste veranderingen in het organisme ten gevolge zou kunnen hebben. Het is wel duidelijk dat topografie al decennia lang in ons lichaam wordt geïntroduceerd, bijvoorbeeld via het ruwe oppervlak van bot implantaten. Maar terwijl er veel studies gedaan worden naar de osseointegratie en de levensduur van zulke implantaten, wordt er weinig of geen onderzoek gedaan naar welke veranderingen er nog meer in de patiënt plaats zouden

kunnen vinden, voor zover die niet gerelateerd zijn aan osseointegratie. Biologische veiligheidsstudies worden in toenemende mate belangrijke in het gehele gebied van de nanotechnologie. De uiteindelijke veiligheid van nanometrische patronen moeten ook in dit verband worden onderzocht. Samenvattend kan worden gezegd, dat het mogelijke scenario van ongunstige bijwerkingen van nanotechnologie in het vakgebied van de implantologie in de toekomst experimenteel geëvalueerd moet worden. Echter, op basis van dit proefschrift moet ook worden geconcludeerd dat de toepassing van topografieën een krachtig instrument vormt, dat kan worden gebruikt voor de studie van fundamentele cellulaire mechanismen. Tenslotte kunnen deze mechanismen worden benut voor het ontwerpen, en de optimalisatie van implantaten en weefsel regeneratie technieken.

9

Acknowledgments
List of Publications
Curriculum Vitae

Acknowledgments

A long time ago, in a city far away, I was asked once what I would like to become when grown up. While other kids had plans to go to space as soviet cosmonauts, or fight the crime as policemen, my answer was "a professor…". "A professor…, or a taxi driver". When asked why a taxi driver, I reasoned that in Ukraine it would be impossible to get a lab without having good connections. Today, in the Netherlands, and more than 20 years later, I have made one further step towards academia. The way has not always been easy, and on some points being a taxi driver would appear so much more attractive. But there have been always people around me, who helped me to stay on track, motivated me to go on, or just made my life very much enjoyable. This book is the final proof of our shared success. In this chapter I would like to thank all of the people, who as I think contributed to this manuscript.

First and foremost, I would like to express my sincere gratitude to my promotor, Prof. dr. John Jansen. Dear John, thank you for giving me the opportunity to join your lab as a member of the biomaterials research group. Although being busy on so many levels, you took your time for all of the PhD students, and helped and guided us through the sometimes frustrating processes of the academic path. It was sometimes very impressive to receive a completely reviewed manuscript full of detailed corrections and comments late in the evening, only hours after having sent it to you. Not less impressive was the fact that despite all of your tasks and responsibilities you could find time and energy to go running during the lunch breaks. John, your passion for science and personal discipline will always remain very inspiring and motivating.

Not less, I am also deeply grateful to my co-promotor, Dr. Frank Walboomers. I remember the first time we met during my interview. After discussing the overall aim of the project, you have brought me upstairs to show me the lab. The first room you were starting with was the "sawing room". While after four years in the lab I do understand that the room was very well equipped for the work in the field of biomaterials, the impression that I had back then was …well I was quite astonished. Coming from molecular biology labs, which are expectably clean, tidy, and almost sterile, the "sawing room"

with its rusty tools and a horror-movie workshop atmosphere with all the plasticized jaws and bones did impress me in a slightly different way than you probably had expected. Luckily, the other parts of the lab were more similar to what I was used to. I say luckily, because if I would have decided not to accept the offer to work with you, I would have missed a great time of my life. A time in which I had to realize that for me the workspace is not defined by the fanciness of the next-gen equipment on the lab tables, but by the compilation of the lab colleagues. Dear Frank, I really appreciate it that you agreed for me to join the project on patterns, which is a very close subject to your own PhD work. Although you possess profound knowledge on this topic, you left me enough of freedom in the decisions during the different studies, so that I could experience both the setbacks but also the successes of my own ideas. You were always there when I needed advise, and I can proudly say that under your supervision and with your help I could learn a lot about problem solving. I really enjoyed working with you and hope that your motivational character and "fingerspitzengefühl" for application of the right amount of mental pressure will help many more PhDs to accomplish their tasks in the same joyful atmosphere as I did.

I would like to further express my appreciation for the other supervisors in the lab; Dr. Sander Leeuwenburgh, Dr. Joop Wolke, and Dr. Jeroen van den Beuken. Thank you for being very helpful on many occasions in which I needed help with specific questions in the fields you are definitely experts in. Thank you also for your (mostly ☺) kind and constructive criticisms during the PhD meetings. It is a fact that many of us could profit from your contributions.

A special thank is going to Dr. Fang Yang, who during the four years became much more than just a colleague. Dear Fang, you were always willing to join many of our PhD activities outside of the lab. Whether spare ribs evenings, BBQs, or movie nights, together with Ronald you were always willing to join, and perfectly blended in. You two became very good friends of us, and we hope that one day we can welcome you as neighbors in the metropolis Kranenburg ☺.

I would like to thank the other, not less important, members of the staff for their assistance on many occasions. Dear Vincent, Natasja, Martijn, Monique, Henriette, and Kim, thanks a lot!

My dear Paranymphs! Dear Wanxun, I met you even before I started to work at the Biomaterials department. Together with Xiangzhen, we both were following the same animal experiment course. Interestingly, I have recognized you directly when I met you in the department, while I did not recognize Xiangzhen. Maybe it was because you were the more communicative one. But maybe I just felt that you might feed me one day through the PhD with snacks that you brought for yourself. It was great to share the same office with you (and I mean it not only because of the food). I appreciate that you understood the jokes we made sometimes and did not take it too serious. You were a wonderful colleague and you are a great friend. I am also very happy that you and Arnold, and Thordis and me are still in frequent contact, and I hope it will stay like this for a while ☺.

Dear Jiankang! The time you arrived in the lab, you got to sit in our office at the spot behind me. I was very impressed by your drive to learn the Dutch language, which was obvious from the thick notebooks you were carrying with you, and which you were reading every now and then. "Hhhet meeeeeijsje loooopt. Is this correct?" you asked with a hopeful look in your face. I confirmed. "Miiiijjn geziiiicht is vies. Is this correct?" and so on, and so on…tireless and for tens of minutes. However, I could see that the effort you spend was paying off, and although you are not willing to talk Dutch most of the time, I know that you understand a lot of what is discussed around you. Jiankang, I met only a few Chinese, who have adapted to the western world as strongly and as fast, as you did. You were the most innocent Chinese male person I have ever met before. That changed ☺. You are a good guy, a very intelligent scientist and a great friend. For my own sake I hope that your affinity for the Dutch language is as big as your affinity for the life here, and that after your PhD you will decide to stay here a little bit more.

I would like to mention also the two persons, who I have spent the most time discussing all possible topics, and solving all possible world problems with. The two princes of Persia; Kambiz and Mani. Dear friends, you made my time in the department a real pleasure and entertainment. Thank you for your company, the Nowruz, and rose water. Kambiz, my hotel-buddy. Thordis is the only person I shared the bed more often with than with you during the last four years. Our road trips and conferences in US, GB and Poland I will always remember. I hope the best for you and Farahnaz, and

we for sure will keep in touch. P.S.: Thank you for protecting me from the gangs in New Jersey, because…well you know.

Dear Mani! My office-room-buddy. I will never forget your "Aha, interesting", "amazing", and belated understanding of jokes. "Aha". Also thanks for organizing the amazing international movie nights. I hope all the best for you, stay sensitive, and break some more records! "Ahaaaaaaaaaaaaaaaaaaa". P.S.: Also after I have achieved my PhD, it is fine if you call me by my first name ☺.

Dear Yang! It was great to have you always around. Also sometimes when you were not with us, we could feel your entertaining and easy going spirit with us. Unfortunately, we have not been there for you, when you needed us most. Couple of years ago. In Paris. We would have told you that putting a bag full of valuable things (including the US visa you would need a month later) unwatched, on the ground at the main square of Paris, might be not the best idea. I hope by now you can laugh about it. Yang, you are the person with the most positive vibes that I have met in the department (except myself of course). Please keep this attitude.

Dear Dana! The Romanian girl with the sense of humor of Vlad the Impaler. …and probably the same temper. Oh what hard times you had, having people like me, Kambiz and Mani around. All these stupid jokes that we constantly made. Terrible! I however enjoyed having you around and believe though that you will miss us a lot once we have left the department.

Dear Simone. I cannot believe that there can be a person so much relaxed and easy going as you are. Stay like this and don't let anything stress you out! After me leaving you are the senior PhD of Frank. This is a big responsibility. P.S.: Take care of Dana after we leave.

Dear Astghik! We started at more or less the same time with our PhD projects and did both finish by now. Although you were often busy with your family, we have spent some time together during all kind of social activities. Whether work related such as during our conference trips to the US and Poland, or private by joining your family for the BBQ parties you often organized. Thank you for being a great colleague and I wish you, David and Armen all the best in the future. I assume that since we are neighbors, we will see each other also in the future ☺.

Dear Xinjie! Although you have been in Nijmegen only for a short part of

your PhD, you made a lot of friends here. I assume it is because of your ever happy aura. I cannot remember a day on which I have not seen you smiling. I know that your time here has not always been easy, but you kept on smiling. Now you are back to China and building up your life there. I hope that by now you have moved into your apartment with your future wife, and that the PhD phase is also finishing soon with good results. It was a pleasure to meet you, and maybe we see each other again.

Dear Daniel! You were part of our small nerdy group. I think from the whole department we two shared the most interests like movies, books, series, games and technology. When I started the PhD you were assembling the computer you wanted to buy. Three years later you did it and we could finally indulge also our gaming addiction ☺. Although you left the department more than one year ago we still see each other regularly and became close friends. I hope you and Saskia will do great in the future and we can let our children "fight" each other in Jedi and Sith costumes soon ☺.

Dear Kemal. Your friendship and colleagueship during the period we were both in the department were very valuable to me. You are a very nice, friendly and funny guy, who I really enjoyed sharing the office with. But not only the office, you shared also the funny videos from the Hürriyet website with me. This is why you were sometimes talking in Turkish to me, because "oh shey, I always talk Turkish to you, because you look Turkish to me", I could understand you. My dear friend, I hope your life is great in California, but also that you will visit us one time.

Dear Paula and Ricardo! It was a great pleasure to meet you two great people. Unfortunately, you were here only for a too short period. A period in which Ricardo broke his Achilles tendon. A period in which you Paula recovered him by motivating him to run and do the insanity workouts. In general you were helpful to many people in the department and made the department a great working place. Seeing you playing with gels colored with food dye while talking about the "magic" ingredients was priceless. Indeed also your cooking skills are unforgettable. Guys, all the best in London and I hope you will be as happy as it can be.

Of course I would also like to thank all of the other colleagues and friends that were always there and created a friendly environment. Dear Nathan, Robin, Eline, Alessandro, Winston, Sonia, Hatice, Antonio, Jinlong, Jinling,

Xiangzhen, Wei, Jie, Roel, Jidong, Jing, Hongbo, Muhanad, Rosa, Eva, Reza, Bart, Huanan, Yue, Floor, Hamdan, Ruggero, Esther, Johnny, Steven, Raffaela, Claire, Pedro, Reza, Michele, Take, Paulo, Kelly, Angela, Carla, and Weihua. Some of you have already finished your work in the department, and continued with their carrier elsewhere. I hope you guys are doing great! For the ones that are still busy and nervous about the finishing there is the old saying that we have in the department: everybody finishes! (at least their contract).

Also the fellas from the department of Orthodontics contributed to a good atmosphere in the lab. Dear Frank, Hans, Aysel, Kriti, Ditte, Katrien, Bas, Paola and Laury. I really appreciate to have met you all and hope that you all will do great in the future.

And now some words that most of you will not be able to read. To my family.

Дорогая мама. Я хочу чтобы ты знала, что всего чего я достиг, я никогда бы не достиг без твоей помощи. Без тебя все это было бы не возможным. Я не только имею в виду, что без тебя не было бы и меня. Я имею в виду, что отец и ты многим пожертвовали, когда решили переезжать в Германию. Вы поменяли профессию, друзей и родину на благополучие и высокие шансы для ваших детей. Мы находимся здесь из-за вас. Я благодарю вас за вашу поддержку во время моей учёбы и докторской диссертации. Мама, ты всегда меня поддерживала, и я хочу, чтобы ты знала, что и я буду всегда поддерживать тебя.

 Любимая бабушка. Хотя моя диссертация только вторая лучшая вещь которую могу я тебе предоставить в этом году, я всё равно знаю, что ты мной очень гордишься. Но ты также можешь гордиться собой. Без твоего вклада сегодняшний день никогда не был бы возможен. По моему мнению, ты сегодня стала доктором на 25 процентов, в твои 86 лет. А очень скоро ты станешь в третий раз на 100 процентов прабабушкой. Я бабуля не большой писатель речей, увы, не в тебя. Я просто надеюсь, что мы вместе с тобою будем испытывать еще много таких позитивных моментов как сегодня.

Liebe Alina, Oliver, Mischa, Stella, Didi und Werner! Vielen Dank auch an euch! Bei euch konnte ich mich immer ablenken und entspannen. Es ist sehr schön, dass es euch gibt und dass ich immer auf euch zählen kann.

List of publications related to this thesis

1. <u>Alexey Klymov</u>, Ljupcho Prodanov, Edwin Lamers, John A Jansen, X Frank Walboomers., *Understanding the role of nano-topography on the surface of a bone-implant.* (Biomaterials Science 2013;1:135-51)

2. <u>Alexey Klymov</u>, Charlotte T Rodrigues Neves, Joost te Riet, Martijn JH Agterberg, Emmanuel AM Mylanus, Ad FM Snik, John A Jansen, X Frank Walboomers., *Nanogrooved Surface-Patterns induce cellular organization and axonal outgrowth in neuron-like PC12-Cells.* (Hearing research 2015;320:11-7.)

3. <u>Alexey Klymov</u>, Ewald M Bronkhorst, Joost te Riet, John A Jansen, X Frank Walboomers., *Bone marrow-derived mesenchymal cells feature selective migration behavior on submicro-and nano-dimensional multi-patterned substrates.* (Acta biomaterialia 2015;16:117-25.)

4. <u>Alexey Klymov</u>, Jiankang Song, Xinjie Cai, Joost te Riet, Sander Leeuwenburgh, John A Jansen and X Frank Walboomers., *Increased acellular and cellular surface mineralization induced by nanogrooves in combination with a calcium-phosphate coating.* (Acta biomaterialia, accepted 2015)

5. <u>Alexey Klymov</u>, Joost te Riet, Peter Mulder, Han Gardeniers, John A Jansen and X Frank Walboomers., *Nanometer-grooved topography stimulates trabecular bone regeneration around a concave implant in a rat femoral medulla model.* (Nanomedicine: Nanotechnology, Biology and Medicine, revision 2015)

6. Esther Tejeda-Montes, <u>Alexey Klymov</u>, M Reza Nejadnik, Matilde Alonso, J Carlos Rodriguez-Cabello, X Frank Walboomers, Alvaro Mata., *Mineralization and bone regeneration using a bioactive elastin-like recombinamer membrane.* (Biomaterials 2014;35:8339-47.)

Curriculum Vitae

December 13, 1983:
>   Born in Kiew, Ukraine.

1995 - 2004:
>   General qualification for university entrance (allgemeine
>   Hochschulreife), Otto-Pankok Gymnasium, Mülheim an der Ruhr,
>   Germany.

2006 - 2009:
>   Bachelor of Science in Medical Biology,
>   Radboud University Nijmegen, Nijmegen, The Netherlands.

2009 - 2011:
>   Master of Science in Medical Biology,
>   Radboud University Nijmegen, Nijmegen, The Netherlands.

2011 - 2015:
>   PhD student,
>   Department of Biomaterials, Radboud University Medical Center,
>   Nijmegen, The Netherlands